Candidate Inorganic Photovoltaic Materials from Electronic Structure-Based Optical Absorption and Charge Transport Proxies

Douglas H. Fabini,[†,‡] Mitchell Koerner,[¶] and Ram Seshadri[*,†,§]

†*Materials Department and Materials Research Laboratory*
University of California, Santa Barbara, California 93106, United States
‡*Current address: Max Planck Institute for Solid State Research*
Heisenbergstraße 1, 70569 Stuttgart, Germany
¶*Physics Program, College of Creative Studies*
University of California, Santa Barbara, California 93106, United States
§*Department of Chemistry and Biochemistry*
University of California, Santa Barbara, California 93106, United States

E-mail: seshadri@mrl.ucsb.edu

Abstract

Approximately 33,000 valence-precise, ordered, inorganic compounds tabulated in the Inorganic Crystal Structures Database have been screened for their potential as photovoltaic (PV) absorbers. This has been accomplished through the use of proxies for charge carrier mobilities and optical absorption properties from electronic structure calculations, in addition to constraints on thermodynamic stability. Preliminary screening of computed properties tabulated in the Materials Project database, with subsequent high(er)-fidelity electronic structure calculations of optical properties and band gap corrections indicate $\approx$200 known compounds on or near the convex hull which exhibit Spectroscopic Limited Maximum Efficiency (SLME) in excess of 25 % for a 500 nm thin film, in addition to possessing low effective masses for both electrons and holes. Among the predicted high-performers are nearly all the known commercial inorganic thin-film PV materials as well as several previously unexplored candidates. The new candidates are drawn from a diversity of chemical and structural families, including many chalcogenides and pnictides as well as anti-perovskites, skutterudites, and semiconducting intermetallics. Carrier effective masses, SLME, corrected band gaps, and other relevant information for $\approx$800 compounds are made available for further analyses via the Materials Project MPContribs Framework.

Introduction

In recent decades, advances in approximate methods for quantum chemical calculations have enabled the creation of databases of predicted properties for tens of thousands of inorganic crystalline materials.[1–3] This has in turn empowered a new approach to materials design and selection wherein desired properties or functionalities are specified, and candidate materials are identified by comparison with tabulated property predictions. This new approach is potentially advantageous over the more usual one of making materials and measuring their properties serially. The traditional approach is typified by the recent example of lead halide perovskite photovoltaic (PV) absorbers: The time from first preparation[4] to crystal structure determination and discovery of photoconductivity[5] to wildly successful first application in solar cells[6] spans more than 100 years.

Augmenting these high-throughput ab initio property databases with progressively higher fidelity calculations and increasingly restrictive screening criteria has become a standard approach to the problem of computational materials design or selection, with examples found in the search for several types of functional materials, including transparent conducting oxides,[7,8] scintillators,[9] photoelectrochemical water-splitting catalysts,[10] and topological insulators.[11] Across functional materials classes, defining effective screening criteria is a persistent challenge as performance often involves a palette of several interconnected properties, some of which may not be easily computed from first principles. Often then, a proxy (alternatively, a "functionality metric")[12] is designed which serves as a computationally tractable stand-in for materials function, grounded in physical or chemical theory and domain knowledge. Examples include the ratio of electron and hole effective masses as a proxy for non-proportional response in scintillators,[9] host structure Debye temperature as a proxy for photoluminescence quantum yield in Ce^{3+} phosphors,[13] and magnetic (unit cell) deformation as a proxy for isothermal magnetic entropy change in magnetocalorics.[14]

The search to identify new solar cell absorbers is a prime example of the challenges of predicting complex function, with photovoltaic performance dictated by a range of optical, electronic, defect-related, and morphological properties. Shockley and Queisser first established a limiting efficiency for p–n junction solar cells which depends only on the electronic band gap of the absorber.[15] This criterion provides an excellent first-order estimate of losses incurred due to transparency to below-gap photons, carrier thermalization, radiative recombination current, and the deficit between cell voltage and band gap, but it is unable to account for the extremely wide range of performance exhibited by materials with comparable band gaps. Yu and Zunger proposed the Spectroscopic Limited Maximum Efficiency (SLME) as a material-dependent addendum to the Shockley-Queisser limit by taking into explicit account the spectral overlap of the material's optical absorption and the incident light from the sun, as well as a proxy for non-radiative recombination for materials for which the fundamental band gap is not both direct and dipole-allowed.[16] In this and a subsequent report, the authors used the SLME metric to screen a few hundred I_x–III_y–VI_z ternary chalcogenides chemically related to chalcopyrite for their potential as PV absorbers.[16,17] In these works, computationally expensive hybrid functional density functional theory (DFT) and many-body quasiparticle calculations limit the number of phases that may be tractably explored.

More recently, two efforts have sought to approximate the impact of defects, and have considered a broad chemical and structural scope by screening entire databases.[18,19] Brandt and coworkers[18] screened electronic structures in the Materials Project database[2] for compounds with s orbital character at the top of the valence band (which can also be readily predicted by electron counting) as a proxy for defect-tolerance. This effort identified dozens of semiconductors containing heavy lone pair-bearing main-group cations, but the predictive power of this approach has proven modest to date.[20] Kuhar and coworkers[19] screened experimentally-realized unary, binary, and ternary phases from the Open Quantum Materials Database[3] for toxicity and elemental abundance, band gaps and line effective masses at the semilocal Gritsenko–van Leeuwen–van Lenthe–Baerends (GLLB)[21] level, and the energetics of single-atom neutral vacancies at a rather modest level of fidelity. Other approaches have been recently reported based on the complex refractive index, carrier density, scattering mechanisms, and the particulars of device structure.[22,23] Still others have considered hypothetical or yet-unrealized materials, as in the screening of millions of organic molecular motifs,[24] hundreds of van der Waals heterostructures,[25] or dozens of elpasolite halides.[26]

Here we focus on proxies that involve only intrinsic materials properties which are relatively easily computed in order to identify promising PV absorber candidates from among most of the corpus of known, ordered, valence-precise (closed-shell) inorganic crystals. By screening the Materials Project database[2] based on band gap, formation energies, diamagnetism, smallest direct electronic transition, and estimated carrier effective masses, $\approx$800 phases are selected for further study as PV absorbers. Optical absorption spectra, transition dipole matrix elements, and band gap corrections are computed ab initio for these 800 compounds, and SLME is predicted based on these results. Close to 200 materials with high SLME ($> 25\,\%$ for 500 nm absorber thickness) are identified in a set of compounds exhibiting great chemical and structural diversity. Because of the approximate nature of computationally-tractable electronic structure calculations, the goal of this effort is not to find solitary and well-tuned, “needle-in-haystack” materials, but rather to highlight previously overlooked families in chemical and structural space, not unlike the situation with main-group halide perovskites only a decade back. Steps for further study and insights for design of other functional materials are discussed. Additionally, data from ab initio calculations are made freely available for further analyses via the Materials Project MPContribs Framework[27,28] at https://materialsproject.org/mpcontribs/ScreeningInorganicPV.

Results & Discussion

Overview of screening process

A schematic overview of the screening methodology is depicted in Figure 1. Beginning with the $\approx$46,000 insulators in the Materials Project Database in early 2018,[2] several preliminary screens are applied. First, only the $\approx$33,000 insulators with a computed electronic bandstructure are considered, as subsequent screening criteria require information on band edge curvatures and the smallest direct transitions. Second, only ordered materials whose relaxed structures reflect experimental entries in the Inorganic Crystal Structures Database (ICSD) are retained—this eliminates orderings of disordered phases which have not been observed experimentally as well as a number of user-submitted hypothetical phases. Third, only valence-precise (closed-shell, diamagnetic) compounds are included, on the grounds that as a general rule, magnetic compounds will exhibit weak low-energy optical absorption due to forbidden transitions between valence and conduction states of opposite spin. Rather than testing for closed-shell configurations based on electron-counting (assigning oxidation-states in an automated fashion presents challenges for certain polyanions and in many intermetallics) or based on the Stoner criterion (calculated densities of states in the MP database are of somewhat low fidelity), valence-precise compounds are selected simply as gapped phases that are not spin-polarized according to the calculations already present in the MP database. Only semiconducting phases are included, as defined by those exhibiting a band gap of $0\,\text{eV} < E_g \leq 2.5\,\text{eV}$. Notably, the underestimation of band gaps in DFT calculations leveraging the generalized gradient approximation (GGA) means that some “false-negatives” which appear metallic but are indeed semiconducting are generated at this step (e.g. CuInSe_2). Lastly, only phases on or near the total energy convex hull ($E - E_{\text{hull}} \leq 50\,\text{meV}\,\text{atom}^{-1}$) are included, as a proxy for thermodynamic stability or practical metastability (further discussion in the Methods section).

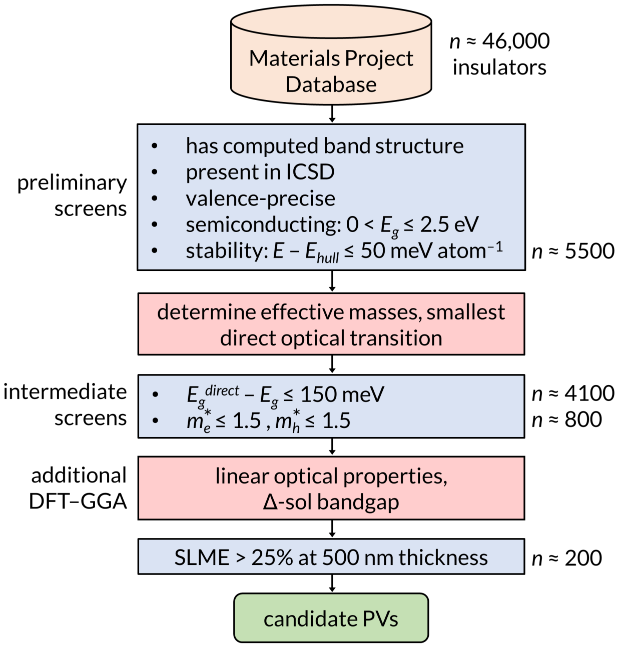

Figure 1: Schematic overview of the computational screening process, summarizing data sources, screening criteria, and approximate number of phases at each screening step.

Together, ≈5500 phases (≈12 % of all insulators in the MP database) remain after the preliminary screens. Next, three parameters are extracted from the calculated band structure in the MP database: (i) the electron effective mass, m_e^*, (ii) the hole effective mass, m_h^*, and (iii) the energy of the smallest direct gap, denoted E_g^{d}. Details of the effective mass determination and comparison with published results[29] are given in the Methods section and the Supporting Information. E_g^{d} is trivially determined as the minimum energy difference between occupied and unoccupied bands at the same crystal momentum.

Based on these parameters extracted from the tabulated band structures, several “intermediate screens” are applied. First, both the electron and hole effective mass must be less than 1.5 times the electron rest mass, m_0, as a proxy for the need for reasonable ambipolar carrier mobilities to extract carriers in a p–i–n device. Certainly, other architectures are possible which can relax the mobility requirements for one or the other carrier type, hence the not-particularly-restrictive value of 1.5m_0 at this stage of screening. Second, the smallest direct gap E_g^{d} must be no more than 150 meV wider than the fundamental band gap. Assuming carriers relax to the band edges before extraction (and thus ignoring concepts like hot carrier extraction), phases with too great of an $E_g^\mathrm{d} - E_g$ deficit will suffer from reduced cell voltages and diminished optical absorption, rendering them unlikely to be promising photovoltaic absorbers (Figure S5).

Close to 800 phases remain after applying these intermediate screens based on estimated carrier masses and the nature of the band gap. For these candidate materials, we conduct additional DFT calculations to determine the optical absorption coefficients and transition dipole matrix elements, as well as to reduce the known band gap errors associated with the GGA. Details of the calculations are given in the Methods section, as well as in the original reports of the methodologies for calculating linear optical properties[30] and the Δ-sol band gap correction.[31] Briefly, the Δ-sol method is an adaptation of the well-known ΔSCF method (for molecules) to extended solids, wherein the bandgap is calculated as the difference between the electron affinity and the ionization energy using total energies of neutral and charged supercells, rather than between the Kohn-Sham eigenvalues corresponding to the lowest unoccupied state and the highest occupied state. In practice, this method achieved a $\approx$70% reduction in mean-absolute band gap error relative to band gaps based on GGA eigenvalues for a test set of $\approx$100 materials.[31] As the Δ-sol requires only three GGA or LDA total energy calculations (one neutral, two charged), it may be preferable to significantly more expensive exact exchange or quasiparticle methods when screening hundreds or thousands of materials. Given the importance of spin-orbit coupling for heavy elements, this interaction is included for band gap corrections on compounds with period 6 elements (those with 5d, 6s, or 6p electrons). These band gap corrections are applied as a scissor operator to the unoccupied bands, and the SLME is subsequently computed, as detailed in the Supporting Information.

Before discussing the materials which emerge from this screening as promising PV candidates, we first examine the parameters computed for three well known systems as partial validation of our approach. Band structures, parabolic band fits, and absorption spectra

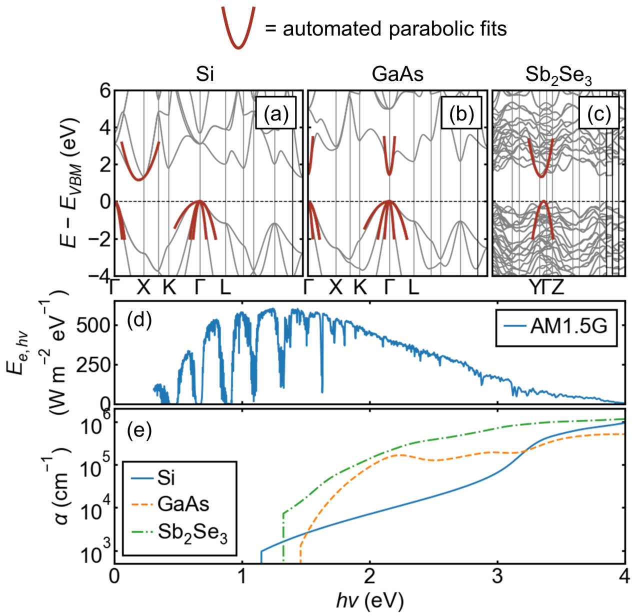

Figure 2: (a–c) Representative band structures and parabolic line effective mass fitting for known photovoltaic materials indirect gap Si, direct gap GaAs, and nearly-direct gap Sb_2Se_3. (d) Solar spectral irradiance, $E_{e,h\nu}(h\nu)$, from reference ASTM G173. (e) Representative absorption spectra, $\alpha(h\nu)$, for Si, GaAs, and Sb_2Se_3. The band structure abscissae in (a-c) are scaled to the length of the high symmetry path through the Brillouin zone to allow direct visual comparison of band curvatures. Only special point labels near the band edges are shown for clarity, but the high symmetry paths are as in Setyawan and Curtarolo.[32]

Table 1: Comparison of computed and measured parameters for the reference compounds presented in Figure 2. Favorable agreement is observed between experiment and the band gaps and effective masses computed here. The SLME metric is not suitable for thick, wafer-based, indirect gap c-Si and is omitted for this compound.

Formula		E_g (eV)	m^* (m_0)		SLME (%)
			m_e^*	m_h^*	L=500 nm
Si	calc.	1.15	1.00	0.59	n/a
	expt.	1.11[33]	1.06[34]	0.59[34]	
GaAs	calc.	1.45	0.08	0.62	27.8
	expt.	1.43[33]	0.07[35]	≈0.5[36]	
Sb_2Se_3	calc.	1.32	0.42	0.31	29.9
	expt.	1.06[37]			

for indirect gap Si, direct gap GaAs, and nearly-direct gap Sb_2Se_3 are given in Figure 2 with a comparison of computed and experimental parameters in Table 1. We see that the Δ-sol correction has roughly recovered the experimental band gaps from the severe underestimates of the GGA (see the Supporting Information, Figure S2), and the automatic parabolic band fitting has correctly detected the 3-fold valence band degeneracy in Si and GaAs at the zone center and has approximated the dispersion near the band edges well. Further, the absorption spectra match expectations, with Si exhibiting weak absorption in the solar spectrum due to its indirect band gap (the upturn in the absorption coefficient at 3.1 eV reflects the smallest direct transition, at Γ) and GaAs and Sb_2Se_3 exhibiting much sharper onsets. The somewhat higher absorption for Sb_2Se_3 than for GaAs accords with the thicknesses of these layers employed in devices (Sb_2Se_3: $\approx$400 nm;[38,39] GaAs: $\approx 2\,\mu$m; Si: $> 100\,\mu$m wafer).

By the logic of these proxies, materials which exhibit a high SLME are then expected to be candidates for high-performance photovoltaics, with strong optical absorption in the visible, predominantly radiative recombination, low carrier masses, and likely stability or metastability. Of the $\approx$800 phases passing the intermediate screens, we find $\approx$200 which exhibit SLME $>$ 25 % for a 500 nm thick absorber, including $\approx$40 with SLME $>$ 30 % at the same thickness. As discussed in the introduction, several other considerations are important for photovoltaic performance and practical viability, and further study of band alignments, defect energetics, processibility, and stability of the candidates proposed here will be essential.

As additional partial validation of this screening methodology, many high performing PV absorbers as well as emerging systems currently under study are present among the candidate phases. All commercial, crystalline thin-film photovoltaics come through these intermediate screens, and nearly all are predicted to have high SLMEs, including GaAs and other III–Vs as well as $CuInS_2$ and other ordered compositions of the chalcopyrite CIGS family. Notably, CdTe is predicted to have only moderate performance due to overestimation of the experimental band gap (see Figure S2). While the Δ-sol method significantly reduces the bias of GGA-calculated band gaps, significant variance remains,[31] and CdTe, CdSe, and CdS appear to be at the tail of the error distribution in our analysis.

In addition to these commercial PV materials, our screening predicts high performance for numerous compounds under research scrutiny in recent years, including kesterite Cu_2ZnGeS_4,[40] two polymorphs of $NaSbS_2$,[41,42] skutterudite $IrSb_3$,[43] halide perovskites $CsSnI_3$[44–46] and $CsPbBr_3$,[47] several II–IV–V_2 phases,[48,49] $BaZrS_3$ and related chalcogenide perovskites,[50] Sb_2Se_3,[38] $PbBi_2S_4$,[51] (Sb,Bi)SeI,[52,53] $Cu_2(Ge,Sn)S_3$,[54,55] and mixed-valence $Cs_2Au^{I}Au^{III}I_6$.[56]

On the other hand, these preliminary and intermediate screens narrowly exclude orthorhombic SnS[57] (direct-to-fundamental gap deficit 6 meV wider than the screening threshold), $CuSbS_2$[58] (hole mass ≈2× too large), $CuTaS_3$[59] (electron and hole masses ≈3× too large), a-Si (only crystalline materials present in the ICSD and MP database), and c-Si (the SLME metric is not suitable for thick, wafer-based, indirect gap photovoltaics). As noted above, this approach narrowly misses the smallest-gap end-member of the CIGS family, $CuInSe_2$, which appears metallic under the GGA. The anti-perovskite Cu_3N[60] is also excluded on the basis of lying well above the convex hull and having too great of a direct-to-fundamental gap deficit.

The calculated SLME for the ≈800 candidate phases is plotted against band gap in Figure 3 for various absorber thicknesses. Several known high-performance and research-scale photovoltaics are highlighted for comparison. It can be seen that the Shockley-Queisser limit (red line, "S–Q") places an upper bound on SLME, reflecting the underlying physics of the two models (see Supporting Information). In the infinite thickness case, the screening threshold on the deficit between direct and fundamental band gaps places a lower bound on SLME (black dashed line) except when our subsequent DFT calculations reveal the smallest direct transition to be dipole-forbidden (lighter gray dots). Dipole-allowed, direct band gap phases always converge to the Shockley-Queisser limit for

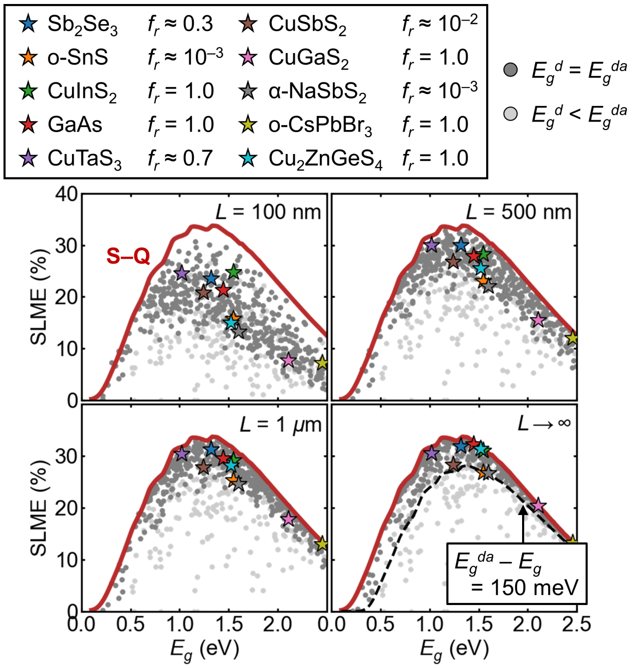

Figure 3: Calculated spectroscopically-limited maximum efficiency (SLME) for $\approx$800 phases passing the intermediate screens at four different absorber thicknesses, L. Several reference compounds are overlaid and their radiative recombination fractions, f_r, from the SLME framework are indicated. Red lines indicate the Shockley-Queisser limit. For infinite thickness, the screening criterion of $E_g^{\mathrm{d}} - E_g \leq 150$ meV sets a lower bound on performance (for phases with a dipole-allowed smallest direct transition) based on the approximation for non-radiative recombination in the SLME model, indicated by the black dashed line.

infinite absorber thickness.

Discussion of selected candidate materials

SLME, absorption spectra, effective masses, band structures, and crystal structures for several candidate materials are given in Figure 4, with key parameters summarized in Table 2. These examples are drawn from the families of candidate materials discussed below, and are not intended to be a representative subset of the high performance candidates which we identify.

Table 2: Computed parameters for the selected candidate phases presented in Figure 4. Band gap parameters are the fundamental band gap (E_g), smallest direct gap (E_g^{d}), and smallest dipole-allowed direct gap (E_g^{da}), and are corrected from GGA-PBE values by the Δ-sol method[31] as discussed in the text. Energies above the convex hull (ΔE_{hull}) are reported directly from the Materials Project database.[2]

Formula	Space Group	SLME (%)		Band gap (eV)			m^* (m_0)		ΔE_{hull}
		L=500 nm	L=1 μ m	E_g	E_g^{d}	E_g^{da}	m_e^*	m_h^*	(meV atom^{-1})
$NaSbS_2$	$C2/m$ (#12)	32.4	32.7	1.405	⊢ 1.408	⊣	0.08	0.14	20.5
Sr_3SiO	$Pnma$ (#62)	30.0	30.8	⊢	1.041	⊣	0.44	0.63	-
$Co_2Ge_3Se_3$	$R\bar{3}$ (#148)	28.8	30.9	⊢	1.218	⊣	0.72	0.27	-
$LiAsS_2$	Cc (#9)	25.4	27.0	1.698	⊢ 1.744	⊣	0.19	0.78	-
NaBaP	$P\bar{6}2m$(#189)	26.5	29.2	⊢	1.515	⊣	0.43	0.66	-
Li_2AgSb	$F\bar{4}3m$(#216)	29.2	29.9	⊢	0.990	⊣	0.12	0.53	-
LaCuSTe	$P2_1/c$ (#14)	28.1	31.1	⊢	1.341	⊣	0.26	0.53	-
$BaCd_2As_2$	$P\bar{3}m1$(#164)	30.9	32.1	⊢	1.358	⊣	0.13	0.47	-

(1) Oxides and chalcogenides with lone pair cations: Numerous chalcogenides (and even several oxides) with lone pair-bearing heavy main-group metal cations appear as promising candidates, a few of which are highlighted here. Interestingly, both monoclinic polymorphs of $NaSbS_2$[61–63] exhibit high SLME and light carriers, with the quenched β-phase (space group $C2/m$, #12) more favorable in both measures. Indeed, $NaSbS_2$ was quite recently identified as a promising PV absorber after forming as an unintentional byproduct during synthesis of Sb_2S_3.[41,42] The whole family of related I–(Sb,Bi)$^{3+}$–VI_2 semiconductors appears to be somewhat underexplored. While these compounds are composed of relatively abundant and low-cost elements, a preliminary survey of the literature sug-

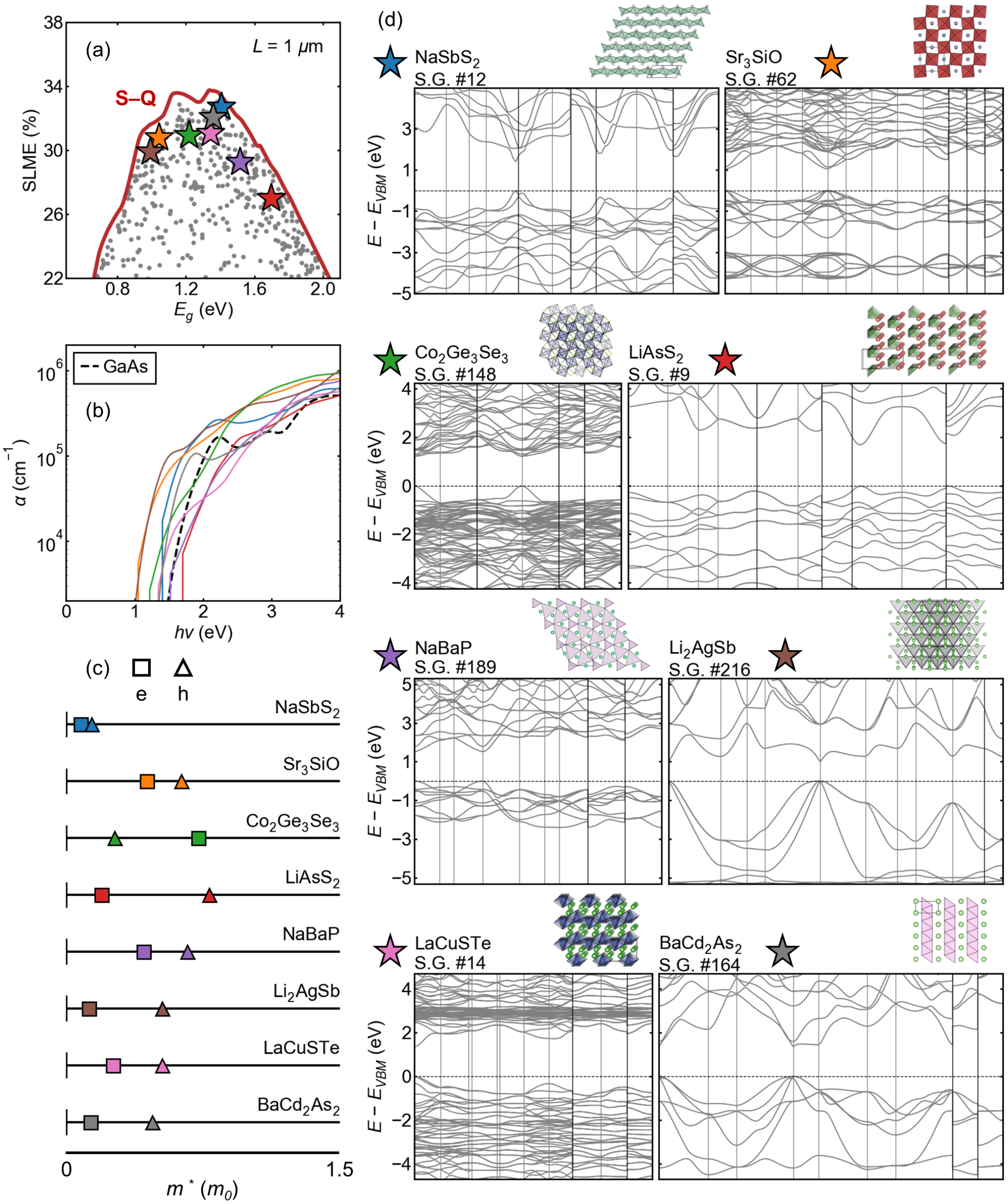

Figure 4: Selected candidate materials from ab initio optical absorption and charge transport proxy screening. Parameters are summarized in Table 2 for these phases, and in the Supporting Information for the ≈800 phases passing the intermediate screens. (a) Spectroscopically-limited maximum efficiency (SLME) for a 1 μm thick absorber, with selected candidate materials indicated. (b) Absorption spectra, with GaAs for comparison. (c) Electron (square) and hole (triangle) effective masses. (d) Crystal and electronic structures. The band structure axes are scaled to allow direct visual comparison of band curvatures. Brillouin zone path labels are omitted for clarity, but they follow the standard paths of Setyawan and Curtarolo.[32]

gests potential challenges related to cation antisite disorder due to the nearly identical sizes of ion pairs like Li^+/Sb^{3+} and Na^+/Bi^{3+} despite their very different charge states.[64–67]

Among the small handful of oxides which exhibit high SLME, mixed-valence $Ag_2Bi^{III,V}O_3$ (space group $Pnn2$, #34)[68,69] is an interesting candidate. Experimental reports indicate stability in air and moisture up to 750 K and confirm the semiconducting, diamagnetic nature.[68,69] Our calculations suggest a band gap of 1.07 eV, while the limited property measurements reported suggest a gap of only 0.7 eV from temperature-dependent impedance spectroscopy.[68] However, activation energies from conductivity frequently underestimate optical band gaps due to the participation of defect levels and other complexities in charge transport. While this phase exhibits 3-D connectivity (chains of edge-sharing BiO_6 octahedra along a, alternating Bi^{3+}/Bi^{5+}, which are then corner-sharing in the bc-plane, as well as Ag–Ag distances along a only 5% longer than in fcc-Ag), carriers are on the heavy end of our screening range likely owing to the high electronegativity of oxygen as well as the Bi charge ordering. One expects also that the electronegativity of oxygen may make for an unfavorably deep valence band, though the maximum may be pushed up somewhat by the interaction with the s orbitals of Bi^{3+}.[70,71]

Several naturally occurring sulfide minerals also appear as candidates, including krupkaite ($CuPbBi_3S_6$, space group $Pmc2_1$, #26)[72–74] and aikinite ($CuPbBiS_3$, space group $Pnma$, #62).[75] Similarly, the well-studied binaries, galena (PbS, NaCl-type) and bismuthinite (Bi_2S_3, Sb_2S_3-type), appear though they are known to exhibit rather narrow gaps in bulk form in experiments. Band gap widening via nanostructuring has been successfully applied to these latter materials for use as absorbers or sensitizers in solar cells.[76–78]

The chalcohalides BiSe(Br,I), BiTe(Cl,I), and SbSeI are identified by our proxies as candidate PV absorbers. Bi(S,Se)I and SbSeI have been studied in recent years for this application, with researchers finding favorable optical absorption and band curvatures, but anisotropic charge transport,[52,53] deep defects under typical synthetic conditions,[79] and deep valence band maxima,[52] as reported previously for other low-dimensional bismuth halides.[80,81]

The candidate $LiAsS_2$ phase, with the lone pair-bearing As^{3+} cation, is polar and exhibits a large second-harmonic generation (SHG) response,[82] raising the intriguing possibility of testing the bulk photovoltaic effect in semiconducting phases[83] rather than wide gap oxides.[84,85] The bulk PV effect is of course beyond the scope of the SLME model applied here, but our results nonetheless suggest favorable absorption in the solar spectrum as well as light carriers. Numerous Tl(I) and mixed-valence Tl(I,III) chalcogenides (including Pt_2TlS_3, Tl_3AsSe_3, Tl_2SnSe_3, and $TlSbSe_2$, to name a few) are predicted to exhibit high performance, but are not considered further here due to the substantial toxicity of thallium.

(2) Layered transition metal chalcogenides: Several layered transition metal chalcogenides appear promising, including hexagonal variants of $(Mo,W)Te_2$ ($P6_3/mmc$, #194), $K_2Ag_4Se_3$ ($C2/m$, #12),[86] and LaCuSTe ($P2_1/c$, #14).[87] The broader family of $(Mo,W)Q_2$ compounds also presents a wide range of structural modifications and the ability to exfoliate down to monolayer or few-layer structures, leading to a wide range of electronic properties and suggesting a substantial phase space for property tuning. While $K_2Ag_4Se_3$ exhibits high SLME and light carriers, Ag–Ag bonding suggests possible susceptibility to oxidation or chemical attack, despite the ostensible nobility of silver metal. For LaCuSTe, empty La^{3+} states enhance the absorption of blue/near-UV photons, and one can expect the details to change with a more sophisticated treatment of the empty d and f states for which electron correlation is typically important.

(3) Skutterudites: $IrSb_3$ (quite recently suggested as a promising PV absorber)[43] as well as the anion-ordered $Co_2Ge_3Se_3$[88,89] and $Co_2Sn_3(Se,Te)_3$[90,91] all exhibit high SLMEs and light carriers (particularly holes), as well as high symmetry. Many skutterudites have been investigated for thermoelectric applications, and it remains to be seen if the true band gaps are indeed wide enough for single-junction photovoltaics.

(4) Anti-perovskites: Many compositions of the anti-perovskites $(Ca,Sr)_3(Si,Ge)O$[92] and $(Ca,Sr,Ba)_3(Sb,Bi)N$[93] appear quite favorable, with high SLMEs and light carriers (though stability is likely to be limited). Additionally, layered Ba_4Pn_2O phases, which adopt the perovskite-derived anti-K_2NiF_4 structure (anti-Ruddlesden-Popper, $n = 1$; Pn = As, Sb: space group $I4/mmm$, #139; Pn = P: space group $Cmca$, #64)[94,95] are favorable by our metrics, though with somewhat heavier holes and layered connectivity.

(5) Pnictides in the ZrNiAl structure: Several pnictides in the ZrNiAl structure type (ordered Fe_2P-type, space group $P\bar{6}2m$, #189) exhibit high SLME and light carriers. NaBaP is composed entirely of non-toxic, reasonably abundant elements and occurs as black crystals.[96] On the other hand, while CaAgPn (Pn = P, As) are predicted to exhibit very high SLME, these phases appear to actually be slightly metallic in experiments.[97]

(6) Layered hexagonal-net pnictides: A number of closed-shell 1:1:1-stoichiometry layered compounds appear as candidates for high performance, including LiBaP[98] and SrAgP (ZrBeSi-type, space group $P6_3/mmc$, #194),[99] KZnSb (KZnAs-type, space group P_3/mmc, #194),[100] and LiBaP and LiBaAs (BaPtSb-type, space group $P\bar{6}m2$, #187).[101] These phases are minimally explored, but the few reports that exist seem to confirm the semiconducting nature of these compounds (for instance, LiBaP in space group #194 is dark red).[98] Further, while the original report describes a silvery luster for KZnSb (suggesting metallicity or proximity thereof), KZnP is described as black-brown.[100]

(7) Other layered pnictides: $(Sr,Ba)Cd_2As_2$ and $BaCd_2P_2$ (space group $P\bar{3}m1$, #164) appear promising, and $BaCd_2P_2$ is further described as gray and stable against air and moisture.[102,103]

(8) Heuslers and related phases: The half-Heusler LiMgBi (space group $F\bar{4}3m$, #216),[104] Heusler Na_2KSb (space group $Fm\bar{3}m$, #225), and Heusler-related Li_2AgSb

(CuHg$_2$Ti-type, space group $F\bar{4}3m$, #216)[105] are interesting, high-symmetry candidates if their band gaps are indeed as wide as predicted.

(9) Zintl phases: Many Zintl compounds are predicted to exhibit high SLME and light carriers, including $Sr_3Ge_2As_4$ and $Na_2Al_2As_3$ (space group $P2_1/c$, #14)[106,107] and $Sr_{11}InSb_9$ (space group $Iba2$, #45).[108] However, air stability is likely to be a challenge with some or most of these, with main-group–main-group bonding in the Zintl ions sometimes causing vulnerability to oxidation.

The aforementioned compounds are merely examples of the ≈200 high SLME candidates. A complete list of computed band gaps, SLME, and effective masses for the ≈800 phases passing the intermediate screens is presented in the Supporting Information. These parameters, as well as computed absorption spectra and electronic densities of states are additionally available in structured digital form at https://materialsproject.org/mpcontribs/ScreeningInorganicPV.

This screening scheme represents a first step in identifying new high performance photovoltaic absorbers. Further investigation will be necessary, particularly in the areas of property anisotropy, stability, band alignments, and defect energetics. For example, though they may lie on or near the total energy convex hull, many phosphides may oxidize to phosphates in air or may release phosphine upon hydrolysis, rendering them both dangerous and ineffective. As another example, many layered materials exhibit strong optical absorption in the through-plane direction, but favorable carrier transport in the in-plane directions.[59] Such anisotropy does not lend the material then to a planar solar cell configuration where carriers are extracted at the front and back cell surfaces, and may require exotic architectures like core-shell microwires which separate the length-scales and directions for light absorption and carrier separation.[109]

A note on polar compounds: Inspired by the example of $LiAsS_2$ above with a strong nonlinear optical response, we note that 114 of the phases passing the intermediate screens crystallize in one of the 68 polar space groups, including 24 compounds with SLME above 25% for a 500 nm thick absorber. Among these polar, high-SLME phases are mixed-valence Ag_2BiO_3 (shown to exhibit strong second harmonic generation, SHG),[69] Cu_2GeS_3 (shown to exhibit strong SHG and birefringence in the mid-IR),[110] $LiAsS_2$ and hydrogenated Zintl compounds SrGa(Ge,Sn)H (predicted to exhibit a substantial bulk photovoltaic effect from ab initio calculations),[111,112] BiTeI (shown to exhibit a large Rasha spin-splitting originating from the bulk),[113] krupkaite $CuPbBi_3S_6$, and several others. These phases may offer fertile ground for exploration of the bulk photovoltaic effect in semiconductors. Additionally, those which contain heavy elements may enable more systematic study of possible effects of spin-orbit-induced Rashba and Dresselhaus spin texture on carrier transport and lifetimes in photovoltaics. Such possible effects[114] have been proposed to enhance performance of halide perovskite solar cells,[115,116] a hypothesis which has been met with recent criticism[117–119] in these materials which exhibit local, dynamic polar distortions[120–123] rather than long-range broken inversion symmetry.

Inter-parameter correlations and chemical trends

The distribution of electron and hole effective masses is given in Figure 5, with the screening thresholds indicated. One can see that the screening criterion is more restrictive for holes than for electrons (with only 26 % of phases exhibiting sufficiently light holes, versus 60 % for electrons). This matches expectation: For closed-shell, heteroatomic compounds, the valence bands are typically derived from tightly-held, anion p-states (e.g. O $2p$ in oxides, S $3p$ in sulfides) or rather localized d^{10} cation d-states (as for Cu^+ and Zn^{2+}), while the situation for the conduction bands is much more varied and involves the participation of larger unoccupied orbitals, typically on the cations. Compounds containing heavy main-group cations with lone pairs are an exception: The filled $5s$ or $6s$ states mix with the anion p states at the top of the valence band, leading to significant dispersion, lighter holes, and reduced ionization energies. Light hole effective masses, then, are typically observed in systems proximate to metallicity, while even insulators can have light electron effective masses (consider diamagnetic metal oxides with conduction bands derived from large, s orbitals, like perovskite BaSnO$_3$ [124,125]). Support for this interpretation is given by the empirical relationship between band gap and carrier effective masses (Supporting Information, Figure S4).

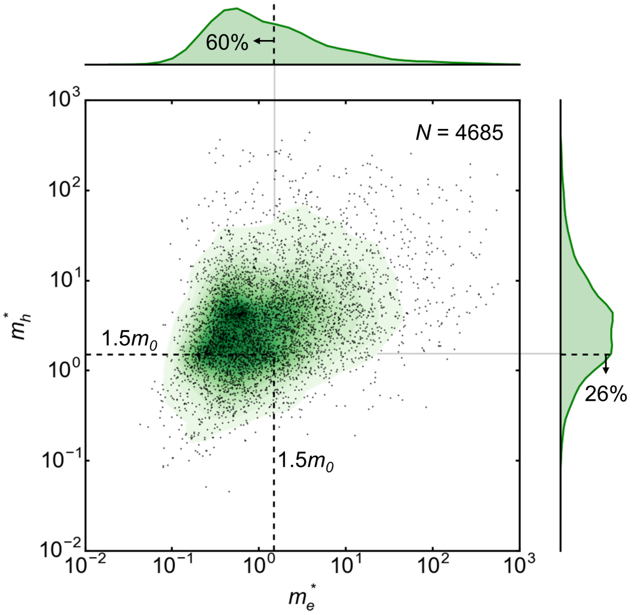

Figure 5: Scatter plot of electron (m_e^*) and hole (m_h^*) effective masses for ≈4700 phases passing the preliminary screens, in units of the electron rest mass (m_0). The green shading indicates the 2-D distribution of the points (via kernel density estimation), while the top and right panes are 1-D histograms. The maximum carrier effective mass ($1.5m_0$) for subsequent screening is indicated, and is shown to be more restrictive for holes than for electrons.

Figure 6 depicts the correlation between SLME and carrier effective masses. One might presume that there is necessarily a fundamental tradeoff between high optical absorption and low carrier mobilities, because the wide band widths which lead to light carrier masses typically also lead to a low joint density-of-states near the absorption onset. However, calculations of the matrix elements reveal that many such compounds have high oscillator strengths near the absorption onset, frequently offsetting this effect. Together with the uncorrelated nature of electron mass and band gap and the positive correlation between hole mass and band gap (Figure S4) for the reasons discussed above, this results in an interesting relationship between high SLME (reflecting strong absorption in the solar spectrum) and light carrier masses (suggesting favorable carrier mobilities). Examining Figure 6 and the Pearson correlation coefficients, SLME is essentially uncorrelated with electron mass, suggesting the two parameters can be optimized somewhat independently. On the other hand, a fortuitous, moderately negative correlation exists between SLME and hole mass, because light holes are typically only observed as the band gap narrows, also leading to stronger absorption of solar photons. Naturally, there is a limit to this behavior: For sufficiently small band gaps, SLME will necessarily begin to drop (Figure 3) as losses from carrier thermalization to the band edges overwhelm any marginal gains from increased photocurrent.

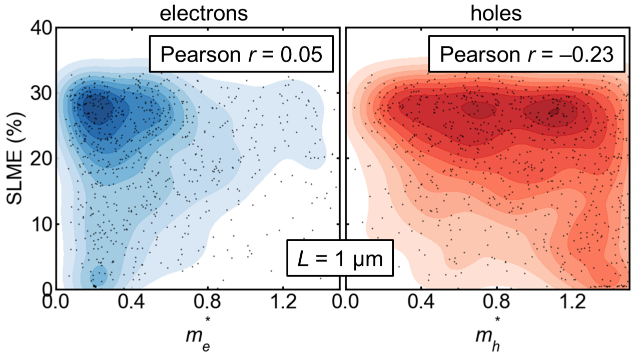

Figure 6: Scatter plots of SLME at $L = 1\,\mu$m absorber thickness against electron and hole effective masses for ≈800 phases passing the intermediate screens. From the Pearson correlation coefficients (annotated) the electron mass is seen to be essentially uncorrelated with SLME, while the hole mass has a fortuitous, moderately negative correlation with SLME: A higher SLME is associated with lighter holes. This is primarily driven by the underlying correlations between carrier masses and band gap (see Figure S4). Blue and red shading indicate the 2-D distribution of the points (via kernel density estimation).

Examination of the chemical and structural trends in these results may offer new insights or design principles for the preparation of new materials. The incidence of the elements in the corpus of ≈800 phases passing the intermediate screens is shown in Figure 7(a), with the number of phases in which each element appears color-coded and annotated. Perhaps unsurprisingly, the distribution looks much like what a solid-state chemist would expect for semiconductors generally, with lots of chalcogens and heavier pnictogens as anions, main-group metals and metalloids and late transition metals as cations, and electropositive alkali and alkaline earth metals and early transition metals presumably functioning as counter-cations in ternary or higher-order multinary compounds. Many sulfides, selenides, tellurides, phosphides, and arsenides appear, reflecting their greater tendency to be semiconducting than nitrides, oxides, and halides with highly electronegative anions. Fortuitously, one expects that the lower electronegativity and larger frontier p orbitals of sulfur, phosphorus, and selenium than of oxygen will also typically lead to shallower, wider valence bands with lighter hole effective masses and more favorable band alignment for hole extraction and p-type doping.

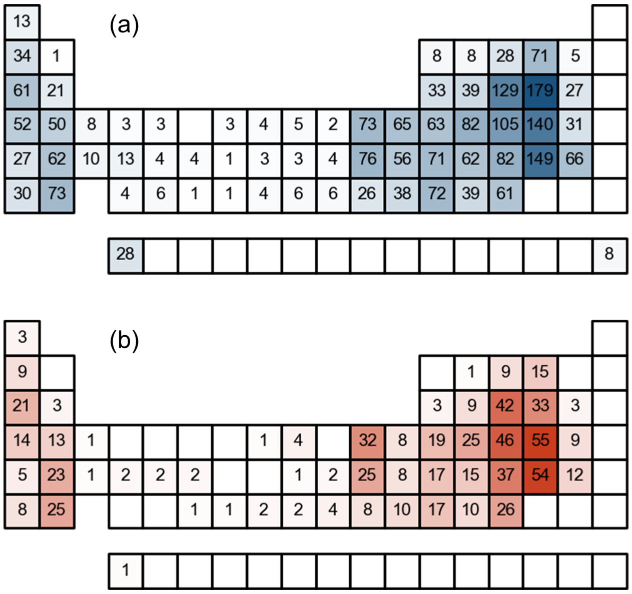

Figure 7: Chemical trends. (a) Incidence of the elements among phases passing the intermediate screens, shaded and annotated as the number of phases in which the element occurs out of ≈800 total. (b) Incidence of the elements among high-SLME phases passing the intermediate screens, shaded and annotated as the number of phases containing the element which exhibit SLME >25 % at 500 nm thickness.

Chemical composition appears to hold some degree of predictive power beyond the intermediate screening, which can be seen in Figure 7(b), with the number of the ≈800 phases passing the intermediate screens which also exhibit high SLME (>25 % at 500 nm thickness) indicated. Of elements which appear at least 20 times in the set of ≈800 candidates, there is a relative paucity among the high-performing phases of Mg, La, Al, Zn, Cd, O, Cl, I, and S. This is rather understandable for Al, O, and Cl, but the finding that Zn, Cd, I, and S are empirically unfavorable is quite unexpected, and warrants further analysis. As an important caveat, this result is biased by which regions of chemical space have been more explored or exhibit more polymorphism. For instance, numerous (≈25) reported ZnS intergrowths pass the intermediate screens due to GGA band gap underestimation, but they are all predicted to have band gaps in excess of 3.5 eV at the Δ-sol level (Figure S3), as observed for both zinc-blende and wurtzite polymorphs in experiments. Were there not so many distinct structures in the database, Zn and S would appear more favorable by this analysis. This particular cautionary example is an extreme one. Nevertheless, we hesitate to draw too many firm conclusions at this stage.

In addition to chemical factors, one presumes that structural features are quite influential, and further analysis of structural dimensionality and connectivity (leveraging graph theoretic techniques)[126–130] and of coordination geometries (leveraging continuous symmetry measures)[131] may prove insightful.

Conclusion

From ≈33,000 ordered, valence-precise, inorganic compounds tabulated in the ICSD, ≈200 candidate thin film photovoltaics have been identified which exhibit a SLME in excess of 25% for a 500 nm thin film, favorable formation energies, and light effective masses for electrons and holes. These materials comprise a diverse set of compositions and crystallize in a wide range of structure types. In addition to correctly identifying nearly all well-known/commercial inorganic thin film materials as well as many compounds under active study, several unexplored or underexplored candidates are identified that include chalcogenides, pnictides, anti-perovskites, skutterudites, and semiconducting intermetallics.

Where previous reports have typically employed screening criteria based on proxies for optical absorption *or* charge transport, this analysis combines these two complementary approaches. Additionally, an extremely broad chemical and structural scope has been considered, expanding significantly the number of inorganic phases for which SLME has been computed. Numerous tools are emerging which will enable the extension of this and other analyses to unrealized inorganic phases[132,133] and to improve the predictive power of such screenings though the inclusion of defect properties,[134,135] dielectric screening,[136–138] solid-aqueous equilibria,[139] and metastability.[140] The data generated here, including high-level parameters as well as ab initio optical absorption spectra and electronic densities of states for ≈800 compounds, are made freely available for further ex post facto analyses and future materials discovery efforts. In particular, the tabulated optical properties present an immediate opportunity to aid in the identification of new photodetectors, including those for near-IR, visible, and hard radiation.

Methods

Preliminary screens: All data for the computational screening (except those generated by our own ab initio calculations, vide infra) were drawn from the Materials Project (MP) database,[2] making extensive use of the PYMATGEN API.[141] The Materials Project contains ab initio relaxed crystal structures and computed properties for tens of thousands of reported ordered, inorganic crystalline phases (predominantly from the Inorganic Crystal Structure Database (ICSD) of FIZ Karlsruhe, but also a number of user-submitted, often hypothetical phases). This computational screening reflects the state of the MP database in early 2018, with 69,640 total entries (including 46,046 insulators, 33,125 of which have computed band structures). Due to the challenges of handling substitutional alloys and partial occupancy in periodic DFT, only ordered phases are present in the database as of this writing, though some disordered phases are automatically ordered, relaxed, and compared to known structures in the ICSD. Our analysis is restricted to those phases which correspond to reported structures in the ICSD, thus excluding user-contributed hypothetical phases and orderings of disordered crystals (unless they relax to match a reported structure present in the ICSD, in which case they are already sampled by our routine).

Further, only valence-precise (full-shell) compounds are considered, reflecting the nominally forbidden nature of optical transitions between occupied and unoccupied states of opposite spin, which will constitute the states near the band gap in spin-polarized semiconductors. While promising magnetic semiconductors for PV may exist, we expect them to be the exception, rather than the rule, and such investigation is beyond the scope of this work. In conjuction with this requirement of valence-precision, we exclude any compounds containing f-block ions, unless they are exclusively La^{3+} $(4f^0)$ or Lu^{3+} $(4f^{14})$. In these cases, the lanthanide f-states typically lie well above the conduction band minimum $(4f^0)$ or well below the valence band maximum $(4f^{14})$. Accordingly, the inaccuracy of DFT treatments of localized f electrons matters much less for the resulting electronic structure and optical absorption than if these states occurred near the band edges.

Accurate prediction of the thermodynamic stability of crystals is difficult, and a field unto itself. To efficiently screen the wide chemical and structural space considered here, we limit our analysis to the computed total energies and associated convex hulls which are tabulated in the MP database. We exclude all compounds which lie more than 50 meV atom^{-1} above the hull in energy, which is in line with typical error bounds in DFT. Notably, this approach potentially excludes the ambient temperature polymorphs of compounds with solid–solid thermal phase transitions brought on by the entropic contribution of very soft vibrations, such as main-group halide perovskites.[142,143] More sophisticated treatments of stability based on solid-aqueous equilibria[139] and prediction of metastability[140] may provide further insight.

As a primary goal of this work is to be as chemically and structurally comprehensive as possible, we summarize here those phases which are excluded from our analysis, but may be of interest in future investigations. Phases without a computed band structure in the MP database, disordered phases, magnetic phases, phases far above the (currently known) total energy convex hull, and those which are semiconducting in reality but which appear metallic under GGA-DFT are excluded here. Apart from these "deterministic" exclusions, ≈30 phases (amounting to ≈3.5 % of our final set of ≈800 phases) are ultimately excluded due to persistent lack of convergence or other problems in our ab initio calculations. For completeness, these phases are listed in the Supporting Information, and are reported in structured form in the accompanying digital datasets (https://materialsproject.org/mpcontribs/ScreeningInorganicPV). In all, roughly 5500 phases pass these preliminary screens of the ≈46,000 insulators in the database.

Intermediate screens: Phases which pass these preliminary screens, as summarized in Figure 1, are subsequently winnowed by criteria based on effective masses and the nature of the band gap. Estimation of electron and hole effective masses is accomplished by a parabolic fitting to the band dispersions at the band extrema, using the electronic band structure stored in the Materials Project database. Details are given in the Supporting Information. Notably, this use of "line" effective masses will necessarily result in a lower fidelity estimate than the use of dense k-meshes about the band extrema in new DFT calculations, a necessary compromise to screen the vast chemical space of most known, ordered, valence-precise, inorganic crystals. Comparison with recent results based on the BoltzTraP code[29] is given in the Supporting Information.

All direct gap phases meeting the effective mass criterion are carried forward for additional ab initio calculations, while indirect gap phases are only propagated if the smallest direct transition lies less than 150 meV above the fundamental band gap. This reflects the fact that if carriers are thermalized to the band edges, a large difference between fundamental and direct gaps will result in weak optical absorption and low cell voltages (Figure S5). As shown in Figure 3, this avoids expensive computation for phases which will necessarily exhibit SLME well below the Shockley-Queisser limit for their band gap, like several of the compounds described in the original report of the SLME metric.[16] Close to 800 phases pass these intermediate screens, and ≈10 additional reference compounds which do not pass these or the preliminary screens are included in subsequent calculations for comparison.

Additional ab initio calculations: All calculations were performed with the Vienna Ab initio Simulation Package (VASP),[144–147] which implements the Kohn-Sham formulation of density functional theory (DFT) using a plane wave basis set and the projector augmented wave formalism.[148,149] The generalized gradient approximation was employed using the exchange and correlation functional of Perdew, Burke, and Ernzerhof (GGA-PBE).[150] The plane wave basis set cutoff energy (800 eV for systems with ions from periods 1 or 2, 500 eV otherwise) and k-point mesh density ($\approx$1200 k-points per reciprocal atom for the self-consistent charge density and for total energy calculations used in the Δ-sol estimation of band gaps, $\approx$10,000 k-points per reciprocal atom for computing dielectric functions, densities of states, and matrix elements, all Γ-centered Monkhorst-Pack sampling[151]) were chosen based on convergence of the total energy for a sample of representative phases. Frequency-dependent dielectric functions were calculated via the method of Gajdoš and coworkers, as implemented in VASP,[30] transformed to an isotropic equivalent, and subsequently to isotropic absorption spectra. Absorption spectra were then transformed by a scissor operator, where the band gap was corrected to that estimated by the Δ-sol method without monopole or dipole corrections (details below and in the original report,[31] and our own partial validation is given in the Supporting Information). Such a scissor operation-type band gap correction does not rigorously correct the energies of the excited states across the entirety of the Brillouin zone, but represents a significant improvement over the uncorrected case at reasonable computational cost. Spin-orbit coupling (SOC) was included in the band gap corrections of compounds containing period 6 elements (those with 5d, 6s, or 6p electrons).

The Δ-sol method was applied as a computationally efficient means to reduce errors in calculated band gaps arising from the lack of derivative discontinuity and delocalization error of semilocal exchange and correlation functionals. Rather than taking the band gap to be the difference between the Kohn-Sham eigenvalues corresponding to the lowest unoccupied state and the highest occupied state, the Δ-sol method takes the band gap to be the difference between the electron affinity and the ionization energy, as determined by total energies of charged and neutral supercells. Specifically, the total energy is evaluated for the neutral case, the case with n additional electrons, and the case with n electrons removed. The fundamental gap is then computed as $E_{FG} = [E(N_0 + n) + E(N_0 - n) - 2E(N_0)]/n$, where N_0 is the number of valence electrons in the neutral supercell.[31] The choice of the value of $N^* = N_0/n$ is essential, and was determined semi-empirically for various local and semilocal functionals and classes of compounds based on test sets of $\approx$80 to $\approx$120 compounds each.[31] The fitted values were found to agree well with an estimate based on the dielectric screening properties of the homogeneous electron gas at densities typical in condensed matter, lending further credibility.[31] We use recommended values of N^* for use with the PBE exchange-correlation functional (72 for compounds with transition metals, 68 for those with only main-group elements).[31] No monopole or dipole corrections were applied for the charged supercells (in agreement with Chan and Ceder, we found in our own tests that monopole corrections increased errors relative to experiment). Ultimately, while band gaps predicted from Δ-sol for $\approx$100 reference compounds still display some random error with respect to experiments, the mean absolute error is reduced by $\approx$70% with respect to typical calculations based on Kohn-Sham eigenvalues.[31] Our own partial validation (Figure S2) shows a significant reduction in systematic error as well.

Data were analyzed and visualized with custom python code, leveraging the PYMATGEN API,[141] and the SEABORN and MATPLOTLIB packages. Crystal structures were visualized with VESTA.[152]

Supporting Information

Computed parameters for the ≈800 candidate phases, and further methodological details. Additionally, structured digital datasets of computed absorption spectra, densities of states, SLME, effective masses, and a list of all ≈33,000 phases which were screened are available at https://materialsproject.org/mpcontribs/ScreeningInorganicPV.
The authors declare no competing financial interest.

Acknowledgement

This work was supported by the U.S. Department of Energy, Office of Science, Basic Energy Sciences under award number DE-SC-0012541. DHF thanks the National Science Foundation Graduate Research Fellowship Program for support under Grant DGE 1144085. We thank the Materials Project for the enabling contribution to this effort. DHF thanks Joshua Bocarsly, Samuel Teicher, and Wennie Wang for useful discussions. Computation made use of the facilities of the Center for Scientific Computing at UCSB supported by the California NanoSystems Institute, the Materials Research Science and Engineering Center (MRSEC) at UCSB (NSF DMR 1720256) and NSF CNS-1725797.

References

(1) Curtarolo, S.; Setyawan, W.; Wang, S.; Xue, J.; Yang, K.; Taylor, R. H.; Nelson, L. J.; Hart, G. L.; Sanvito, S.; Buongiorno-Nardelli, M.; Mingo, N.; Levy, O. AFLOWLIB.ORG: A Distributed Materials Properties Repository from High-Throughput Ab Initio Calculations. *Comput. Mater. Sci.* **2012**, *58*, 227 – 235.

(2) Jain, A.; Ong, S. P.; Hautier, G.; Chen, W.; Richards, W. D.; Dacek, S.; Cholia, S.; Gunter, D.; Skinner, D.; Ceder, G.; Persson, K. A. Commentary: The Materials Project: A Materials Genome Approach to Accelerating Materials innovation. *APL Mater.* **2013**, *1*, 011002.

(3) Saal, J. E.; Kirklin, S.; Aykol, M.; Meredig, B.; Wolverton, C. Materials Design and Discovery with High-Throughput Density Functional Theory: The Open Quantum Materials Database (OQMD). *JOM* **2013**, *65*, 1501–1509.

(4) Wells, H. L. Über die Cäsium–und Kalium–Bleihalogenide. *Z. Anorg. Chem.* **1893**, *3*, 195–210.

(5) Møller, C. K. Crystal Structure and Photoconductivity of Caesium Plumbohalides. *Nature* **1958**, *182*, 1436.

(6) Kojima, A.; Teshima, K.; Shirai, Y.; Miyasaka, T. Organometal Halide Perovskites as Visible-Light Sensitizers for Photovoltaic Cells. *J. Am. Chem. Soc.* **2009**, *131*, 6050–6051.

(7) Hautier, G.; Miglio, A.; Ceder, G.; Rignanese, G.-M.; Gonze, X. Identification and Design Principles of Low Hole Effective Mass p-Type Transparent Conducting Oxides. *Nat. Commun.* **2013**, *4*, 2292.

(8) Hautier, G.; Miglio, A.; Waroquiers, D.; Rignanese, G.-M.; Gonze, X. How Does

Chemistry Influence Electron Effective Mass in Oxides? A High-Throughput Computational Analysis. *Chem. Mater.* **2014**, *26*, 5447–5458.

(9) Setyawan, W.; Gaume, R. M.; Lam, S.; Feigelson, R. S.; Curtarolo, S. High-Throughput Combinatorial Database of Electronic Band Structures for Inorganic Scintillator Materials. *ACS Comb. Sci.* **2011**, *13*, 382–390.

(10) Castelli, I. E.; Hüser, F.; Pandey, M.; Li, H.; Thygesen, K. S.; Seger, B.; Jain, A.; Persson, K. A.; Ceder, G.; Jacobsen, K. W. New Light-Harvesting Materials Using Accurate and Efficient Bandgap Calculations. *Adv. Energy Mater.* **2015**, *5*, 1400915.

(11) Yang, K.; Setyawan, W.; Wang, S.; Buongiorno Nardelli, M.; Curtarolo, S. A Search Model for Topological Insulators with High-Throughput Robustness Descriptors. *Nat. Mater.* **2012**, *11*, 614–619.

(12) Rondinelli, J. M.; Poeppelmeier, K. R.; Zunger, A. Research Update: Towards Designed Functionalities in Oxide-Based Electronic Materials. *APL Mater.* **2015**, *3*, 080702.

(13) Brgoch, J.; DenBaars, S. P.; Seshadri, R. Proxies From Ab Initio Calculations for Screening Efficient Ce^{3+} Phosphor Hosts. *J. Phys. Chem. C* **2013**, *117*, 17955–17959.

(14) Bocarsly, J. D.; Levin, E. E.; Garcia, C. A. C.; Schwennicke, K.; Wilson, S. D.; Seshadri, R. A Simple Computational Proxy for Screening Magnetocaloric Compounds. *Chem. Mater.* **2017**, *29*, 1613–1622.

(15) Shockley, W.; Queisser, H. J. Detailed Balance Limit of Efficiency of p–n Junction Solar Cells. *J. Appl. Phys.* **1961**, *32*, 510–519.

(16) Yu, L.; Zunger, A. Identification of Potential Photovoltaic Absorbers Based on First-Principles Spectroscopic Screening of Materials. *Phys. Rev. Lett.* **2012**, *108*, 068701.

(17) Yu, L.; Kokenyesi, R. S.; Keszler, D. A.; Zunger, A. Inverse Design of High Absorption Thin-Film Photovoltaic Materials. *Adv. Energy Mater.* **2013**, *3*, 43–48.

(18) Brandt, R. E.; Stevanović, V.; Ginley, D. S.; Buonassisi, T. Identifying Defect-Tolerant Semiconductors with High Minority-Carrier Lifetimes: Beyond Hybrid Lead Halide Perovskites. *MRS Commun.* **2015**, *5*, 265–275.

(19) Kuhar, K.; Pandey, M.; Thygesen, K. S.; Jacobsen, K. W. High-Throughput Computational Assessment of Previously Synthesized Semiconductors for Photovoltaic and Photoelectrochemical Devices. *ACS Energy Lett.* **2018**, *3*, 436–446.

(20) Brandt, R. E.; Poindexter, J. R.; Gorai, P.; Kurchin, R. C.; Hoye, R. L. Z.; Nienhaus, L.; Wilson, M. W. B.; Polizzotti, J. A.; Sereika, R.; Žaltauskas, R.; Lee, L. C.; MacManus-Driscoll, J. L.; Bawendi, M.; Stevanović, V.; Buonassisi, T. Searching for "Defect-Tolerant" Photovoltaic Materials: Combined Theoretical and Experimental Screening. *Chem. Mater.* **2017**, *29*, 4667–4674.

(21) Gritsenko, O.; van Leeuwen, R.; van Lenthe, E.; Baerends, E. J. Self-Consistent Approximation to the Kohn-Sham Exchange Potential. *Phys. Rev. A* **1995**, *51*, 1944–1954.

(22) Blank, B.; Kirchartz, T.; Lany, S.; Rau, U. Selection Metric for Photovoltaic Materials Screening Based on Detailed-Balance Analysis. *Phys. Rev. Applied* **2017**, *8*, 024032.

(23) Kirchartz, T.; Rau, U. Linking Structural Properties with Functionality in Solar Cell Materials – the Effective Mass and Effective Density of States. *Sustainable Energy Fuels* **2018**, *2*, 1550–1560.

(24) Hachmann, J.; Olivares-Amaya, R.; Jinich, A.; Appleton, A. L.; Blood-Forsythe, M. A.; Seress, L. R.; Román-Salgado, C.; Trepte, K.; Atahan-Evrenk, S.; Er, S.; Shrestha, S.; Mondal, R.; Sokolov, A.; Bao, Z.; Aspuru-Guzik, A. Lead candidates for high-performance organic photovoltaics from high-throughput quantum

chemistry – the Harvard Clean Energy Project. *Energy Environ. Sci.* **2014**, *7*, 698–704.

(25) Linghu, J.; Yang, T.; Luo, Y.; Yang, M.; Zhou, J.; Shen, L.; Feng, Y. P. High-Throughput Computational Screening of Vertical 2D van der Waals Heterostructures for High-efficiency Excitonic Solar Cells. *ACS Appl. Mater. Interfaces* **2018**, *10*, 32142–32150.

(26) Zhao, X.-G.; Yang, J.-H.; Fu, Y.; Yang, D.; Xu, Q.; Yu, L.; Wei, S.-H.; Zhang, L. Design of Lead-Free Inorganic Halide Perovskites for Solar Cells via Cation-Transmutation. *J. Am. Chem. Soc.* **2017**, *139*, 2630–2638.

(27) Huck, P.; Jain, A.; Gunter, D.; Winston, D.; Persson, K. A Community Contribution Framework for Sharing Materials Data with Materials Project. 2015 IEEE 11th International Conference on e-Science. 2015.

(28) Huck, P.; Gunter, D.; Cholia, S.; Winston, D.; N'Diaye, A. T.; Persson, K. User applications driven by the community contribution framework MPContribs in the Materials Project. *Concurr. Comp.-Pract. E.* **2015**, *28*, 1982–1993.

(29) Ricci, F.; Chen, W.; Aydemir, U.; Snyder, G. J.; Rignanese, G.-M.; Jain, A.; Hautier, G. An Ab Initio Electronic Transport Database for Inorganic Materials. *Sci. Data* **2017**, *4*, 170085.

(30) Gajdoš, M.; Hummer, K.; Kresse, G.; Furthmüller, J.; Bechstedt, F. Linear Optical Properties in the Projector-Augmented Wave Methodology. *Phys. Rev. B* **2006**, *73*, 1–9.

(31) Chan, M. K. Y.; Ceder, G. Efficient Band Gap Prediction for Solids. *Phys. Rev. Lett.* **2010**, *105*, 196403.

(32) Setyawan, W.; Curtarolo, S. High-Throughput Electronic Band Structure Calculations: Challenges and Tools. *Comput. Mater. Sci.* **2010**, *49*, 299–312.

(33) Kittel, C. *Introduction to Solid State Physics*, 6th ed.; John Wiley: New York, 1986.

(34) Barber, H. Effective Mass and Intrinsic Concentration in Silicon. *Solid-State Electron.* **1967**, *10*, 1039–1051.

(35) Raymond, A.; Robert, J. L.; Bernard, C. The Electron Effective Mass in Heavily Doped GaAs. *J. Phys. C Sol. State Phys.* **1979**, *12*, 2289.

(36) Stormer, H. L.; Schlesinger, Z.; Chang, A.; Tsui, D. C.; Gossard, A. C.; Wiegmann, W. Energy Structure and Quantized Hall Effect of Two-Dimensional Holes. *Phys. Rev. Lett.* **1983**, *51*, 126–129.

(37) Zhou, Y.; Leng, M.; Xia, Z.; Zhong, J.; Song, H.; Liu, X.; Yang, B.; Zhang, J.; Chen, J.; Zhou, K.; Han, J.; Cheng, Y.; Tang, J. Solution-Processed Antimony Selenide Heterojunction Solar Cells. *Adv. Energy Mater.* **2014**, *4*, 1301846.

(38) Zhou, Y.; Wang, L.; Chen, S.; Qin, S.; Liu, X.; Chen, J.; Xue, D.-J.; Luo, M.; Cao, Y.; Cheng, Y.; Sargent, E. H.; Tang, J. Thin-Film Sb_2Se_3 Photovoltaics with Oriented One-Dimensional Ribbons and Benign Grain Boundaries. *Nat. Photonics* **2015**, *9*, 409–415.

(39) Chen, C.; Wang, L.; Gao, L.; Nam, D.; Li, D.; Li, K.; Zhao, Y.; Ge, C.; Cheong, H.; Liu, H.; Song, H.; Tang, J. 6.5% Certified Efficiency Sb_2Se_3 Solar Cells Using PbS Colloidal Quantum Dot Film as Hole-Transporting Layer. *ACS Energy Lett.* **2017**, *2*, 2125–2132.

(40) Ford, G. M.; Guo, Q.; Agrawal, R.; Hillhouse, H. W. Earth Abundant Element $Cu_2Zn(Sn_{1-x}Ge_x)S_4$ Nanocrystals for Tunable Band Gap Solar Cells: 6.8% Efficient Device Fabrication. *Chem. Mater.* **2011**, *23*, 2626–2629.

(41) Rahayu, S. U.; Chou, C.-L.; Suriyawong, N.; Aragaw, B. A.; Shi, J.-B.; Lee, M.-W. Sodium Antimony Sulfide ($NaSbS_2$): Turning an Unexpected Impurity into a Promising, Environmentally Friendly Novel Solar Absorber Material. *APL Mater.* **2016**, *4*, 116103.

(42) Sun, J.; Singh, D. J. Electronic Properties, Screening, and Efficient Carrier Transport in $NaSbS_2$. *Phys. Rev. Applied* **2017**, *7*, 024015.

(43) Yin, Y.; Huang, Y.; Wu, Y.; Chen, G.; Yin, W.-J.; Wei, S.-H.; Gong, X. Exploring Emerging Photovoltaic Materials Beyond Perovskite: The Case of Skutterudite. *Chem. Mater.* **2017**, *29*, 9429–9435.

(44) Chung, I.; Lee, B.; He, J.; Chang, R. P. H.; Kanatzidis, M. G. All-Solid-State Dye-Sensitized Solar Cells with High Efficiency. *Nature* **2012**, *485*, 486–489.

(45) Chung, I.; Song, J.-H.; Im, J.; Androulakis, J.; Malliakas, C. D.; Li, H.; Freeman, A. J.; Kenney, J. T.; Kanatzidis, M. G. $CsSnI_3$: Semiconductor or Metal? High Electrical Conductivity and Strong Near-Infrared Photoluminescence from a Single Material. High Hole Mobility and Phase-Transitions. *J. Am. Chem. Soc.* **2012**, *134*, 8579–8587.

(46) Xu, P.; Chen, S.; Xiang, H.-J.; Gong, X.-G.; Wei, S.-H. Influence of Defects and Synthesis Conditions on the Photovoltaic Performance of Perovskite Semiconductor $CsSnI_3$. *Chem. Mater.* **2014**, *26*, 6068–6072.

(47) Kulbak, M.; Cahen, D.; Hodes, G. How Important is the Organic Part of Lead Halide Perovskite Photovoltaic Cells? Efficient $CsPbBr_3$ Cells. *J. Phys. Chem. Lett.* **2015**, *6*, 2452–2456.

(48) Lahourcade, L.; Coronel, N. C.; Delaney, K. T.; Shukla, S. K.; Spaldin, N. A.; Atwater, H. A. Structural and Optoelectronic Characterization of RF Sputtered $ZnSnN_2$. *Adv. Mater.* **2013**, *25*, 2562–2566.

(49) Martinez, A. D.; Warren, E. L.; Gorai, P.; Borup, K. A.; Kuciauskas, D.; Dippo, P. C.; Ortiz, B. R.; Macaluso, R. T.; Nguyen, S. D.; Greenaway, A. L.; Boettcher, S. W.; Norman, A. G.; Stevanovi, V.; Toberer, E. S.; Tamboli, A. C. Solar Energy Conversion Properties and Defect Physics of $ZnSiP_2$. *Energy Environ. Sci.* **2016**, *9*, 1031–1041.

(50) Sun, Y.-Y.; Agiorgousis, M. L.; Zhang, P.; Zhang, S. Chalcogenide Perovskites for Photovoltaics. *Nano Lett.* **2015**, *15*, 581–585.

(51) Savory, C. N.; Ganose, A. M.; Scanlon, D. O. Exploring the PbS–Bi_2S_3 Series for Next Generation Energy Conversion Materials. *Chem. Mater.* **2017**, *29*, 5156–5167.

(52) Ganose, A. M.; Butler, K. T.; Walsh, A.; Scanlon, D. O. Relativistic Electronic Structure and Band Alignment of BiSI and BiSeI: Candidate Photovoltaic Materials. *J. Mater. Chem. A* **2016**, *4*, 2060–2068.

(53) Shi, H.; Ming, W.; Du, M.-H. Bismuth Chalcohalides and Oxyhalides as Optoelectronic Materials. *Phys. Rev. B* **2016**, *93*, 104108.

(54) Kuku, T. A.; Fakolujo, O. A. Photovoltaic Characteristics of Thin Films of Cu_2SnS_3. *Sol. Energy Mater. Sol. Cells* **1987**, *16*, 199–204.

(55) Pogue, E. A.; Paris, M.; Sutrisno, A.; Lafond, A.; Johnson, N.; Shoemaker, D. P.; Rockett, A. A. Identifying Short-Range Disorder in Crystalline Bulk Cu_2SnS_3 Phases: A Solid-State Nuclear Magnetic Resonance Spectroscopic Investigation. *Chem. Mater.* **2018**, *30*, 6624–6635.

(56) Debbichi, L.; Lee, S.; Cho, H.; Rappe, A. M.; Hong, K.-H.; Jang, M. S.; Kim, H. Mixed Valence Perovskite $Cs_2Au_2I_6$: A Potential Material for Thin-Film Pb-Free Photovoltaic Cells with Ultrahigh Efficiency. *Adv. Mater.* **2018**, *30*, 1707001.

(57) Ramakrishna Reddy, K. T.; Koteswara Reddy, N.; Miles, R. W. Photovoltaic Properties of SnS Based Solar Cells. *Sol. Energy Mater. Sol. Cells* **2006**, *90*, 3041 – 3046.

(58) Dufton, J. T. R.; Walsh, A.; Panchmatia, P. M.; Peter, L. M.; Colombara, D.; Islam, M. S. Structural and Electronic Properties of $CuSbS_2$ and $CuBiS_2$: Potential Absorber Materials for Thin-Film Solar Cells. *Phys. Chem. Chem. Phys.* **2012**, *14*, 7229–7233.

(59) Heo, J.; Yu, L.; Altschul, E.; Waters, B. E.; Wager, J. F.; Zunger, A.; Keszler, D. A. $CuTaS_3$: Intermetal d–d Transitions Enable High Solar Absorption. *Chem. Mater.* **2017**, *29*, 2594–2598.

(60) Birkett, M.; Savory, C. N.; Fioretti, A. N.; Thompson, P.; Muryn, C. A.; Weerakkody, A. D.; Mitrovic, I. Z.; Hall, S.; Treharne, R.; Dhanak, V. R.; Scanlon, D. O.; Zakutayev, A.; Veal, T. D. Atypically Small Temperature-Dependence of the Direct Band Gap in the Metastable Semiconductor Copper Nitride Cu_3N. *Phys. Rev. B* **2017**, *95*, 115201.

(61) Volk, K.; Schäfer, H. Die Kristallstruktur von β-$NaSbS_2$. *Z. Naturforsch. B Chem. Sci.* **1978**, *33*, 827–828.

(62) Olivier-Fourcade, J.; Philippot, E.; Maurin, M. Structure des Composés $NaSbS_2\alpha$ et $NaSbS_2\beta$. Etude de L'Influence de la Paire Electronique E de L'Antimonine III dans la Transition $NaSbS_2\alpha \rightarrow NaSbS_2\beta$. *Z. Anorg. Allg. Chem.* **1978**, *446*, 159–168.

(63) Cenzual, K.; Gelato, L. M.; Penzo, M.; Parthé, E. Inorganic Structure Types with Revised Space Groups. I. *Acta Crystallogr. B* **1991**, *47*, 433–439.

(64) Glemser, O.; Filcek, M. Über Alkalithiowismutate(III). *Z. Anorg. Allg. Chem.* **1955**, *279*, 321–323.

(65) Gattow, G.; Zemann, J. Beitrag zur Kristallchemie komplexer Wismutchalkogenverbindungen. *Z. Anorg. Allg. Chem.* **1955**, *279*, 324–327.

(66) Gabrelian, B. V.; Lavrentyev, A. A.; Nikiforov, I. Y. To the Explanation of the "White" Line in the X-Ray K-Absorption Spectrum of Sulfur in $NaBiS_2$. *Bull. Russ. Acad. Sci.: Phys.* **2009**, *73*, 1001–1003.

(67) Boon, J. W. The Crystal Structure of $NaBiS_2$ and $KBiS_2$. *Recl. Trav. Chim. Pays-Bas* **2010**, *63*, 32–34.

(68) Deibele, S.; Jansen, M. Bismuth in Ag_2BiO_3: Tetravalent or Internally Disproportionated? *J. Solid State Chem.* **1999**, *147*, 117–121.

(69) Oberndorfer, C. P.; Dinnebier, R. E.; Ibberson, R. M.; Jansen, M. Charge Ordering in Ag_2BiO_3. *Solid State Sci.* **2006**, *8*, 267–276.

(70) Brgoch, J.; Lehner, A. J.; Chabinyc, M.; Seshadri, R. Ab Initio Calculations of Band Gaps and Absolute Band Positions of Polymorphs of $RbPbI_3$ and $CsPbI_3$: Implications for Main-Group Halide Perovskite Photovoltaics. *J. Phys. Chem. C* **2014**, *118*, 27721–27727.

(71) Fabini, D. H.; Labram, J. G.; Lehner, A. J.; Bechtel, J. S.; Evans, H. A.; Van der Ven, A.; Wudl, F.; Chabinyc, M. L.; Seshadri, R. Main-Group Halide Semiconductors Derived from Perovskite: Distinguishing Chemical, Structural, and Electronic Aspects. *Inorg. Chem.* **2016**, *56*, 11–25.

(72) Horiuchi, H.; Wuensch, B. J. Lindströmite, $Cu_3Pb_3Bi_7S_{15}$: Its Space Group and Ordering Scheme for Metal Atoms in the Crystal Structure. *Can. Mineral.* **1977**, *15*, 527–535.

(73) Topa, D.; Makovicky, E.; Balić-Žunić, T. The Structural Role of Excess Cu and Pb in Gladite and Krupkaite Based on New Refinements of their Structure. *Can. Mineral.* **2002**, *40*, 1147.

(74) Topa, D.; Petříček, V.; Dušek, M.; Makovicky, E.; Balić-Žunić, T. Simultaneous Refinement of Two Components of an Exsolution Intergrowth: Crystal Structures of the Lindströmite–Krupkaite Pair. *Can. Mineral.* **2008**, *46*, 525.

(75) Ohmasa, M.; Nowacki, W. A Redetermination of the Crystal Structure of Aikinite $[\mathrm{BiS_2|S|Cu^{IV}Pb^{VII}}]$. *Z. Kristallogr.* **1970**, *132*, 71–86.

(76) Vogel, R.; Hoyer, P.; Weller, H. Quantum-Sized PbS, CdS, Ag_2S, Sb_2S_3, and Bi_2S_3 Particles as Sensitizers for Various Nanoporous Wide-Bandgap Semiconductors. *J. Phys. Chem.* **1994**, *98*, 3183–3188.

(77) Rath, A. K.; Bernechea, M.; Martinez, L.; Konstantatos, G. Solution-Processed Heterojunction Solar Cells Based on p-Type PbS Quantum Dots and n-Type Bi_2S_3 Nanocrystals. *Adv. Mater.* **2011**, *23*, 3712–3717.

(78) Semonin, O. E.; Luther, J. M.; Choi, S.; Chen, H.-Y.; Gao, J.; Nozik, A. J.; Beard, M. C. Peak External Photocurrent Quantum Efficiency Exceeding 100% via MEG in a Quantum Dot Solar Cell. *Science* **2011**, *334*, 1530–1533.

(79) Ganose, A. M.; Matsumoto, S.; Buckeridge, J.; Scanlon, D. O. Defect Engineering of Earth-Abundant Solar Absorbers BiSI and BiSeI. *Chem. Mater.* **2018**, *30*, 3827–3835.

(80) Lehner, A. J.; Wang, H.; Fabini, D. H.; Liman, C. D.; Hébert, C.-A.; Perry, E. E.; Wang, M.; Bazan, G. C.; Chabinyc, M. L.; Seshadri, R. Electronic Structure and Photovoltaic Application of BiI_3. *Appl. Phys. Lett.* **2015**, *107*, 131109.

(81) Lehner, A. J.; Fabini, D. H.; Evans, H. A.; Hébert, C.-A.; Smock, S. R.; Hu, J.; Wang, H.; Zwanziger, J. W.; Chabinyc, M. L.; Seshadri, R. Crystal and Electronic Structures of Complex Bismuth Iodides $A_3Bi_2I_9$ (A = K, Rb, Cs) Related to Perovskite: Aiding the Rational Design of Photovoltaics. *Chem. Mater.* **2015**, *27*, 7137–7148.

(82) Bera, T.; Song, J.-H.; Freeman, A.; Jang, J.; Ketterson, J.; Kanatzidis, M. Soluble Direct-Band-Gap Semiconductors $LiAsS_2$ and $NaAsS_2$: Large Electronic Structure Effects from Weak As···S Interactions and Strong Nonlinear Optical Response. *Angew. Chem. Int. Ed.* **2008**, *47*, 7828–7832.

(83) Rangel, T.; Fregoso, B. M.; Mendoza, B. S.; Morimoto, T.; Moore, J. E.; Neaton, J. B. Large Bulk Photovoltaic Effect and Spontaneous Polarization of Single-Layer Monochalcogenides. *Phys. Rev. Lett.* **2017**, *119*, 067402.

(84) Glass, A. M.; von der Linde, D.; Negran, T. J. High-Voltage Bulk Photovoltaic Effect and the Photorefractive Process in $LiNbO_3$. *Appl. Phys. Lett.* **1974**, *25*, 233–235.

(85) Yang, S. Y.; Seidel, J.; Byrnes, S. J.; Shafer, P.; Yang, C.-H.; Rossell, M. D.; Yu, P.; Chu, Y.-H.; Scott, J. F.; Ager III, J. W.; Martin, L. W.; Ramesh, R. Above-Bandgap Voltages from Ferroelectric Photovoltaic Devices. *Nat. Nanotechnol.* **2010**, *5*, 143–147.

(86) Bronger, W.; Schils, H. $K_2Ag_4Se_3$, Darstellung und Kristallstruktur. *J. Less Common Met.* **1982**, *83*, 287–291.

(87) Huang, F. Q.; Ibers, J. A. Syntheses, Structures, and Theoretical Study of LaCuSTe and SmCuSTe. *Inorg. Chem.* **1999**, *38*, 5978–5983.

(88) Partik, M.; Kringe, C.; Lutz, H. D. X-Ray Structure Determination of Pseudomerohedrally Twinned $CoGe_{1.5}S_{1.5}$ and $CoGe_{1.5}Se_{1.5}$, Absorption Correction. *Z. Krist.* **1996**, *211*, 304–312.

(89) Korenstein, R.; Soled, S.; Wold, A.; Collin, G. Preparation and Characterization of the Skutterudite-Related Phases $CoGe_{1.5}S_{1.5}$ and $CoGe_{1.5}Se_{1.5}$. *Inorg. Chem.* **1977**, *16*, 2344–2346.

(90) Laufek, F.; Navrátil, J.; Plášil, J.; Plecháček, T.; Drašar, C. Synthesis, Crystal Structure and Transport Properties of Skutterudite-Related $CoSn_{1.5}Se_{1.5}$. *J. Alloys Compd.* **2009**, *479*, 102 – 106.

(91) Laufek, F.; Návrátil, J.; Goliáš, V. Synthesis and Rietveld Refinement of Skutterudite-Related Phase $CoSn_{1.5}Te_{1.5}$. *Powder Diffr.* **2008**, *23*, 15–19.

(92) Velden, A.; Jansen, M. Zur Kenntnis der Inversen Perowskite M_3TO (M = Ca, Sr, Yb; T = Si, Ge, Sn, Pb). *Z. Anorg. Allg. Chem.* **2004**, *630*, 234–238.

(93) Chern, M. Y.; Vennos, D.; Disalvo, F. Synthesis, Structure, and Properties of Anti-Perovskite Nitrides Ca_3MN, M = P, As, Sb, Bi, Ge, Sn, and Pb. *J. Solid State Chem.* **1992**, *96*, 415 – 425.

(94) Hadenfeldt, C.; Terschüren, H.-U. Darstellung und Kristallstruktur der Strontium- und Bariumpnictidoxide Sr_4P_2O, Sr_4As_2O, Ba_4P_2O und Ba_4As_2O. *Z. Anorg. Allg. Chem.* **1991**, *597*, 69–78.

(95) Röhr, C.; George, R. Crystal Structure of Barium Antimonide Oxide, Ba_4Sb_2O. *Z. Kristallogr.* **1996**, *211*, 478.

(96) Carrillo-Cabrera, W.; Somer, M.; Peters, E.-M.; Peters, K.; von Schnering, H. G. Crystal Structure of Sodium Barium Phosphide, NaBaP. *Z. Krist.* **1996**, *211*, 191.

(97) Okamoto, Y.; Inohara, T.; Yamakage, A.; Yamakawa, Y.; Takenaka, K. Low Carrier Density Metal Realized in Candidate Line-Node Dirac Semimetals CaAgP and CaAgAs. *J. Phys. Soc. Jpn.* **2016**, *85*, 123701.

(98) Dong, Y.; DiSalvo, F. J. Synthesis and Single Crystal Structures of Ternary Phosphides Li_4SrP_2 and AAeP (A = Li, Na; Ae = Sr, Ba). *J. Solid State Chem.* **2007**, *180*, 432 – 439.

(99) Mewis, A. ABX-Verbindungen mit Ni_2In-Struktur: Darstellung und Struktur der Verbindungen CaCuP(As), SrCuP(As), SrAgP(As) und EuCuAs / ABX Compounds with the Structure Ni_2In: Preparation and Crystal Structure of CaCuP(As), SrCuP(As), SrAgP(As), and EuCuAs. *Z. Naturforsch. B* **1978**, *33*, 983–986.

(100) Savelsberg, G.; Schäfer, H. Ternäre Pnictide und Chalkogenide von Alkalimetallen und IB-bzw. IIB-Elementen / On Ternary Pnictides and Chalkogenides of Alkaline Metals and IB-Resp. IIB-Elements. *Z. Naturforsch. B* **1978**, *33*, 370–373.

(101) Albering, J.; Ebel, T.; Jeitschko, W. Präparation, Kristallstruktur und Magnetische Eigenschaften der Verbindungen LiAX (A = Ca, Sr, Ba, Eu, Yb; X = P, As, Sb, Bi). *Z. Kristallogr.* **1997**, *12*, 242.

(102) Klüfers, P.; Neumann, H.; Mewis, A.; Schuster, H.-U. AB_2X_2-Verbindungen im $CaAl_2Si_2$-Typ, VIII [1]. *Z. Naturforsch. B Chem. Sci.* **1980**, *35*, 1317–1318.

(103) Klüfers, P.; Mewis, A. AB_2X_2-Verbindungen mit $CaAl_2Si_2$-Struktur. *Z. Krist.* **1984**, *169*, 135–147.

(104) Nowotny, H.; Holub, F. Untersuchungen an Metallischen Systemen mit Flußspatphasen. *Monatsh. Chem.* **1960**, *91*, 877–887.

(105) Pauly, H.; Weiss, A.; Witte, H. The Crystal Structure of the Ternary Intermetallic Phases Li_2EX: E = Cu, Ag, Au, and X = Al, Ga, In, Tl, Si, Ge, Sn, Pb, Sb, and Bi. *Z. Metallkd.* **1968**, *59*, 47–58.

(106) Eisenmann, B.; Schäfer, H. Zintl-Phasen mit Komplexen Anionen: $Sr_3Si_2As_4$ und $Sr_3Ge_2As_4$. *Angew. Chem.* **1980**, *92*, 480–481.

(107) Cordier, G.; Ochmann, H. Crystal Structure of Disodium Phyllo-Triarsenidodialuminate, $Na_2Al_2As_3$. *Z. Kristallogr.* **1991**, *197*, 283–284.

(108) Hullmann, J.; Xia, S.; Bobev, S. $Sr_{11}InSb_9$ Grown from Molten In. *Acta Cryst. E* **2007**, *63*, i178.

(109) Kelzenberg, M. D.; Boettcher, S. W.; Petykiewicz, J. A.; Turner-Evans, D. B.; Putnam, M. C.; Warren, E. L.; Spurgeon, J. M.; Briggs, R. M.; Lewis, N. S.; Atwater, H. A. Enhanced Absorption and Carrier Collection in Si Wire Arrays for Photovoltaic Applications. *Nat. Mater.* **2010**, *9*, 239–244.

(110) Liang, F.; Kang, L.; Lin, Z.; Wu, Y.; Chen, C. Analysis and Prediction of Mid-IR Nonlinear Optical Metal Sulfides with Diamond-Like Structures. *Coord. Chem. Rev.* **2017**, *333*, 57–70.

(111) Brehm, J. A.; Young, S. M.; Zheng, F.; Rappe, A. M. First-Principles Calculation of the Bulk Photovoltaic Effect in the Polar Compounds $LiAsS_2$, $LiAsSe_2$, and $NaAsSe_2$. *J. Chem. Phys.* **2014**, *141*, 204704.

(112) Brehm, J. A. Predicted Bulk Photovoltaic Effect in Hydrogenated Zintl Compounds. *J. Mater. Chem. C* **2018**, *6*, 1470–1475.

(113) Ishizaka, K. et al. Giant Rashba-Type Spin Splitting in Bulk BiTeI. *Nat. Mater.* **2011**, *10*, 521–526.

(114) Kim, M.; Im, J.; Freeman, A. J.; Ihm, J.; Jin, H. Switchable $S = 1/2$ and $J = 1/2$ Rashba Bands in Ferroelectric Halide Perovskites. *Proc. Natl. Acad. Sci. USA* **2014**, *111*, 6900–6904.

(115) Zheng, F.; Tan, L. Z.; Liu, S.; Rappe, A. M. Rashba Spin–Orbit Coupling Enhanced Carrier Lifetime in $CH_3NH_3PbI_3$. *Nano Lett.* **2015**, *15*, 7794–7800.

(116) Azarhoosh, P.; McKechnie, S.; Frost, J. M.; Walsh, A.; van Schilfgaarde, M. Research Update: Relativistic Origin of Slow Electron-Hole Recombination in Hybrid Halide Perovskite Solar Cells. *APL Mater.* **2016**, *4*, 091501.

(117) Frohna, K.; Deshpande, T.; Harter, J.; Peng, W.; Barker, B. A.; Neaton, J. B.; Louie, S. G.; Bakr, O. M.; Hsieh, D.; Bernardi, M. Inversion Symmetry and Bulk Rashba Effect in Methylammonium Lead Iodide Perovskite Single Crystals. *Nat. Commun.* **2018**, *9*, 1829.

(118) Zhang, X.; Shen, J.-X.; Van de Walle, C. G. Three-Dimensional Spin Texture in Hybrid Perovskites and Its Impact on Optical Transitions. *J. Phys. Chem. Lett.* **2018**, *9*, 2903–2908.

(119) Zhang, X.; Shen, J.-X.; Wang, W.; Van de Walle, C. G. First-Principles Analysis of Radiative Recombination in Lead-Halide Perovskites. *ACS Energy Lett.* **2018**, *3*, 2329–2334.

(120) Fabini, D. H.; Laurita, G.; Bechtel, J. S.; Stoumpos, C. C.; Evans, H. A.; Kontos, A. G.; Raptis, Y. S.; Falaras, P.; Van der Ven, A.; Kanatzidis, M. G.; Seshadri, R. Dynamic Stereochemical Activity of the Sn^{2+} Lone Pair in Perovskite $CsSnBr_3$. *J. Am. Chem. Soc.* **2016**, *138*, 11820–11832.

(121) Laurita, G.; Fabini, D. H.; Stoumpos, C. C.; Kanatzidis, M. G.; Seshadri, R. Chemical Tuning of Dynamic Cation Off-Centering in the Cubic Phases of Hybrid Tin and Lead Halide Perovskites. *Chem. Sci.* **2017**, *8*, 5628–5635.

(122) Yaffe, O.; Guo, Y.; Tan, L. Z.; Egger, D. A.; Hull, T.; Stoumpos, C. C.; Zheng, F.; Heinz, T. F.; Kronik, L.; Kanatzidis, M. G.; Owen, J. S.; Rappe, A. M.; Pimenta, M. A.; Brus, L. E. Local Polar Fluctuations in Lead Halide Perovskite Crystals. *Phys. Rev. Lett.* **2017**, *118*, 136001.

(123) Wu, X. et al. Light-Induced Picosecond Rotational Disordering of the Inorganic Sublattice in Hybrid Perovskites. *Sci. Adv.* **2017**, *3*, e1602388.

(124) Mizoguchi, H.; Eng, H. W.; Woodward, P. M. Probing the Electronic Structures of

Ternary Perovskite and Pyrochlore Oxides Containing Sn^{4+} or Sb^{5+}. *Inorg. Chem.* **2004**, *43*, 1667–1680.

(125) Krishnaswamy, K.; Himmetoglu, B.; Kang, Y.; Janotti, A.; Van de Walle, C. G. First-Principles Analysis of Electron Transport in $BaSnO_3$. *Phys. Rev. B* **2017**, *95*, 205202.

(126) Blatov, V. A.; Shevchenko, A. P.; Serenzhkin, V. N. Crystal Space Analysis by Means of Voronoi–Dirichlet Polyhedra. *Acta Crystallogr. A* **1995**, *51*, 909–916.

(127) Blatov, V. A. Search for Isotypism in Crystal Structures by Means of the Graph Theory. *Acta Crystallogr. A* **2000**, *56*, 178–188.

(128) Baburin, I.; Blatov, V.; Carlucci, L.; Ciani, G.; Proserpio, D. Interpenetrating Metal-Organic and Inorganic 3D Networks: A Computer-Aided Systematic Investigation. Part II [1]. Analysis of the Inorganic Crystal Structure Database (ICSD). *J. Solid State Chem.* **2005**, *178*, 2452–2474.

(129) O'Keeffe, M.; Yaghi, O. M. Deconstructing the Crystal Structures of Metal–Organic Frameworks and Related Materials into Their Underlying Nets. *Chem. Rev.* **2011**, *112*, 675–702.

(130) Ward, L.; Liu, R.; Krishna, A.; Hegde, V. I.; Agrawal, A.; Choudhary, A.; Wolverton, C. Including Crystal Structure Attributes in Machine Learning Models of Formation Energies via Voronoi Tessellations. *Phys. Rev. B* **2017**, *96*, 024104.

(131) Ok, K. M.; Halasyamani, P. S.; Casanova, D.; Llunell, M.; Alemany, P.; Alvarez, S. Distortions in Octahedrally Coordinated d^0 Transition Metal Oxides: A Continuous Symmetry Measures Approach. *Chem. Mater.* **2006**, *18*, 3176–3183.

(132) Gautier, R.; Zhang, X.; Hu, L.; Yu, L.; Lin, Y.; Sunde, T. O. L.; Chon, D.; Poeppelmeier, K. R.; Zunger, A. Prediction and Accelerated Laboratory Discovery of Previously Unknown 18-Electron ABX Compounds. *Nat. Chem.* **2015**, *7*, 308–316.

(133) Davies, D.; Butler, K.; Jackson, A.; Morris, A.; Frost, J.; Skelton, J.; Walsh, A. Computational Screening of all Stoichiometric Inorganic Materials. *Chem* **2016**, *1*, 617–627.

(134) Goyal, A.; Gorai, P.; Peng, H.; Lany, S.; Stevanović, V. A Computational Framework for Automation of Point Defect Calculations. *Comput. Mater. Sci.* **2017**, *130*, 1–9.

(135) Broberg, D.; Medasani, B.; Zimmermann, N. E.; Yu, G.; Canning, A.; Haranczyk, M.; Asta, M.; Hautier, G. PyCDT: A Python Toolkit for Modeling Point Defects in Semiconductors and Insulators. *Comput. Phys. Commun.* **2018**, *226*, 165–179.

(136) Du, M.-H.; Singh, D. J. Enhanced Born Charge and Proximity to Ferroelectricity in Thallium Halides. *Phys. Rev. B* **2010**, *81*, 144114.

(137) Siemons, W.; McGuire, M. A.; Cooper, V. R.; Biegalski, M. D.; Ivanov, I. N.; Jellison, G. E.; Boatner, L. A.; Sales, B. C.; Christen, H. M. Dielectric-Constant-Enhanced Hall Mobility in Complex Oxides. *Adv. Mater.* **2012**, *24*, 3965–3969.

(138) He, X.; Singh, D. J.; Boon-on, P.; Lee, M.-W.; Zhang, L. Dielectric Behavior as a Screen in Rational Searches for Electronic Materials: Metal Pnictide Sulfosalts. *J. Am. Chem. Soc.* **2018**, Advance Article.

(139) Persson, K. A.; Waldwick, B.; Lazic, P.; Ceder, G. Prediction of Solid-Aqueous Equilibria: Scheme to Combine First-Principles Calculations of Solids with Experimental Aqueous States. *Phys. Rev. B* **2012**, *85*, 235438.

(140) Sun, W.; Dacek, S. T.; Ong, S. P.; Hautier, G.; Jain, A.; Richards, W. D.; Gamst, A. C.; Persson, K. A.; Ceder, G. The Thermodynamic Scale of Inorganic Crystalline Metastability. *Sci. Adv.* **2016**, *2*.

(141) Ong, S. P.; Richards, W. D.; Jain, A.; Hautier, G.; Kocher, M.; Cholia, S.; Gunter, D.; Chevrier, V. L.; Persson, K. A.; Ceder, G. Python Materials Genomics (pymatgen):

A Robust, Open-Source Python Library for Materials Analysis. *Comput. Mater. Sci.* **2013**, *68*, 314–319.

(142) Bechtel, J. S.; Van der Ven, A. Octahedral Tilting Instabilities in Inorganic Halide Perovskites. *Phys. Rev. Materials* **2018**, *2*, 025401.

(143) Bechtel, J. S.; Van der Ven, A. First-Principles Thermodynamics Study of Phase Stability in Inorganic Halide Perovskite Solid Solutions. *Phys. Rev. Materials* **2018**, *2*, 045401.

(144) Kresse, G.; Hafner, J. Ab Initio Molecular Dynamics for Liquid Metals. *Phys. Rev. B* **1993**, *47*, 558–561.

(145) Kresse, G.; Hafner, J. Ab Initio Molecular-Dynamics Simulation of the Liquid-Metal-Amorphous-Semiconductor Transition in Germanium. *Phys. Rev. B* **1994**, *49*, 14251–14269.

(146) Kresse, G.; Furthmüller, J. Efficient Iterative Schemes for Ab Initio Total-Energy Calculations Using a Plane-Wave Basis Set. *Phys. Rev. B* **1996**, *54*, 11169–11186.

(147) Kresse, G.; Furthmüller, J. Efficiency of Ab-Initio Total Energy Calculations for Metals and Semiconductors Using a Plane-Wave Basis Set. *Comput. Mater. Sci.* **1996**, *6*, 15–50.

(148) Blöchl, P. E. Projector Augmented-Wave Method. *Phys. Rev. B* **1994**, *50*, 17953–17979.

(149) Kresse, G.; Joubert, D. From Ultrasoft Pseudopotentials to the Projector Augmented-Wave Method. *Phys. Rev. B* **1999**, *59*, 1758–1775.

(150) Perdew, J. P.; Burke, K.; Ernzerhof, M. Generalized Gradient Approximation Made Simple. *Phys. Rev. Lett.* **1996**, *77*, 3865–3868.

(151) Monkhorst, H. J.; Pack, J. D. Special Points for Brillouin-Zone Integrations. *Phys. Rev. B* **1976**, *13*, 5188–5192.

(152) Momma, K.; Izumi, F. VESTA3 for Three-Dimensional Visualization of Crystal, Volumetric and Morphology Data. *J. Appl. Crystallogr.* **2011**, *44*, 1272–1276.

Graphical TOC Entry

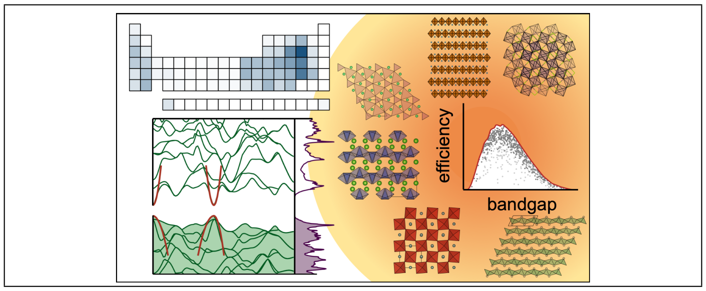

— Supporting Information —

Candidate Inorganic Photovoltaic Materials from Electronic Structure-Based Optical Absorption and Charge Transport Proxies

Douglas H. Fabini,[†,‡] Mitchell Koerner,[¶] and Ram Seshadri[*,†,§]

†Materials Department and Materials Research Laboratory
University of California, Santa Barbara, California 93106, United States
‡Current address: Max Planck Institute for Solid State Research
Heisenbergstraße 1, 70569 Stuttgart, Germany
¶Physics Program, College of Creative Studies
University of California, Santa Barbara, California 93106, United States
§Department of Chemistry and Biochemistry
University of California, Santa Barbara, California 93106, United States

E-mail: seshadri@mrl.ucsb.edu

Variable definitions, manipulation of spectral quantities

Irradiance: E_e (e.g. W m^{-2}) (subscripted "e" refers to radiometric, rather than photometric, quantities throughout)

Spectral irradiance: $E_{e,\lambda}$ (e.g. W m^{-2} nm^{-1}) or $E_{e,h\nu}$ (e.g. W m^{-2} eV^{-1})

Spectral radiance: $L_{e,\Omega,\lambda}$ (e.g. W sr^{-1} m^{-2} nm^{-1}) or $L_{e,\Omega,h\nu}$ (e.g. W sr^{-1} m^{-2} eV^{-1})

Interconversion of spectral irradiance between wavelength units and photon energy units:

$$E_{e,h\nu} = \frac{\partial E_e}{\partial(h\nu)} = \frac{\partial E_e}{\partial\lambda}\left(\frac{\partial\lambda}{\partial(h\nu)}\right) = E_{e,\lambda}\left(\frac{\partial\lambda}{\partial(h\nu)}\right) \tag{1}$$

using

$$\lambda = \frac{c}{\nu} \quad \rightarrow \quad \frac{\partial\lambda}{\partial(h\nu)} = -\frac{hc}{(h\nu)^2} \tag{2}$$

Blackbody spectrum (Planck's law):

$$L_{e,\Omega,\lambda}(\lambda,T) = \frac{2hc^2}{\lambda^5}\frac{1}{e^{\frac{hc}{\lambda kT}}-1} \tag{3}$$

Equations implementing scissor operations

Scissor operations to use Δ-sol method[1] to correct bandgap and absorption spectrum:

$$\Delta = E_{\mathrm{g},\Delta\mathrm{sol}} - E_{\mathrm{g,KS}} \tag{4}$$

$$E_{\mathrm{g}} = E_{\mathrm{g,KS}} + \Delta = E_{\mathrm{g},\Delta\mathrm{sol}} \tag{5}$$

$$E_{\mathrm{g}}^{\mathrm{d}} = E_{\mathrm{g,KS}}^{\mathrm{d}} + \Delta \tag{6}$$

$$E_{\mathrm{g}}^{\mathrm{da}} = E_{\mathrm{g,KS}}^{\mathrm{da}} + \Delta \tag{7}$$

$$\alpha(h\nu) = \alpha_{\mathrm{KS}}(h\nu + \Delta) \tag{8}$$

where $E_{\mathrm{g,KS}}$, $E^{\mathrm{d}}_{\mathrm{g,KS}}$, $E^{\mathrm{da}}_{\mathrm{g,KS}}$, and $\alpha_{\mathrm{KS}}(h\nu)$ are the fundamental bandgap, smallest direct transition, smallest dipole-allowed direct transition, and absorption spectrum from Kohn-Sham eigenvalues, and $E_{\mathrm{g},\Delta\mathrm{sol}}$ is the bandgap from the Δ-sol method.

Equations implementing the SLME metric[2]

Photon absorptivity:

$$a(\lambda, L) = 1 - e^{-2\alpha(\lambda)L} \tag{9}$$

where $\alpha(\lambda)$ is the absorption coefficient and L is the absorber thickness.

Ideal diode solar cell $j - V$ characteristic:

$$j(V) = j_{sc} - j_0 \left(e^{\frac{q_0 V}{kT}} - 1 \right) \tag{10}$$

where j_{sc} and j_0 are the short-circuit current density and the reverse saturation current density, respectively, and q_0 is the electron charge.

Radiative recombination fraction under the SLME approximation:

$$f_r = e^{-\frac{E_g^{\mathrm{da}} - E_g}{kT}} \tag{11}$$

Short-circuit current density under the SLME approximation:

$$j_{sc}(L) = e \int_0^\infty a(h\nu, L) \frac{E^{\mathrm{sun}}_{e,h\nu}}{h\nu} d(h\nu) \tag{12}$$

where $E^{\mathrm{sun}}_{e,h\nu}$ is the spectral irradiance from the sun (measured, AM1.5G).

Reverse saturation current density under the SLME approximation:

$$j_0(L) = \frac{1}{f_r} q_0 \int_0^\infty a(h\nu, L) \frac{\Omega_{bg} L_{e,\Omega,h\nu}(h\nu, T)}{h\nu} d(h\nu) \tag{13}$$

where $\Omega_{bg} = \pi$ is the solid angle subtended by the background (bath) for a flat-plate solar cell and $L_{e,\Omega,h\nu}(h\nu, T)$ is the blackbody radiation from the background.

The Shockley–Queisser limit[3] can be recovered by setting $f_r = 1$ and setting the photon absorptivity to be:

$$a(\lambda, L) = \begin{cases} 1, & \text{if } \lambda < \frac{hc}{E_g}, \\ 0, & \text{otherwise.} \end{cases} \tag{14}$$

Calculation of optical properties from dielectric properties

The isotropic equivalent of the dielectric function, $\epsilon(h\nu)$ is taken to be one-third of the sum of the eigenvalues of the full, anisotropic tensor dielectric function, $\epsilon_{ij}(h\nu)$.

Complex refractive index:

$$N(h\nu) = \sqrt{\epsilon'(h\nu) + i\epsilon''(h\nu)} \tag{15}$$

Optical absorption coefficient:

$$\alpha(h\nu) = \frac{4\pi}{hc} h\nu \, \Im[N(h\nu)] \tag{16}$$

Details of effective mass fitting

"Line" effective masses are determined from the electronic band structures computed and stored in the Materials Project database[4] by fitting parabolic dispersions (Eqn. 17) from the band extrema along each direction present in the high-symmetry path through the Brillouin zone. A tolerance of 10 meV is used for determining band degeneracies at the band edges. As a simple proxy with no additional ab initio computation required, we then take the effective mass to be the arithmetic mean of the various line effective masses associated with each carrier type. This simplified approach is not strictly equivalent to a density-of-states effective mass, which would require a more rigorous treatment of carrier pocket degeneracies and point symmetries at the band edge wavevectors (an excellent discussion is given by Setyawan and coworkers).[5] Additionally, in the case where one or both band extrema occur away from Brillouin zone special points, additional ab initio calculations will always be needed to obtain the full effective mass tensor (consider Si, where the conduction band minimum occurs at an intermediate point on the $\overline{\Gamma\mathrm{X}}$ line, and no information about the dispersion in directions orthogonal to $\overline{\Gamma\mathrm{X}}$ is present in a band structure that is only computed along the standard high-symmetry path).

$$E(k) \approx E_0 \pm \frac{\hbar^2 (k - k_0)^2}{2m^*} \tag{17}$$

Ricci and coworkers have recently published a large database of ab initio transport properties, including the principle components of the p-type and n-type conductivity effective mass tensors for most insulators in the Materials Project database.[6] These values are reported for a carrier concentration of 10^{18} cm^{-3} and a temperature of 300 K. Comparison of the isotropic equivalent of the effective mass ellipsoids they report and those which we utilize based on line effective masses is given in Figure S1 below.

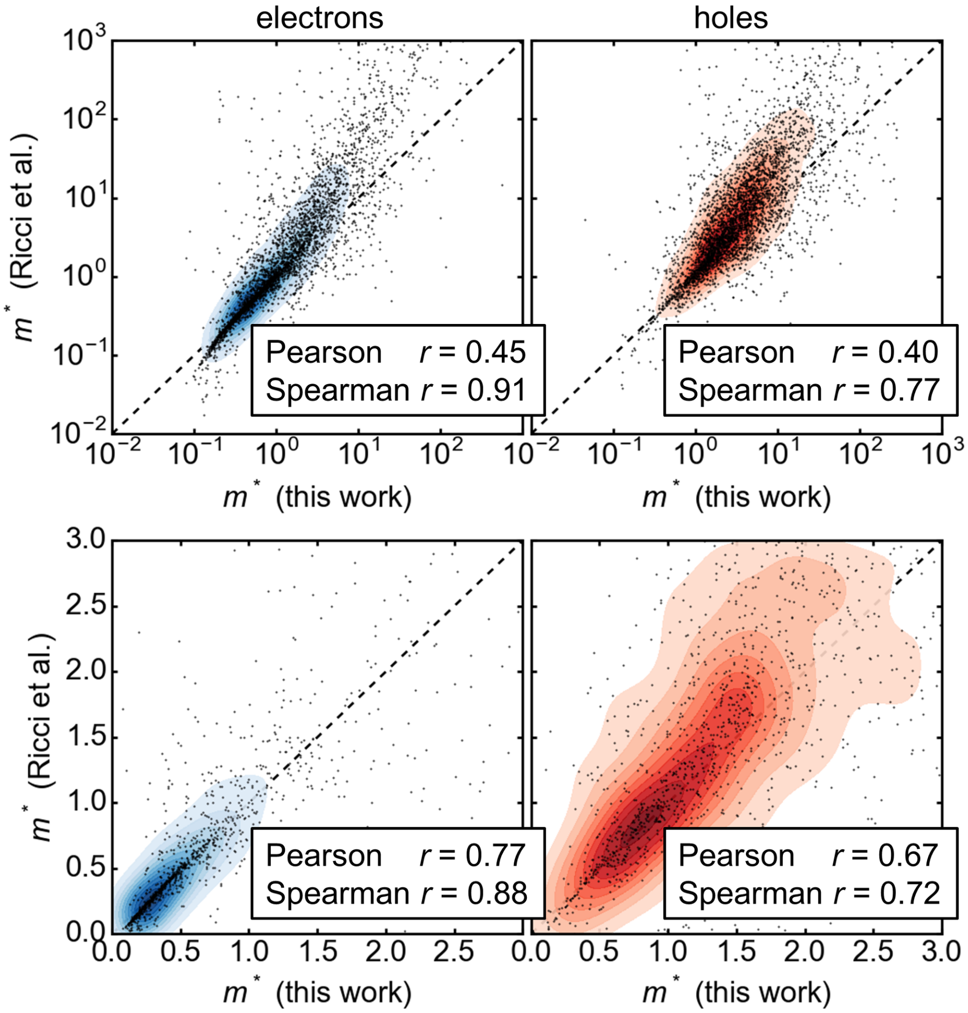

Figure S1: Comparison of effective masses reported here (methodology above) and those reported by Ricci and coworkers ($n = 10^{18}\,\mathrm{cm}^{-3}$, $T = 300\,\mathrm{K}$) based on BoltzTraP calculations[6] ($N \approx 3800$ phases). Blue and red shading indicate the 2-D distribution of the points (via kernel density estimation).

While these two quantities should not be exactly equivalent due to their different definitions, they should be strongly correlated and close in value. Indeed, the top panes of Figure S1 reveal zero-bias correspondence for intermediate effective masses, while our approach returns slightly higher (lower) values in the small (large) effective mass regime. The modest, positive Pearson correlation coefficients are highly skewed by disagreement for very large carrier masses (flat bands cause masses well beyond the upper limits of this plot), while the near-unity Spearman correlation coefficients reveal strong agreement of the qualitative ordering of the estimates from the two approaches. In the bottom panes, if we restrict this analysis only to the region of interest from 0 to

$3m_0$ (twice our screening threshold), the correlations are significantly stronger and have minimal bias.

Notably, our approach did not require additional ab initio calculations, only utilizing the existing calculated band structures from the Materials Project database. However, now that the more rigorous results of Ricci and coworkers are available for the case of heavy doping, future work should utilize these data as appropriate.[6]

Effect of Δ-sol bandgap corrections

The motivation, application, and more extensive validation of the Δ-sol method is discussed in detail in the original report by Chan and Ceder.[1] Sufficient practical details to reproduce our results are presented in the Methods section of the manuscript. Below we briefly present our own partial validation (Figure S2) and the effects of including spin-orbit coupling for compounds with 6s, 5d, and 6p ions.

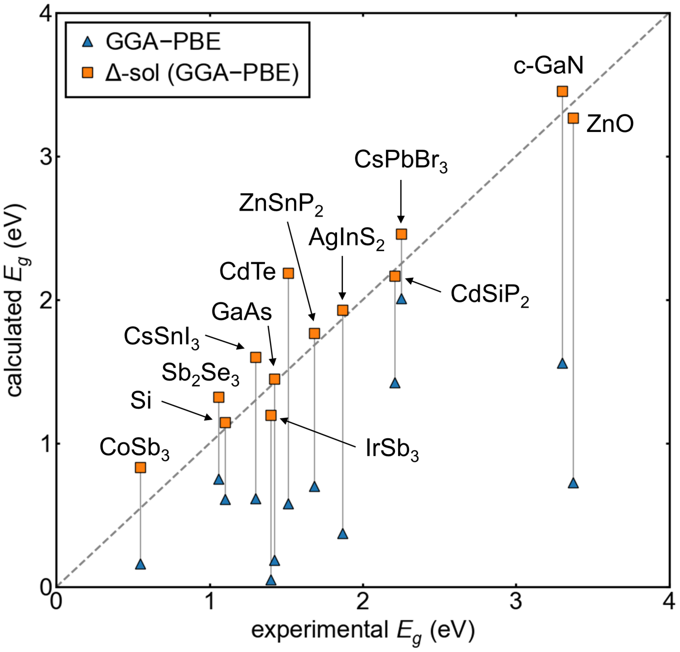

Figure S2: Computed bandgap ("uncorrected," and "corrected" via the Δ-sol method) versus experimental bandgap for several reference compounds. The GGA-PBE functional is used in both cases, but the uncorrected bandgap is based on the Kohn-Sham eigenvalues, while the corrected, Δ-sol bandgap is based on the difference between electron affinity and ionization energy. Spin-orbit coupling (SOC) is included in Δ-sol calculations for compounds with 6s, 5d, and 6p ions. More complete validation is given in the original report of the method.[1]

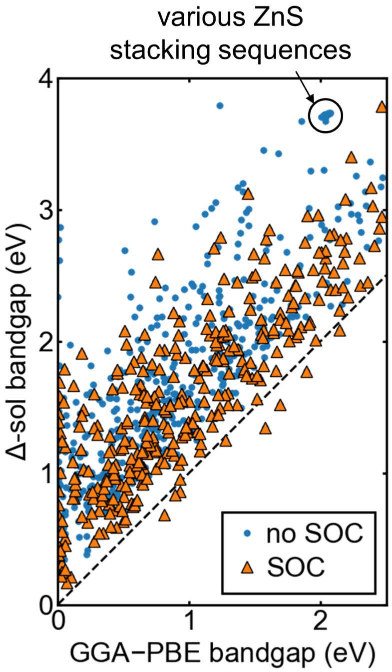

Figure S3: "Corrected" Δ-sol bandgap versus "uncorrected" bandgap for ≈800 phases passing the intermediate screens. The GGA-PBE functional is used in both cases, but the uncorrected bandgap is based on the Kohn-Sham eigenvalues, while the corrected, Δ-sol bandgap is based on the difference between electron affinity and ionization energy. Spin-orbit coupling (SOC) is included in Δ-sol calculations for compounds with $6s$, $5d$, and $6p$ ions, and is seen to partially or fully cancel the bandgap widening effect of the Δ-sol corrections (as for $CsPbBr_3$ in Figure S2 above).

Correlation between bandgap and effective masses

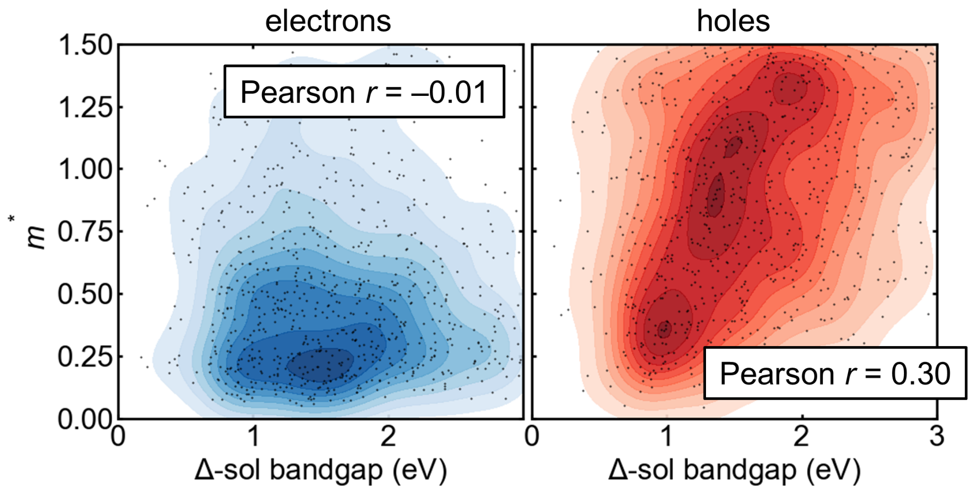

Figure S4: Scatter plots of effective mass versus bandgap for the ≈800 phases passing the intermediate screens. Pearson correlation coefficients reveal that electron mass is essentially uncorrelated with bandgap, while there is a modest tendency for narrower gap materials to exhibit lighter holes. A discussion of likely chemical origins of this behavior and its consequences for SLME is given in the main text. Blue and red shading indicate the 2-D distribution of the points (via kernel density estimation).

Effect of gap nature on efficiency

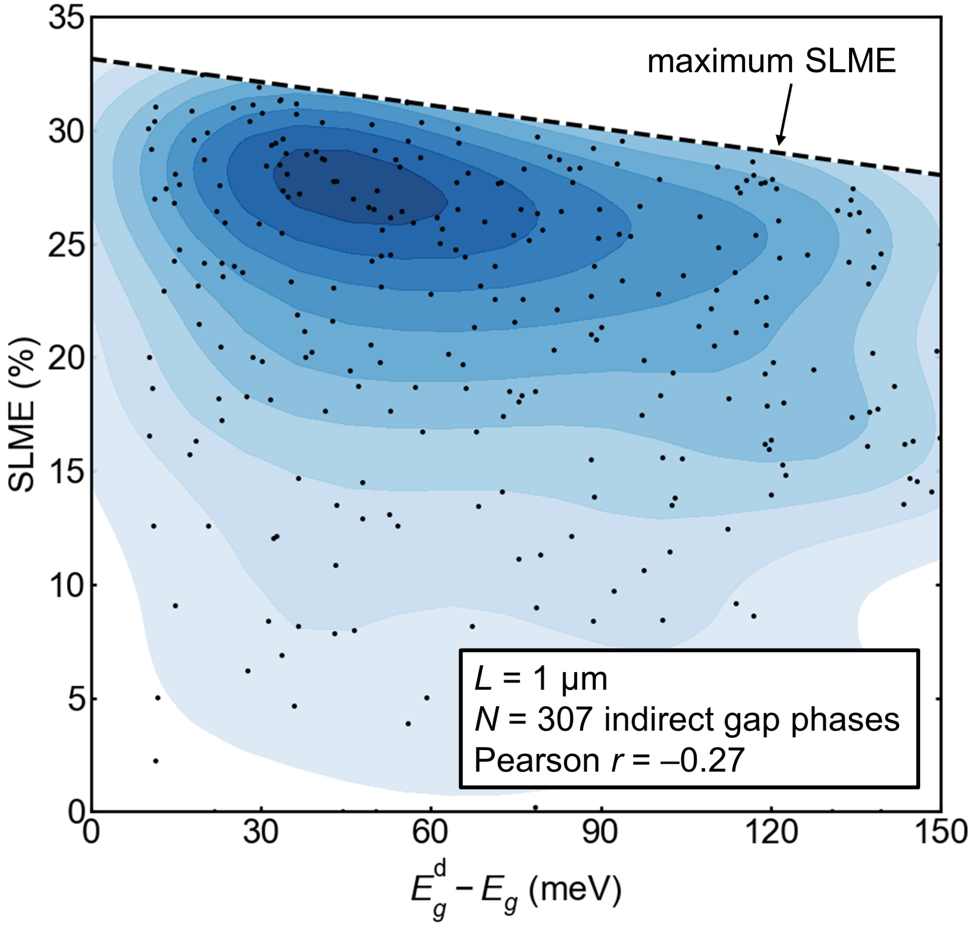

Figure S5: Scatter plot of SLME versus difference between direct and fundamental bandgaps for the ≈300 indirect bandgap phases passing the intermediate screens. Blue shading indicates the 2-D distribution of the points (via kernel density estimation).

Example of dipole-allowed and -forbidden bandgaps

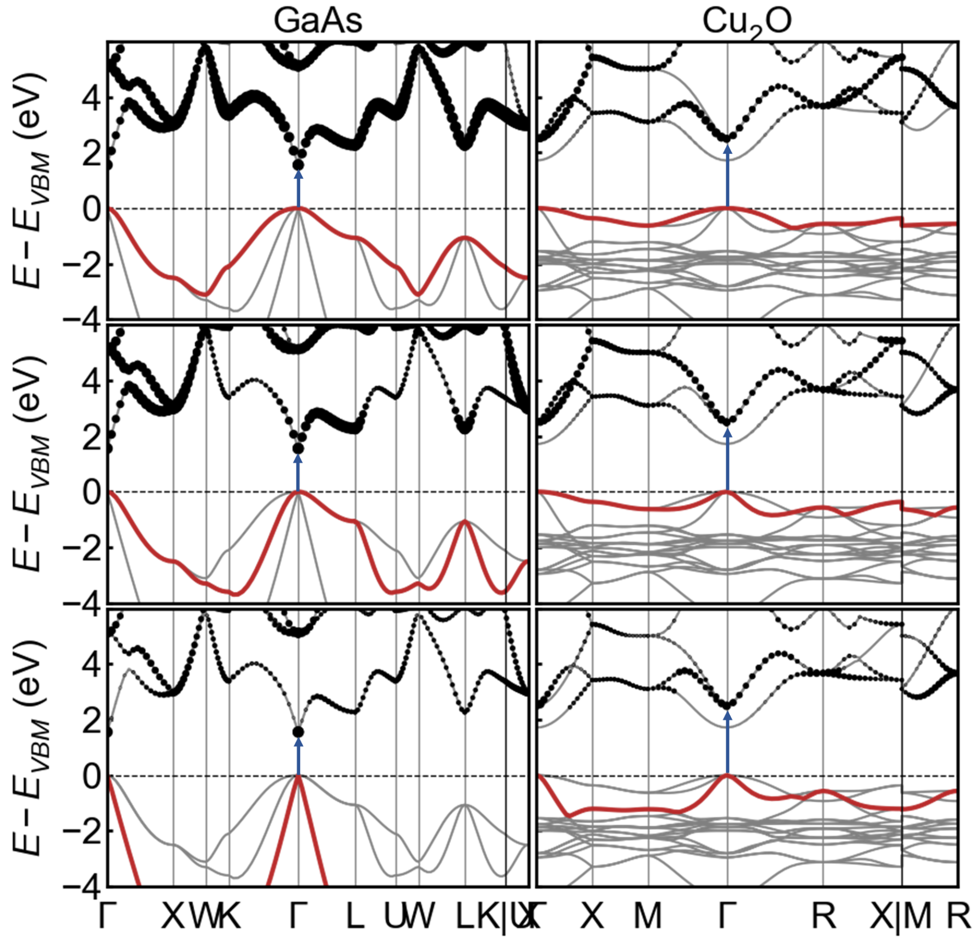

Figure S6: Electronic band structures for GaAs (left) and Cu_2O (right) with the square of the transition dipole matrix elements from each of the three highest occupied bands overlaid. The initial state (occupied band) is indicated in red, and the square of the matrix elements to each final state (unoccupied bands) are indicated by the size of the black markers. The smallest dipole-allowed transition is indicated with a blue arrow. The smallest direct transition in Cu_2O is seen to be forbidden, in contrast to the strongly-allowed direct gap in GaAs.

Parameters for Phases Passing the Intermediate Screens

The table below summarizes key computed parameters for the ≈800 phases passing the intermediate screen, with the phases ordered by descending spectroscopic limited maximum efficiency (SLME) at absorber thickness $L = 500\,\text{nm}$. The Materials Project ID and space group symmetry of each phase are given as identifiers. Chemical formulae are given with the elements in group order from left to right, with the exception of hydrogen, which is placed at the end (*e.g.* YH_3 instead of H_3Y). Within a group, elements are listed in period order from top to bottom. The structure of polyanions or other chemical groupings is not reflected in the naming (*e.g.* strontium amide appears as SrN_2H_4 rather than $Sr(NH_2)_2$). Bandgap parameters are the fundamental bandgap (E_g), smallest direct gap ($E_g^{\rm d}$), and smallest dipole-allowed direct gap ($E_g^{\rm da}$), and are corrected from GGA-PBE values by the Δ-sol method[1] as discussed in the text. "Optical Type" is as defined in Yu and Zunger.[2] Effective masses are averages of line effective masses as discussed in the text. Energies above the convex hull ($\Delta E_{\rm hull}$) are reported directly from the Materials Project database.[4] Note that these values may change as new stable phases are added to the database or higher fidelity formation energies are computed. (*) Asterisks indicate a few well-known materials which do not pass the intermediate screens, but are nonetheless included for comparison. These data and many others are available in structured, digital form as described in the main text via the Materials Project MPContribs Framework[7,8] at https://materialsproject.org/mpcontribs/ScreeningInorganicPV.

	Formula	Materials	Space	SLME (%)		Optical	Bandgap (eV)			$\Delta E_{\rm hull}$	m^* (m_0)	
		Project ID	Group	L=500 nm	L=1 μm	Type	E_g	$E_g^{\rm d}$	$E_g^{\rm da}$	(meV atom^{-1})	m_e^*	m_h^*
1.	$CsAuI_3$	mp-28453	$I4/mmm$ (#139)	32.8	32.9	OT1	1.159	1.159	1.159	-	0.46	0.43
2.	Pt_2TlS_3	mp-9272	$P\bar{3}m1$ (#164)	32.7	33.0	OT1	1.380	1.380	1.380	-	0.56	0.64
3.	$NaSbS_2$	mp-557179	$C2/m$ (#12)	32.4	32.7	OT1	1.405	1.408	1.408	20.5	0.08	0.14
4.	$K_2Ag_4Se_3$	mp-573891	$C2/m$ (#12)	32.3	32.5	OT1	1.302	1.305	1.305	-	0.17	0.81
5.	Cs_2GaSb_2	mp-29372	$Pnma$ (#62)	32.2	32.5	OT1	1.171	1.176	1.176	-	0.34	1.36
6.	$BiSeI$	mp-23020	$Pnma$ (#62)	32.1	32.4	OT3	1.344	1.364	1.364	11.7	1.23	0.88
7.	$Sr_{11}InSb_9$	mp-578752	$Iba2$ (#45)	31.8	32.5	OT1	1.207	1.207	1.207	-	0.44	0.58
8.	Tl_3AsSe_3	mp-7684	$R3m$ (#160)	31.3	32.3	OT1	1.230	1.230	1.230	-	0.41	0.70
9.	$CaAgP$	mp-12277	$P\bar{6}2m$ (#189)	31.2	31.5	OT1	1.471	1.471	1.471	-	0.21	0.12
10.	$MoTe_2$	mp-602	$P6_3/mmc$ (#194)	31.1	31.2	OT3	1.340	1.396	1.396	-	0.48	1.45
11.	$YPtSb$	mp-4964	$F\bar{4}3m$ (#216)	31.1	31.7	OT1	1.088	1.088	1.088	-	0.15	0.43
12.	$IrSb_3$	mp-1239	$Im\bar{3}$ (#204)	31.1	31.6	OT1	1.200	1.200	1.200	-	0.24	0.13
13.	Ba_3As_{14}	mp-524	$P2_1/c$ (#14)	31.0	31.2	OT3	1.359	1.415	1.415	-	0.43	0.90
14.	$BaCd_2As_2$	mp-8281	$P\bar{3}m1$ (#164)	30.9	32.1	OT1	1.358	1.358	1.358	-	0.13	0.47
15.	$Si_{19}Te_8$	mp-31135	$R3c$ (#161)	30.9	31.9	OT3	1.373	1.402	1.402	34.9	0.30	1.36
16.	Ag_2BiO_3	mp-23558	$Pnn2$ (#34)	30.8	31.2	OT1	1.066	1.066	1.066	-	1.23	1.26
17.	Ba_4P_2O	mp-28164	$Cmca$ (#64)	30.8	32.0	OT1	1.441	1.441	1.441	2.0	1.25	1.25

	Formula	Materials	Space	SLME (%)		Optical	Bandgap (eV)			ΔE_{hull}	m^* (m_0)	
		Project ID	Group	L=500 nm	L=1 μm	Type	E_g	E_g^{d}	E_g^{da}	(meV atom^{-1})	m_e^*	m_h^*
18.	LiBaP	mp-13277	$P6_3/mmc$ (#194)	30.8	32.4	OT1	1.323	1.323	1.323	-	0.64	0.63
19.	Tl_2SnSe_3	mp-29237	$Pnma$ (#62)	30.7	32.1	OT1	1.315	1.321	1.321	-	0.59	0.76
20.	Sc_4C_3	mp-15661	$I\bar{4}3d$ (#220)	30.7	31.9	OT1	1.149	1.149	1.149	-	0.75	0.26
21.	Ba_4Sb_2O	mp-9774	$I4/mmm$ (#139)	30.7	32.1	OT1	1.160	1.160	1.160	-	0.42	1.43
22.	SrAgP	mp-10667	$P6_3/mmc$ (#194)	30.7	31.5	OT1	1.174	1.174	1.174	-	0.14	0.38
23.	Ba_3SnP_3	mp-540923	$P2_1/c$ (#14)	30.6	31.2	OT3	1.134	1.171	1.171	6.4	0.68	0.35
24.	$AgInTe_2$	mp-22386	$I\bar{4}2d$ (#122)	30.5	31.5	OT1	1.360	1.360	1.360	-	0.10	0.49
25.	PbO_2	mp-20725	$P4_2/mnm$ (#136)	30.4	30.6	OT2	1.304	1.312	1.361	-	0.51	0.31
26.	Ba_4As_2O	mp-8300	$I4/mmm$ (#139)	30.4	31.9	OT1	1.235	1.235	1.235	-	0.43	0.94
27.	Os_2Ge_3	mp-16610	$Pbcn$ (#60)	30.4	31.9	OT1	1.214	1.214	1.214	3.3	1.01	0.44
28.	$Ca_3In_2As_4$	mp-650513	$Pnnm$ (#58)	30.3	30.4	OT1	0.988	0.988	0.988	-	0.08	0.50
29.	Te_2I	mp-27655	$Pnma$ (#62)	30.3	31.9	OT1	1.177	1.177	1.177	-	0.60	1.18
30.	P	mp-157	$Cmca$ (#64)	30.3	31.9	OT1	1.307	1.312	1.312	30.0	0.57	0.69
31.	Na_2AgAs	mp-8411	$C222_1$ (#20)	30.2	31.8	OT1	1.273	1.273	1.273	-	0.75	0.81
32.	Na_2AsTe_2	mp-29381	$P2_12_12_1$ (#19)	30.2	30.4	OT3	1.278	1.336	1.336	10.8	1.42	1.02
33.	Bi_2S_3	mp-22856	$Pnma$ (#62)	30.2	31.0	OT3	1.523	1.534	1.534	-	0.54	1.15
34.	$CsAuBr_3$	mp-569548	$I4/mmm$ (#139)	30.2	30.3	OT1	1.593	1.593	1.593	-	0.43	0.39
35.	$PdBi_{14}Br_{16}$	mp-542522	$P\bar{1}$ (#2)	30.1	31.0	OT2	1.440	1.440	1.478	30.5	1.39	1.44
36.	BiSeBr	mp-569707	$Pnma$ (#62)	30.1	30.9	OT3	1.523	1.541	1.541	8.6	0.87	1.06
37.	LiBaP	mp-10615	$P\bar{6}m2$ (#187)	30.1	31.8	OT1	1.214	1.214	1.214	33.4	0.44	0.92
38.	Sr_3SiO	mp-30949	$Pnma$ (#62)	30.0	30.8	OT1	1.041	1.041	1.041	-	0.44	0.63
39.	Bi_3Se_4Br	mp-29857	$C2/m$ (#12)	30.0	31.4	OT3	1.318	1.351	1.351	24.3	0.55	1.50
40.	$Sr_3Ge_2As_4$	mp-17504	$P2_1/c$ (#14)	30.0	31.1	OT3	1.155	1.183	1.183	-	1.21	0.62
41.	Sb_2Se_3	mp-2160	$Pnma$ (#62)	29.9	31.3	OT3	1.323	1.356	1.356	-	0.42	0.31
42.	$TaCuS_3$*	mp-3102	$Pnma$ (#62)	29.9	30.4	OT3	1.022	1.034	1.034	-	4.50	3.96
43.	Ca_3NBi	mp-31149	$Pm\bar{3}m$ (#221)	29.8	30.8	OT1	1.049	1.049	1.049	-	0.38	0.26
44.	AgTlSe	mp-29238	$Pnma$ (#62)	29.7	31.5	OT1	1.148	1.148	1.148	-	0.49	0.83
45.	$CuInTe_2$	mp-22261	$I\bar{4}2d$ (#122)	29.7	29.7	OT3	1.168	1.247	1.247	-	0.10	1.28
46.	CaP_3	mp-9122	$P\bar{1}$ (#2)	29.7	29.9	OT3	1.014	1.035	1.035	-	0.45	0.26
47.	CsSn	mp-11055	$I4_1/acd$ (#142)	29.7	30.7	OT1	1.037	1.037	1.037	5.9	0.38	0.80
48.	K_2PdSe_{10}	mp-505138	$I2_12_12_1$ (#24)	29.7	30.7	OT1	1.547	1.547	1.547	-	0.96	1.33
49.	KZnSb	mp-7438	$P6_3/mmc$ (#194)	29.6	30.9	OT1	1.491	1.491	1.491	-	0.27	1.37
50.	Ca_3SiO	mp-11649	$Pnma$ (#62)	29.6	30.2	OT1	0.996	0.996	0.996	-	0.51	0.37
51.	Sr_3GeO	mp-30950	$Pnma$ (#62)	29.6	30.3	OT1	0.987	0.987	0.987	-	0.47	0.64
52.	Ca_3GeO	mp-17193	$Imma$ (#74)	29.5	30.2	OT1	0.990	0.990	0.990	-	0.28	0.36
53.	CaAgAs	mp-5615	$P\bar{6}2m$ (#189)	29.5	30.8	OT3	1.284	1.314	1.314	-	0.16	0.10
54.	$TlSbSe_2$	mp-567318	$P2_1$ (#4)	29.4	30.7	OT3	1.151	1.187	1.187	-	0.17	0.32
55.	$RbSb_3Se_5$	mp-4721	$P2_1/c$ (#14)	29.3	29.7	OT1	1.613	1.619	1.619	-	0.54	1.47
56.	$InBi_2Se_4Br$	mp-571169	$C2/m$ (#12)	29.3	30.1	OT3	1.447	1.512	1.512	12.3	0.77	1.25
57.	Nb_2Te_6I	mp-28745	$P2_1/c$ (#14)	29.3	29.4	OT1	0.919	0.919	0.923	-	1.08	1.39
58.	$Na_2In_2Sb_3$	mp-541692	$P2_1/c$ (#14)	29.2	30.0	OT1	0.978	0.985	0.985	8.4	0.62	1.28
59.	$Nb_2CuTl_3Se_{12}$	mp-570757	$P2_1/c$ (#14)	29.2	29.9	OT2	1.343	1.345	1.437	-	1.18	1.30
60.	Li_2AgSb	mp-16238	$F\bar{4}3m$ (#216)	29.2	29.9	OT1	0.990	0.990	0.990	-	0.12	0.53
61.	PbS	mp-21276	$Fm\bar{3}m$ (#225)	29.1	31.4	OT1	1.178	1.178	1.178	-	0.20	0.20
62.	$CuPbBi_3S_6$	mp-542302	$Pmc2_1$ (#26)	29.1	30.8	OT1	1.085	1.085	1.085	4.7	0.91	1.35
63.	AlSb	mp-2624	$F\bar{4}3m$ (#216)	29.1	31.0	OT3	1.430	1.455	1.455	-	0.52	0.70
64.	$MgAs_4$	mp-7623	$P4_12_12$ (#92)	29.1	30.1	OT4	1.183	1.193	1.242	-	1.30	0.85
65.	CuP_2BiSe_6	mp-569715	$P\bar{3}1c$ (#163)	29.1	30.4	OT3	1.175	1.216	1.216	13.9	0.54	1.39
66.	LiBaAs	mp-10616	$P\bar{6}m2$ (#187)	29.1	30.5	OT1	1.044	1.044	1.044	-	0.36	0.95
67.	KTe	mp-2072	$P6_3/mmc$ (#194)	29.1	31.5	OT1	1.178	1.178	1.178	-	0.44	1.39
68.	AgTlTe	mp-5874	$Pnma$ (#62)	29.0	29.9	OT1	0.991	0.998	0.998	-	0.23	0.80
69.	WTe_2	mp-1019322	$P6_3/mmc$ (#194)	28.9	29.2	OT3	1.274	1.362	1.362	25.4	0.42	0.94
70.	Cu_2HgGeS_4	mp-557574	$Pmn2_1$ (#31)	28.9	29.7	OT1	1.537	1.537	1.537	2.4	0.14	1.49

	Formula	Materials	Space		SLME (%)		Optical	Bandgap (eV)			ΔE_{hull}	m^* (m_0)	
		Project ID	Group		L=500 nm	L=1 μm	Type	E_g	E_g^{d}	E_g^{da}	(meV atom^{-1})	m_e^*	m_h^*
71.	Ca_3NAs	mp-7223	$Pm\bar{3}m$	(#221)	28.9	31.0	OT1	1.457	1.457	1.457	6.0	0.44	0.36
72.	$KGaSb_2$	mp-29383	$Cmca$	(#64)	28.8	29.5	OT2	1.108	1.111	1.176	-	1.19	1.21
73.	$Co_2Ge_3Se_3$	mp-5094	$R\bar{3}$	(#148)	28.8	30.9	OT1	1.218	1.218	1.218	-	0.72	0.27
74.	$CuGaSe_2$	mp-4840	$I\bar{4}2d$	(#122)	28.8	29.4	OT1	1.570	1.570	1.570	-	0.07	0.54
75.	Te_3Cl_2	mp-27628	$P2_1/c$	(#14)	28.7	28.7	OT3	1.607	1.661	1.661	13.5	1.33	1.19
76.	$Cu_6Hg_3As_4S_{12}$	mp-6287	$R3$	(#146)	28.7	30.8	OT1	1.345	1.345	1.345	1.4	0.20	1.02
77.	BaP_{10}	mp-28035	$Cmc2_1$	(#36)	28.7	29.4	OT3	1.521	1.586	1.586	-	1.27	0.97
78.	$BaZrS_3$	mp-540771	$Pnma$	(#62)	28.7	29.9	OT2	1.543	1.543	1.573	-	0.41	0.89
79.	NaP	mp-7440	$P2_12_12_1$	(#19)	28.6	30.3	OT3	1.421	1.470	1.470	-	0.77	1.29
80.	$CuGaTe_2$	mp-3839	$I\bar{4}2d$	(#122)	28.5	30.4	OT1	1.273	1.273	1.273	-	0.07	0.46
81.	Na_2AuAs	mp-7773	$Cmcm$	(#63)	28.5	29.9	OT1	1.040	1.044	1.044	-	0.41	0.66
82.	$NaBa_6Cu_3Te_{14}$	mp-569168	$P6_3/mcm$	(#193)	28.5	29.4	OT3	1.062	1.094	1.094	-	0.51	0.93
83.	$Ba_3In_2P_4$	mp-19913	$C2/c$	(#15)	28.5	30.4	OT1	1.544	1.544	1.544	-	0.65	1.11
84.	Cu_2HgGeS_4	mp-10952	$I\bar{4}2m$	(#121)	28.5	29.6	OT1	1.450	1.450	1.457	-	0.10	0.69
85.	Na_2AgSb	mp-7392	$Cmcm$	(#63)	28.5	30.4	OT3	1.187	1.215	1.215	-	0.60	0.70
86.	$CuTlPO_4$	mp-541201	$C2/c$	(#15)	28.5	28.7	OT1	1.688	1.688	1.688	-	0.34	0.67
87.	$CuTlAsO_4$	mp-541202	$C2/c$	(#15)	28.4	29.4	OT3	1.580	1.612	1.612	-	0.25	0.42
88.	Ga_2Te_5	mp-2371	$I4/m$	(#87)	28.4	29.6	OT3	1.400	1.493	1.493	-	0.19	1.48
89.	Cu_2GeS_3	mp-15252	Cc	(#9)	28.4	29.6	OT3	1.124	1.158	1.158	-	0.17	1.07
90.	Cs_2P_3	mp-14652	$Fmmm$	(#69)	28.4	30.8	OT1	1.314	1.317	1.317	-	1.09	1.12
91.	$SrCd_2As_2$	mp-7771	$P\bar{3}m1$	(#164)	28.4	29.6	OT1	1.542	1.542	1.542	-	0.10	0.48
92.	K_2Se_5	mp-18609	$P2_12_12_1$	(#19)	28.3	28.9	OT4	1.279	1.360	1.376	-	1.22	1.49
93.	$CuInS_2$	mp-22736	$I\bar{4}2d$	(#122)	28.3	29.1	OT1	1.548	1.548	1.550	-	0.12	0.93
94.	Cu_4SnS_4	mp-504536	$Pnma$	(#62)	28.2	28.4	OT3	0.929	0.960	0.960	28.4	0.28	0.56
95.	Li_3As_7	mp-680395	$Pbca$	(#61)	28.2	28.8	OT2	1.608	1.608	1.652	0.1	1.33	1.46
96.	Cu_4GeS_4	mp-565590	$P2_1/c$	(#14)	28.2	30.2	OT1	1.368	1.368	1.368	19.2	0.18	0.66
97.	$HgGa_2Te_4$	mp-16337	$I\bar{4}$	(#82)	28.2	30.7	OT1	1.401	1.401	1.401	-	0.15	0.85
98.	$LaCuSTe$	mp-10288	$P2_1/c$	(#14)	28.1	31.1	OT1	1.341	1.341	1.341	-	0.26	0.53
99.	Bi_2STe_2	mp-27910	$R\bar{3}m$	(#166)	28.1	30.1	OT1	1.064	1.064	1.064	-	0.18	0.35
100.	$RbAuI_3$	mp-568666	$C2/m$	(#12)	28.0	28.4	OT3	1.209	1.319	1.319	-	0.47	0.54
101.	Na_5SiP_3	mp-5929	$P2_1/c$	(#14)	28.0	29.5	OT3	1.496	1.552	1.552	-	0.27	0.59
102.	$Na_2Al_2As_3$	mp-17473	$P2_1/c$	(#14)	28.0	29.4	OT1	1.613	1.613	1.613	-	0.95	1.17
103.	$K_3Ag_3As_2$	mp-14206	$R\bar{3}m$	(#166)	28.0	28.4	OT1	1.710	1.710	1.710	-	1.20	1.22
104.	$Co_2Sn_3Se_3$	mp-570152	$R\bar{3}$	(#148)	27.9	29.3	OT1	0.969	0.969	0.969	-	0.62	0.25
105.	$GeSe$	mp-10759	$Fm\bar{3}m$	(#225)	27.9	28.4	OT1	0.889	0.889	0.889	10.1	0.20	0.13
106.	$Bi_2Te_7Cl_8$	mp-30097	$P\bar{1}$	(#2)	27.9	29.6	OT1	1.620	1.623	1.623	-	0.34	0.34
107.	$HgIn_2Te_4$	mp-19765	$I\bar{4}$	(#82)	27.8	30.5	OT1	1.383	1.383	1.383	-	0.14	0.96
108.	Ba_3NBi	mp-567666	$P6_3/mmc$	(#194)	27.8	28.9	OT1	0.918	0.918	0.918	-	0.51	0.33
109.	$GaAs$	mp-2534	$F\bar{4}3m$	(#216)	27.8	29.6	OT1	1.450	1.450	1.450	-	0.08	0.62
110.	SnS	mp-1876	$Fm\bar{3}m$	(#225)	27.8	27.7	OT1	0.877	0.877	0.877	45.2	0.09	0.18
111.	$PbSe$	mp-2201	$Fm\bar{3}m$	(#225)	27.7	29.4	OT1	0.958	0.958	0.958	-	0.18	0.20
112.	$RbAg_3Se_2$	mp-10477	$C2/m$	(#12)	27.7	28.9	OT3	1.440	1.478	1.478	-	0.20	1.11
113.	$Ir_2Sn_3Te_3$	mp-5142	$R\bar{3}$	(#148)	27.7	30.1	OT1	1.281	1.281	1.281	-	0.36	0.18
114.	Li_3RhH_4	mp-697047	$Cmcm$	(#63)	27.7	27.7	OT3	0.989	1.054	1.054	-	0.31	0.23
115.	Cd_3P_2	mp-2441	$P4_2/nmc$	(#137)	27.7	29.0	OT2	1.422	1.422	1.517	21.7	0.09	1.43
116.	$BaSi_2$	mp-1477	$Pnma$	(#62)	27.7	28.3	OT3	1.094	1.179	1.179	-	0.63	0.79
117.	$BaPt_4As_6$	mp-14501	$C2/c$	(#15)	27.7	29.4	OT1	1.031	1.041	1.041	-	0.60	0.64
118.	$GaAs$	mp-8883	$P6_3mc$	(#186)	27.7	29.5	OT1	1.445	1.445	1.445	13.2	0.06	0.63
119.	TlS	mp-561066	$P4_12_12$	(#92)	27.6	30.0	OT1	1.487	1.487	1.487	26.6	0.27	0.68
120.	Tl_2PSe_3	mp-28394	$P2_1/c$	(#14)	27.6	28.1	OT3	1.706	1.721	1.721	-	1.32	0.79
121.	$Bi_{14}S_8Te_{13}$	mp-557619	$R\bar{3}$	(#148)	27.4	29.4	OT1	1.008	1.008	1.008	13.5	0.24	0.63
122.	In_4Se_3	mp-19932	$Pnnm$	(#58)	27.4	29.2	OT3	1.050	1.060	1.060	18.3	0.25	0.98
123.	K_3PSe_{16}	mp-29947	$Fd\bar{3}$	(#203)	27.4	27.8	OT2	1.413	1.413	1.571	2.1	0.82	1.20

	Formula	Materials	Space		SLME (%)		Optical	Bandgap (eV)			ΔE_{hull}	m^* (m_0)	
		Project ID	Group		L=500 nm	L=1 μm	Type	E_g	E_g^{d}	E_g^{da}	(meV atom^{-1})	m_e^*	m_h^*
124.	BiTeI	mp-22965	$P3m1$	(#156)	27.4	28.0	OT3	1.250	1.367	1.367	-	0.51	0.69
125.	$Co_2Sn_3Te_3$	mp-866481	$R\bar{3}$	(#148)	27.4	28.4	OT1	0.903	0.903	0.903	-	0.67	0.25
126.	Na_2KSb	mp-15724	$Fm\bar{3}m$	(#225)	27.3	29.7	OT1	1.518	1.518	1.518	-	0.14	0.78
127.	$HgPbP_{14}$	mp-22574	$Pnma$	(#62)	27.3	28.4	OT3	1.605	1.660	1.660	-	0.86	1.33
128.	$GeAs_4Te_7$	mp-8645	$P\bar{3}m1$	(#164)	27.3	27.3	OT1	0.867	0.867	0.867	12.2	0.35	0.22
129.	Cu_3PSe_4	mp-5756	$Pmn2_1$	(#31)	27.3	27.7	OT3	0.954	0.997	0.997	-	0.11	0.48
130.	$CdBiSe_2I$	mp-570961	$C2/m$	(#12)	27.3	28.8	OT3	1.597	1.638	1.638	42.6	1.04	0.80
131.	$LiNa_2GaAs_2$	mp-9722	$Cmca$	(#64)	27.3	30.2	OT1	1.362	1.362	1.362	-	0.16	0.88
132.	$ZnAs_2$	mp-7262	$P2_1/c$	(#14)	27.3	29.8	OT1	1.291	1.291	1.291	-	0.23	0.78
133.	Na_5SiAs_3	mp-18139	$P2_1/c$	(#14)	27.2	29.6	OT3	1.181	1.199	1.199	-	0.18	0.72
134.	$CuPbBiS_3$	mp-624191	$Pnma$	(#62)	27.2	29.0	OT3	1.085	1.119	1.119	9.5	0.35	0.79
135.	$Pb_5Sb_8S_{17}$	mp-642227	$C2/c$	(#15)	27.1	27.6	OT3	1.738	1.760	1.760	2.9	1.06	0.90
136.	$Ag_3Ge_5P_6$	mp-17862	$I\bar{4}3m$	(#217)	27.1	27.9	OT3	1.257	1.378	1.378	-	0.25	0.48
137.	$BaAg_2Te_2$	mp-18501	$Pnma$	(#62)	27.1	29.3	OT1	1.540	1.540	1.540	-	0.27	1.18
138.	$Pb_9Sb_8S_{21}$	mp-649982	$C2/c$	(#15)	27.1	27.2	OT3	1.740	1.777	1.777	6.2	0.35	1.20
139.	$BaCd_2P_2$	mp-8279	$P\bar{3}m1$	(#164)	27.1	29.1	OT1	1.583	1.583	1.583	-	0.31	0.61
140.	$Tl_4Bi_2S_5$	mp-23408	$Pnma$	(#62)	27.1	28.6	OT3	1.388	1.505	1.505	-	0.32	0.92
141.	Bi_2SeTe_2	mp-29666	$R\bar{3}m$	(#166)	27.0	29.0	OT1	0.962	0.962	0.962	-	0.23	0.64
142.	$RbAuBr_3$	mp-27300	$C2/m$	(#12)	27.0	27.5	OT3	1.579	1.693	1.693	-	0.49	0.55
143.	BaCuN	mp-29199	$C2/c$	(#15)	27.0	27.4	OT3	0.864	0.878	0.878	-	0.60	0.47
144.	Ca_3NP	mp-11824	$Pm\bar{3}m$	(#221)	26.9	29.5	OT1	1.552	1.552	1.552	-	0.45	0.40
145.	$HgAl_2Te_4$	mp-7910	$I\bar{4}$	(#82)	26.9	28.7	OT1	1.654	1.654	1.654	-	0.22	1.13
146.	$Sr_{11}Cd_6Sb_{12}$	mp-3195	$C2/m$	(#12)	26.9	28.6	OT1	0.967	0.967	0.967	-	0.93	0.48
147.	SrGaSnH	mp-978852	$P3m1$	(#156)	26.8	28.1	OT1	0.912	0.912	0.912	-	0.13	0.30
148.	LiMgBi	mp-570213	$F\bar{4}3m$	(#216)	26.8	28.5	OT1	0.951	0.951	0.951	-	0.10	0.81
149.	Cu_2HgI_4	mp-568598	$P\bar{4}2m$	(#111)	26.8	29.1	OT3	1.365	1.405	1.405	6.1	0.30	1.09
150.	$Sr_3In_2P_4$	mp-28324	$Pnnm$	(#58)	26.8	29.8	OT1	1.383	1.383	1.383	-	0.21	1.27
151.	Na_2CuAs	mp-15685	$Cmcm$	(#63)	26.7	28.7	OT3	1.319	1.402	1.402	-	0.67	0.75
152.	$CsAg_3Se_2$	mp-16234	$C2/m$	(#12)	26.7	29.1	OT1	1.481	1.484	1.484	-	0.21	1.10
153.	GaTe	mp-542812	$C2/m$	(#12)	26.7	28.7	OT3	1.600	1.620	1.620	-	0.50	1.00
154.	$CuSbS_2{}^*$	mp-4468	$Pnma$	(#62)	26.7	27.8	OT3	1.243	1.359	1.359	-	1.08	3.75
155.	K_3AuSe_{13}	mp-28606	$P2/c$	(#13)	26.7	27.7	OT3	1.276	1.395	1.395	-	0.46	0.05
156.	$AgGaTe_2$	mp-4899	$I\bar{4}2d$	(#122)	26.7	28.9	OT1	1.428	1.428	1.428	-	0.08	0.39
157.	Sr_3InP_3	mp-616026	$Pnma$	(#62)	26.7	29.2	OT2	1.424	1.424	1.471	-	1.28	1.05
158.	FeP_4	mp-570553	$C2/c$	(#15)	26.6	27.7	OT3	1.264	1.382	1.382	-	0.85	1.12
159.	$CaCd_2As_2$	mp-7067	$P\bar{3}m1$	(#164)	26.6	28.3	OT1	1.593	1.593	1.593	-	0.11	0.47
160.	Tl_3SiTe_3	mp-568020	$P\bar{1}$	(#2)	26.5	27.7	OT4	1.227	1.299	1.346	-	0.83	1.22
161.	$Ba_2Ge_2Te_5$	mp-17885	$Pna2_1$	(#33)	26.5	27.7	OT3	1.074	1.147	1.147	-	0.60	1.12
162.	$ZnGa_2Te_4$	mp-15777	$I\bar{4}$	(#82)	26.5	28.5	OT1	1.655	1.655	1.655	-	0.18	1.09
163.	Sr_3NSb	mp-7752	$Pm\bar{3}m$	(#221)	26.5	29.0	OT1	1.001	1.001	1.001	-	0.35	0.39
164.	NaBaP	mp-9732	$P\bar{6}2m$	(#189)	26.5	29.2	OT1	1.515	1.515	1.515	-	0.43	0.66
165.	In_5Se_5Br	mp-510346	$Pmn2_1$	(#31)	26.5	28.5	OT3	1.397	1.489	1.489	26.0	0.47	0.98
166.	$MoSe_2$	mp-7581	$R3m$	(#160)	26.5	26.5	OT3	1.742	1.806	1.806	0.1	0.69	1.42
167.	$Na_3Sr_3GaAs_4$	mp-10097	$P6_3mc$	(#186)	26.4	29.4	OT1	1.271	1.271	1.271	-	0.18	0.72
168.	$Ge_{19}P_4Br_4$	mp-27625	$P\bar{4}3n$	(#218)	26.4	26.5	OT3	1.760	1.814	1.814	-	0.32	0.93
169.	Ba_3GaP_3	mp-541715	$Cmca$	(#64)	26.4	28.1	OT3	1.002	1.037	1.037	-	0.89	1.26
170.	Sr_3NBi	mp-570008	$Pm\bar{3}m$	(#221)	26.4	27.0	OT1	0.861	0.861	0.861	-	0.40	0.35
171.	$SrGa_2As_2$	mp-972120	$P2/m$	(#10)	26.4	29.3	OT1	1.146	1.146	1.146	-	0.14	0.43
172.	$CsAg_5Se_3$	mp-10480	$P4_2/mnm$	(#136)	26.4	27.7	OT4	1.295	1.380	1.394	-	0.24	0.88
173.	NaTe	mp-28353	$Pbcn$	(#60)	26.4	26.7	OT2	1.004	1.004	1.092	6.7	0.21	0.65
174.	Rb_2P_3	mp-2079	$Fmmm$	(#69)	26.3	29.3	OT1	1.272	1.272	1.272	-	0.91	1.04
175.	K_2P_3	mp-8262	$Fmmm$	(#69)	26.3	29.2	OT1	1.213	1.213	1.213	0.1	0.94	1.14
176.	$Re_3Tl_2Se_6$	mp-616190	$C2/c$	(#15)	26.3	27.4	OT3	1.293	1.427	1.427	-	1.47	1.13

	Formula	Materials	Space		SLME (%)		Optical	Bandgap (eV)			ΔE_{hull}	m^* (m_0)	
		Project ID	Group		L=500 nm	L=1 μm	Type	E_g	E_g^{d}	E_g^{da}	(meV atom^{-1})	m_e^*	m_h^*
177.	Sr_4GeP_4	mp-14213	$P\bar{4}3n$	(#218)	26.3	27.6	OT2	1.252	1.252	1.371	-	1.36	1.11
178.	$AgPbSbS_3$	mp-605863	$P2_1/c$	(#14)	26.2	28.1	OT3	1.108	1.175	1.175	47.1	0.60	0.81
179.	Ca_3NAs	mp-4192	$Pnma$	(#62)	26.2	28.6	OT1	1.601	1.601	1.601	-	0.69	0.52
180.	Ag_2S_3Te	mp-29163	Cc	(#9)	26.2	26.9	OT1	1.788	1.788	1.788	-	0.56	1.45
181.	$ZnIn_2Te_4$	mp-20832	$I\bar{4}$	(#82)	26.2	28.4	OT1	1.612	1.612	1.612	-	0.16	1.16
182.	CuP_2	mp-927	$P2_1/c$	(#14)	26.2	28.8	OT3	1.428	1.486	1.486	-	0.57	1.12
183.	AsSeI	mp-505373	$P2_1/c$	(#14)	26.2	27.3	OT1	1.754	1.761	1.761	-	0.32	1.45
184.	NaSi	mp-2402	$C2/c$	(#15)	26.1	27.1	OT4	1.501	1.535	1.653	-	0.29	0.39
185.	As_2Te_3	mp-9897	$R\bar{3}m$	(#166)	26.1	26.2	OT1	0.837	0.837	0.837	11.4	0.21	0.26
186.	$CsAsSe_2$	mp-28563	$Pbca$	(#61)	26.1	27.1	OT1	1.771	1.771	1.771	2.6	1.37	1.25
187.	Na_2AuSb	mp-7774	$Cmcm$	(#63)	26.0	27.6	OT3	0.940	0.955	0.955	-	0.57	0.57
188.	SrGaGeH	mp-978847	$P3m1$	(#156)	26.0	27.8	OT1	0.965	0.965	0.965	-	0.10	0.30
189.	BiTeCl	mp-28944	$P6_3mc$	(#186)	26.0	27.0	OT3	1.567	1.701	1.701	-	0.59	1.02
190.	$Cu_6As_4S_9$	mp-28717	$P1$	(#1)	26.0	27.3	OT3	1.015	1.066	1.066	-	0.48	1.47
191.	K_2AuSb	mp-867335	$Cmcm$	(#63)	26.0	28.4	OT3	1.445	1.531	1.531	-	0.53	1.28
192.	K_3GeTe_3	mp-27331	$C2/c$	(#15)	26.0	27.4	OT3	1.503	1.623	1.623	-	0.54	1.37
193.	Ag_5GeO_4	mp-5563	$P2_1/c$	(#14)	25.9	27.8	OT3	1.441	1.541	1.541	-	0.76	1.35
194.	$SrCu_2SnS_4$	mp-17322	$P3_221$	(#154)	25.9	28.3	OT1	1.570	1.571	1.571	5.9	0.15	0.88
195.	CaSrGe	mp-12418	$Pnma$	(#62)	25.9	26.1	OT1	0.841	0.841	0.841	-	0.52	1.26
196.	$GeAs_2$	mp-17524	$Pbam$	(#55)	25.9	28.3	OT3	1.342	1.418	1.418	-	0.26	0.67
197.	$SrCu_2SnS_4$	mp-16988	$P3_121$	(#152)	25.9	28.3	OT1	1.570	1.571	1.571	5.9	0.15	0.87
198.	$SrZrS_3$	mp-5193	$Pnma$	(#62)	25.9	26.8	OT1	1.793	1.793	1.793	0.5	0.54	0.68
199.	Bi_2Se_2Te	mp-31406	$R\bar{3}m$	(#166)	25.9	26.3	OT3	0.951	1.030	1.030	37.1	1.18	1.38
200.	NaP_5	mp-31086	$Pnma$	(#62)	25.9	27.2	OT1	1.752	1.752	1.752	10.5	0.50	0.83
201.	$Ag_2Hg_7P_8I_6$	mp-672339	$C2/m$	(#12)	25.8	27.3	OT3	1.527	1.642	1.642	12.0	0.57	0.70
202.	$Sr_2Cu_2O_6TeBr_2$	mp-555814	$P2_1/c$	(#14)	25.8	26.1	OT1	1.817	1.817	1.817	22.2	0.26	0.37
203.	$Ba_2GeSe_2Te_2$	mp-570803	$P2_1/m$	(#11)	25.8	29.4	OT1	1.345	1.345	1.345	-	0.36	1.18
204.	$SrPt_4As_6$	mp-14500	$C2/c$	(#15)	25.8	27.3	OT3	0.964	0.998	0.998	-	0.51	0.78
205.	Tl_5Se_2I	mp-23488	$I4/mcm$	(#140)	25.7	27.8	OT2	1.189	1.189	1.277	-	0.44	0.59
206.	Ga_2BiSe_4	mp-571085	$P4/nnc$	(#126)	25.6	25.9	OT4	1.769	1.826	1.845	-	0.46	1.46
207.	SbSeI	mp-22996	$Pnma$	(#62)	25.6	26.1	OT3	1.776	1.829	1.829	-	0.69	0.95
208.	Bi_2Se_3	mp-541837	$R\bar{3}m$	(#166)	25.6	28.3	OT1	1.061	1.061	1.061	-	0.24	0.38
209.	Tl_3AsS_3	mp-559356	$Pbca$	(#61)	25.6	25.9	OT3	1.817	1.847	1.847	-	0.55	1.39
210.	$Na_3Sr_3GaP_4$	mp-10096	$P6_3mc$	(#186)	25.5	28.9	OT1	1.478	1.478	1.478	-	0.32	0.89
211.	Cu_2ZnGeS_4	mp-6408	$I\bar{4}2m$	(#121)	25.4	28.2	OT1	1.526	1.526	1.526	-	0.15	1.12
212.	Ag_7PSe_6	mp-8594	$P2_13$	(#198)	25.4	28.0	OT1	1.562	1.562	1.562	-	0.20	1.16
213.	AgP_2	mp-8200	$P2_1/c$	(#14)	25.4	28.5	OT3	1.378	1.411	1.411	14.4	0.50	0.28
214.	$LiAsS_2$	mp-555874	Cc	(#9)	25.4	27.0	OT3	1.698	1.744	1.744	-	0.19	0.78
215.	SnSe	mp-2693	$Fm\bar{3}m$	(#225)	25.3	25.3	OT1	0.802	0.802	0.802	3.8	0.10	0.11
216.	$CaCd_2Sb_2$	mp-7430	$P\bar{3}m1$	(#164)	25.3	26.2	OT3	1.109	1.216	1.216	-	1.00	0.38
217.	$MgGeAs_2$	mp-1016200	$I\bar{4}2d$	(#122)	25.2	28.2	OT1	1.482	1.482	1.482	19.8	0.12	0.39
218.	K_2GeAs_2	mp-8930	$Ibam$	(#72)	25.2	26.5	OT3	1.056	1.146	1.146	-	1.38	1.15
219.	$AgInSe_2$	mp-20554	$I\bar{4}2d$	(#122)	25.2	26.6	OT3	1.560	1.609	1.609	-	0.11	0.32
220.	Os_2Si_3	mp-16608	$Pbcn$	(#60)	25.2	27.2	OT2	1.517	1.517	1.622	-	1.02	0.52
221.	Tl_3AsS_3	mp-9791	$R3m$	(#160)	25.1	26.5	OT3	1.594	1.725	1.725	9.8	0.58	1.09
222.	$Pb_2Bi_2Se_5$	mp-570930	$P\bar{3}m1$	(#164)	25.1	27.7	OT1	0.990	0.990	0.990	7.1	0.24	0.30
223.	$Ba_2Zn_3As_2O_2$	mp-14769	$I4/mmm$	(#139)	25.1	26.8	OT1	1.664	1.664	1.664	12.1	0.17	1.12
224.	Ba_3ZnN_2O	mp-545788	$P4/mmm$	(#123)	25.1	26.5	OT3	1.018	1.094	1.094	7.2	1.09	1.09
225.	$CoSb_3$	mp-1317	$Im\bar{3}$	(#204)	25.1	25.9	OT1	0.837	0.837	0.837	-	0.29	0.18
226.	Hg_2SnSe_4	mp-10955	$I\bar{4}$	(#82)	25.0	27.2	OT1	1.601	1.601	1.601	0.7	0.10	1.32
227.	$CdGa_2Te_4$	mp-13949	$I\bar{4}$	(#82)	25.0	26.9	OT1	1.747	1.747	1.747	-	0.17	0.98
228.	FeSbS	mp-27904	$P2_1/c$	(#14)	25.0	25.4	OT3	0.938	1.034	1.034	-	1.19	1.34
229.	$MgBi_2O_6$	mp-28447	$P4_2/mnm$	(#136)	24.9	27.8	OT4	1.388	1.431	1.481	-	0.33	0.24

	Formula	Materials	Space	SLME (%)		Optical	Bandgap (eV)			ΔE_{hull}	m^* (m_0)	
		Project ID	Group	L=500 nm	L=1 μm	Type	E_g	E_g^{d}	E_g^{da}	(meV atom^{-1})	m_e^*	m_h^*
230.	In_4SnSe_4	mp-628768	$Pa\bar{3}$ (#205)	24.8	26.9	OT1	1.725	1.725	1.725	2.1	0.17	1.07
231.	$Cs_2AgAuCl_6$	mp-567776	$I4/mmm$ (#139)	24.8	25.0	OT3	1.831	1.892	1.892	-	0.67	0.98
232.	$KTaTe_3$	mp-568318	$P2_1/c$ (#14)	24.8	25.2	OT1	0.803	0.803	0.803	-	0.58	1.07
233.	$LiRb_2Sn_4$	mp-680436	$P\bar{1}$ (#2)	24.8	25.5	OT2	1.142	1.142	1.317	-	0.72	1.04
234.	$CsSnI_3$	mp-568570	$Pnma$ (#62)	24.8	27.5	OT1	1.600	1.600	1.600	3.3	0.69	0.17
235.	$Ba_3Sn_2P_4$	mp-601867	$P2_1/c$ (#14)	24.8	25.6	OT4	1.171	1.251	1.341	-	1.22	0.99
236.	Cu_3PS_4	mp-3934	$Pmn2_1$ (#31)	24.7	26.7	OT1	1.753	1.753	1.753	-	0.36	0.95
237.	$PbBi_2S_4$	mp-641924	$Pnma$ (#62)	24.7	26.0	OT4	1.297	1.366	1.470	1.7	0.39	1.45
238.	MnP_4	mp-569522	$P\bar{1}$ (#2)	24.7	26.1	OT3	0.969	1.030	1.030	-	1.32	1.32
239.	$LaAsTe$	mp-10383	$Pnma$ (#62)	24.7	25.1	OT1	0.809	0.819	0.819	-	0.27	0.30
240.	$TlBiS_2$	mp-554310	$R\bar{3}m$ (#166)	24.6	28.0	OT1	1.191	1.191	1.191	-	0.22	0.29
241.	$CdIn_2Te_4$	mp-21374	$I\bar{4}$ (#82)	24.6	26.8	OT1	1.716	1.716	1.716	-	0.16	1.08
242.	$Ir_2Ge_3Se_3$	mp-975924	$R\bar{3}$ (#148)	24.5	27.2	OT1	1.638	1.638	1.638	-	0.46	0.20
243.	$BaAgP$	mp-9899	$P6_3/mmc$ (#194)	24.5	25.7	OT3	0.959	1.021	1.021	-	0.55	0.36
244.	LiP_5	mp-2412	$Pna2_1$ (#33)	24.5	26.5	OT2	1.680	1.681	1.740	13.0	0.55	0.62
245.	$In_2Sn_3S_7$	mp-616255	$P2_1/m$ (#11)	24.4	27.0	OT4	1.232	1.243	1.304	41.0	0.75	0.59
246.	$CaZrS_3$	mp-7781	$Pnma$ (#62)	24.4	25.6	OT1	1.848	1.848	1.848	36.1	0.70	0.65
247.	TeI	mp-569766	$P\bar{1}$ (#2)	24.3	26.3	OT4	1.328	1.462	1.488	-	0.60	1.01
248.	$Au_7P_{10}I$	mp-27370	$P\bar{6}2m$ (#189)	24.3	26.4	OT3	1.401	1.537	1.537	13.5	0.30	1.17
249.	$LaCuSe_2$	mp-11790	$P2_1/c$ (#14)	24.3	26.7	OT1	1.732	1.732	1.732	-	0.34	0.33
250.	$CuAgS$	mp-8911	$Cmcm$ (#63)	24.2	26.5	OT3	1.439	1.489	1.489	24.3	0.32	1.09
251.	Cs_5Sb_8	mp-628742	$P2_1/c$ (#14)	24.2	24.3	OT1	0.759	0.759	0.759	-	1.20	0.80
252.	$YAgTe_2$	mp-12903	$P\bar{4}2_1m$ (#113)	24.2	27.0	OT2	1.558	1.559	1.631	-	0.51	0.47
253.	Tl_2SnS_3	mp-542623	$C2/m$ (#12)	24.2	27.0	OT2	1.554	1.554	1.611	10.8	0.33	0.47
254.	Al_2BiSe_4	mp-571623	$P4/nnc$ (#126)	24.2	24.2	OT4	1.854	1.904	1.935	-	0.49	1.35
255.	SrP_3	mp-11108	$C2/m$ (#12)	24.2	25.4	OT3	0.912	0.986	0.986	1.8	0.24	0.18
256.	$BaTe_3$	mp-8234	$P\bar{4}2_1m$ (#113)	24.2	25.0	OT3	1.079	1.229	1.229	11.7	0.42	0.98
257.	$Ag_2HgSnSe_4$	mp-10963	$Pmn2_1$ (#31)	24.1	25.6	OT3	1.257	1.394	1.398	-	0.67	0.39
258.	$Hf_3Cu_2Tl_2Se_8$	mp-570700	$C2/m$ (#12)	24.1	26.7	OT3	1.247	1.344	1.344	-	1.22	0.83
259.	$RbBa_4Sb_3O$	mp-559270	$I4/mcm$ (#140)	24.1	26.0	OT3	1.105	1.226	1.226	-	0.49	1.43
260.	K_2SnTe_5	mp-28080	$I4cm$ (#108)	24.1	24.5	OT4	0.920	0.973	1.018	-	0.42	1.44
261.	$BaGe_2$	mp-2139	$Pnma$ (#62)	24.1	24.4	OT3	0.879	0.945	0.945	-	0.55	0.70
262.	Rb_2As_3	mp-15556	$Fmmm$ (#69)	24.0	24.9	OT1	0.813	0.814	0.814	-	1.35	0.79
263.	Rb_3AuGe_4	mp-17830	$Pmmn$ (#59)	23.9	24.2	OT4	1.068	1.088	1.236	-	0.79	0.81
264.	Ag_2HgI_4	mp-570256	$P\bar{4}2m$ (#111)	23.8	25.6	OT1	1.818	1.818	1.818	1.6	0.30	1.13
265.	Tl_3PSe_4	mp-4160	$Pnma$ (#62)	23.8	25.1	OT4	1.724	1.801	1.851	-	1.09	1.41
266.	Cu_3SbS_3	mp-554272	$P2_1/c$ (#14)	23.8	26.4	OT3	1.550	1.633	1.633	28.4	0.72	1.43
267.	$LiSrP$	mp-13276	$P6_3/mmc$ (#194)	23.7	25.4	OT3	1.738	1.831	1.831	-	0.89	0.67
268.	$KSr_2Cd_2Sb_3$	mp-866639	$Pnma$ (#62)	23.7	25.1	OT2	1.032	1.032	1.114	-	0.58	0.71
269.	$KGaTe_2$	mp-17965	$C2/c$ (#15)	23.7	25.7	OT2	1.667	1.667	1.771	-	0.35	0.87
270.	$CsAg_3S_2$	mp-561902	$C2/m$ (#12)	23.7	26.4	OT3	1.637	1.659	1.659	-	0.27	1.15
271.	$TlBiSe_2$	mp-29662	$R\bar{3}m$ (#166)	23.7	26.5	OT1	1.015	1.015	1.015	-	0.14	0.20
272.	$NaBaBi$	mp-31235	$P\bar{6}2m$ (#189)	23.6	25.0	OT1	0.842	0.842	0.842	-	0.10	0.52
273.	$GeBi_4Te_7$	mp-29644	$P\bar{3}m1$ (#164)	23.6	23.9	OT1	0.743	0.743	0.743	3.7	0.43	0.75
274.	Na_2CuP	mp-7639	$Cmcm$ (#63)	23.5	25.7	OT3	1.417	1.577	1.577	-	0.59	0.81
275.	Mg_3As_2	mp-7891	$P\bar{3}m1$ (#164)	23.5	27.5	OT1	1.489	1.489	1.489	18.8	0.13	0.92
276.	$ZnGeAs_2$	mp-4008	$I\bar{4}2d$ (#122)	23.5	25.9	OT3	1.358	1.382	1.384	-	0.05	0.24
277.	KCu_4AsS_4	mp-557728	$P2_1$ (#4)	23.5	24.5	OT3	1.852	1.903	1.903	-	1.37	1.27
278.	$PbPSe_3$	mp-20316	Pc (#7)	23.5	24.0	OT3	1.780	1.938	1.938	-	0.78	1.12
279.	Ag_2HgI_4	mp-23485	$I\bar{4}$ (#82)	23.5	24.7	OT1	1.878	1.878	1.878	-	0.31	1.37
280.	KCu_3Te_2	mp-541622	$C2/m$ (#12)	23.5	26.8	OT3	1.468	1.483	1.483	13.6	0.27	1.15
281.	$NaSrAs$	mp-9775	$P\bar{6}2m$ (#189)	23.5	26.3	OT1	1.689	1.689	1.689	-	0.17	1.01
282.	$CsAuCl_3$	mp-23484	$I4/mmm$ (#139)	23.5	23.5	OT3	1.936	1.959	1.959	-	0.53	0.53

	Formula	Materials	Space		SLME (%)		Optical	Bandgap (eV)			ΔE_{hull}	m^* (m_0)	
		Project ID	Group		L=500 nm	L=1 μm	Type	E_g	E_g^{d}	E_g^{da}	(meV atom^{-1})	m_e^*	m_h^*
283.	Ag_2PSe_3	mp-13956	$P2_12_12_1$	(#19)	23.4	25.5	OT4	1.440	1.473	1.609	-	0.81	0.57
284.	NaGe	mp-29657	$P2_1/c$	(#14)	23.4	24.5	OT2	1.041	1.041	1.174	-	0.22	0.56
285.	$SnPSe_3$	mp-570370	Pc	(#7)	23.4	24.0	OT3	1.805	1.944	1.944	-	0.93	1.45
286.	$Au_4Tl_2S_3$	mp-29898	$Pmmn$	(#59)	23.3	25.6	OT1	1.787	1.787	1.787	-	0.47	0.55
287.	Ba_2CdTe_3	mp-16904	$Pnma$	(#62)	23.3	24.9	OT1	1.857	1.857	1.857	19.5	0.36	1.10
288.	$Ge_2As_2Te_5$	mp-14791	$P\bar{3}m1$	(#164)	23.3	23.1	OT3	0.831	0.882	0.882	14.6	0.35	0.44
289.	Sn_3As_4	mp-570377	$P\bar{4}3m$	(#215)	23.2	24.5	OT3	1.058	1.184	1.184	25.1	0.19	1.28
290.	$BaCu_2Se_2$	mp-4473	$Pnma$	(#62)	23.2	26.0	OT1	1.649	1.649	1.649	3.9	0.21	1.07
291.	$KSbSe_2$	mp-9576	$P\bar{1}$	(#2)	23.2	25.4	OT4	1.629	1.746	1.763	-	0.41	1.17
292.	Na_5SnSb_3	mp-29739	$P2_1/c$	(#14)	23.2	23.5	OT1	0.737	0.737	0.737	-	0.16	0.62
293.	Cd_7P_{10}	mp-29576	$Fdd2$	(#43)	23.2	25.2	OT3	1.720	1.809	1.809	34.7	1.06	0.41
294.	$Ag_2Hg_7P_8Br_6$	mp-571425	$C2/m$	(#12)	23.2	24.7	OT3	1.793	1.857	1.857	10.7	0.54	1.19
295.	$Na_3Ca_3AlAs_4$	mp-15572	$P6_3mc$	(#186)	23.1	26.6	OT1	1.654	1.654	1.654	-	0.36	0.79
296.	$ZrGeTe_4$	mp-13542	$Cmc2_1$	(#36)	23.1	23.8	OT3	0.928	1.042	1.042	-	0.50	0.88
297.	SnS^*	mp-2231	$Pnma$	(#62)	23.0	25.3	OT3	1.551	1.708	1.708	-	0.20	0.53
298.	Se	mp-542461	$P2_1/c$	(#14)	23.0	24.0	OT4	1.882	1.907	1.925	5.6	1.27	1.43
299.	C	mp-169	$R\bar{3}m$	(#166)	23.0	23.2	OT1	1.974	1.974	1.974	21.3	0.09	0.09
300.	$Sr_3Si_2As_4$	mp-11677	$C2/c$	(#15)	23.0	25.4	OT2	1.373	1.373	1.539	-	0.41	1.21
301.	$Cs_2Au_2Se_3$	mp-29194	$C2/c$	(#15)	22.9	24.2	OT4	1.840	1.855	1.905	-	0.42	0.86
302.	$Ba_2As_2S_5$	mp-28134	$Pca2_1$	(#29)	22.8	23.6	OT1	1.942	1.942	1.942	-	0.49	1.32
303.	Ir_4Ge_5	mp-541844	$P\bar{4}c2$	(#116)	22.8	23.6	OT3	0.916	1.020	1.020	-	0.62	0.37
304.	Mg_2CaBi_2	mp-29208	$P\bar{3}m1$	(#164)	22.7	23.8	OT1	0.767	0.767	0.767	-	0.08	0.70
305.	Sr_4P_2O	mp-8298	$I4/mmm$	(#139)	22.5	24.0	OT3	1.844	1.915	1.915	-	0.48	1.32
306.	$Sn_5Sb_2S_9$	mp-29267	$Pbca$	(#61)	22.5	25.6	OT4	1.336	1.387	1.431	39.9	0.91	1.27
307.	$K_4SnSe_2Te_2$	mp-569427	$Pnma$	(#62)	22.5	23.2	OT1	1.956	1.956	1.956	-	0.46	1.24
308.	$CdSnP_2$	mp-5213	$I\bar{4}2d$	(#122)	22.5	24.9	OT1	1.669	1.669	1.669	-	0.07	0.36
309.	LiSrBi	mp-30456	$Pnma$	(#62)	22.4	23.3	OT2	0.771	0.771	0.785	-	0.83	0.56
310.	Sr_3AlSb_3	mp-17667	$Cmca$	(#64)	22.4	24.4	OT2	1.006	1.006	1.092	-	0.53	1.07
311.	Tl_5Se_2Cl	mp-28920	$P4/ncc$	(#130)	22.4	25.0	OT2	1.232	1.232	1.372	-	0.50	0.39
312.	Bi_2TeI	mp-23435	$C2/m$	(#12)	22.4	22.2	OT1	0.677	0.677	0.682	26.9	0.19	0.74
313.	ZnP_2	mp-1392	$P2_1/c$	(#14)	22.4	25.8	OT1	1.699	1.699	1.699	3.2	0.63	1.03
314.	In_4Te_3	mp-617281	$Pnnm$	(#58)	22.4	22.9	OT3	0.742	0.755	0.755	-	0.15	0.44
315.	$MgO_6I_8H_{12}$	mp-707735	$P\bar{1}$	(#2)	22.3	22.5	OT3	1.911	2.028	2.028	-	0.20	0.88
316.	$CdGeAs_2$	mp-4953	$I\bar{4}2d$	(#122)	22.3	24.2	OT3	1.242	1.375	1.375	-	0.13	0.14
317.	$Fe_3Al_2Si_3$	mp-29110	$P\bar{1}$	(#2)	22.3	22.6	OT1	0.706	0.706	0.706	-	1.21	0.34
318.	NaCuTe	mp-7434	$P4/nmm$	(#129)	22.3	25.5	OT1	1.684	1.684	1.684	10.0	0.15	1.36
319.	$ZnSnP_2$	mp-4175	$I\bar{4}2d$	(#122)	22.3	24.9	OT1	1.771	1.771	1.771	-	0.12	0.56
320.	BiI	mp-27708	$C2/m$	(#12)	22.3	23.2	OT3	0.858	0.927	0.927	27.1	1.03	0.97
321.	$PbBi_4Te_7$	mp-23005	$P\bar{3}m1$	(#164)	22.3	22.9	OT1	0.721	0.721	0.721	0.0	0.26	0.34
322.	$SrCd_2P_2$	mp-8277	$P\bar{3}m1$	(#164)	22.2	24.5	OT1	1.826	1.826	1.826	-	0.24	0.66
323.	$BaZn_2As_2$	mp-7427	$Pnma$	(#62)	22.2	24.5	OT2	1.295	1.295	1.413	-	0.66	0.83
324.	Sr_2CdAs_2	mp-867203	$Cmc2_1$	(#36)	22.2	25.3	OT1	1.642	1.642	1.642	-	0.16	0.75
325.	$HfGeTe_4$	mp-567817	$Cmc2_1$	(#36)	22.2	22.8	OT3	0.835	0.895	0.895	-	0.44	0.60
326.	$Sr_2Ge_2Se_5$	mp-18112	$P2_1/c$	(#14)	22.2	24.1	OT2	1.776	1.776	1.871	-	0.51	1.27
327.	Ca_3InP_3	mp-614572	$Pnma$	(#62)	22.1	25.0	OT2	1.611	1.611	1.709	-	0.99	0.94
328.	$PbBi_2Te_4$	mp-676250	$R\bar{3}m$	(#166)	22.0	22.8	OT1	0.715	0.715	0.715	0.8	0.27	0.45
329.	Mg_2SrAs_2	mp-867194	$P\bar{3}m1$	(#164)	22.0	24.4	OT3	1.721	1.843	1.843	-	0.95	0.71
330.	$KAuI_4$	mp-29519	$P2_1/c$	(#14)	22.0	23.2	OT4	0.892	0.911	0.977	0.5	0.67	1.29
331.	$NaSbS_2$	mp-5414	$C2/c$	(#15)	22.0	24.6	OT3	1.603	1.742	1.742	-	0.53	0.69
332.	Na_3AlAs_2	mp-8543	$Ibam$	(#72)	22.0	24.9	OT3	1.556	1.667	1.667	-	0.17	0.43
333.	Ba_3NSb	mp-12814	$P6_3/mmc$	(#194)	22.0	23.3	OT2	1.228	1.228	1.455	-	0.69	0.35
334.	$LiInTe_2$	mp-20782	$I\bar{4}2d$	(#122)	22.0	23.1	OT1	1.957	1.957	1.957	-	0.27	0.59
335.	NaSrP	mp-13275	$P\bar{6}2m$	(#189)	21.9	23.7	OT1	1.907	1.907	1.907	-	0.28	1.04

	Formula	Materials	Space		SLME (%)		Optical	Bandgap (eV)			ΔE_{hull}	m^* (m_0)	
		Project ID	Group		L=500 nm	L=1 μm	Type	E_g	E_g^{d}	E_g^{da}	(meV atom^{-1})	m_e^*	m_h^*
336.	$BaCu_2GeS_4$	mp-17947	$P3_121$	(#152)	21.8	23.8	OT1	1.880	1.883	1.883	-	0.23	1.16
337.	$Ag_4HgGe_2S_7$	mp-542199	Cc	(#9)	21.8	24.1	OT3	1.762	1.785	1.785	-	0.17	1.31
338.	$PbTe$	mp-19717	$Fm\bar{3}m$	(#225)	21.7	22.1	OT1	0.683	0.683	0.683	-	0.22	0.27
339.	$ZnGeP_2$	mp-4524	$I\bar{4}2d$	(#122)	21.7	23.7	OT3	1.871	1.897	1.897	-	0.29	0.43
340.	$CaCd_2P_2$	mp-9570	$P\bar{3}m1$	(#164)	21.7	23.7	OT1	1.881	1.881	1.881	-	0.26	0.82
341.	$Ba_3Si_2As_4$	mp-11692	$C2/c$	(#15)	21.6	22.8	OT2	1.157	1.157	1.387	-	0.39	1.05
342.	InP	mp-20351	$F\bar{4}3m$	(#216)	21.6	24.2	OT1	1.767	1.767	1.767	-	0.10	0.73
343.	$LiSrSb$	mp-7756	$Pnma$	(#62)	21.6	24.8	OT2	1.247	1.247	1.359	-	0.87	0.53
344.	$LiGaTe_2$	mp-5048	$I\bar{4}2d$	(#122)	21.6	22.3	OT1	2.008	2.008	2.008	-	0.32	0.49
345.	$GaGeTe$	mp-8211	$R\bar{3}m$	(#166)	21.6	25.3	OT1	1.228	1.229	1.229	5.6	0.11	1.02
346.	Ca_3AlAs_3	mp-17186	$Pnma$	(#62)	21.5	25.0	OT2	1.447	1.447	1.533	-	0.88	1.17
347.	$CsSnI_3$	mp-616378	$P4/mbm$	(#127)	21.4	24.0	OT1	1.796	1.796	1.796	2.9	0.70	0.17
348.	Ca_3GaAs_3	mp-541062	$Pnma$	(#62)	21.4	23.6	OT2	1.099	1.099	1.213	-	0.51	0.77
349.	$GeBi_2Te_4$	mp-27948	$R\bar{3}m$	(#166)	21.4	21.3	OT3	0.836	0.926	0.926	4.9	0.61	0.70
350.	$K_3Cs_6GaSb_4$	mp-541811	$P6_3/mmc$	(#194)	21.4	22.8	OT2	0.934	0.934	1.050	-	0.32	1.10
351.	$Ge_3As_2Te_6$	mp-541312	$R\bar{3}m$	(#166)	21.3	21.3	OT3	0.784	0.851	0.851	4.9	0.77	0.86
352.	In_5TlS_7	mp-562480	$P2_1/m$	(#11)	21.3	25.5	OT1	1.582	1.582	1.582	-	0.52	0.73
353.	$NaSn$	mp-11051	$I4_1/acd$	(#142)	21.3	21.5	OT3	0.696	0.715	0.715	-	0.31	0.25
354.	$GeSe_2$	mp-10074	$P\bar{4}$	(#81)	21.2	21.9	OT3	2.001	2.038	2.038	15.3	1.23	0.66
355.	GaP	mp-2490	$F\bar{4}3m$	(#216)	21.1	22.7	OT1	1.970	1.970	1.970	-	0.40	0.70
356.	Sc_2PbSe_4	mp-542826	$Pnma$	(#62)	21.1	22.8	OT4	1.495	1.595	1.782	-	0.73	0.99
357.	Mg_2BaBi_2	mp-29209	$P\bar{3}m1$	(#164)	21.1	21.9	OT1	0.696	0.696	0.696	-	0.08	0.46
358.	ZrI_2	mp-570506	$Pmn2_1$	(#31)	21.1	21.0	OT3	0.809	0.897	0.897	-	0.44	0.96
359.	$K_3AuP_2Se_8$	mp-866660	Cc	(#9)	21.1	23.7	OT1	1.857	1.857	1.857	-	0.62	1.40
360.	$LaZn_3As_3$	mp-866648	$Pnma$	(#62)	21.0	23.3	OT3	1.178	1.316	1.323	-	0.48	0.89
361.	$K_3Cs_6AlSb_4$	mp-17120	$P6_3/mmc$	(#194)	21.0	22.8	OT2	1.044	1.044	1.186	-	0.27	1.09
362.	$La_3AgSnSe_7$	mp-17155	$P6_3$	(#173)	21.0	22.7	OT4	1.758	1.846	1.959	-	0.54	1.48
363.	InP	mp-966800	$P6_3mc$	(#186)	21.0	23.8	OT1	1.763	1.763	1.763	5.9	0.11	0.88
364.	$Sr_{21}Cd_4Bi_{18}$	mp-582108	$C2/m$	(#12)	20.9	21.2	OT1	0.670	0.672	0.672	-	0.22	0.63
365.	$RhGeTe$	mp-607818	$Pbca$	(#61)	20.9	22.1	OT3	0.906	1.016	1.016	-	0.72	0.47
366.	ZrI_2	mp-571279	$P2_1/m$	(#11)	20.9	20.8	OT3	0.806	0.895	0.895	0.2	0.45	1.12
367.	$SrCu_2GeS_4$	mp-18685	$P3_2$	(#145)	20.8	22.8	OT1	1.934	1.940	1.940	-	0.23	1.00
368.	Na_8TiAs_4	mp-9071	$Fd\bar{3}m$	(#227)	20.8	22.1	OT2	1.312	1.312	1.607	-	0.70	1.16
369.	$ZnSiAs_2$	mp-3595	$I\bar{4}2d$	(#122)	20.7	23.6	OT1	1.835	1.835	1.835	-	0.15	0.36
370.	$GaTlSe_2$	mp-680555	Cc	(#9)	20.7	23.5	OT1	1.870	1.870	1.870	3.9	0.35	0.61
371.	Os_2Si_3	mp-16609	$P\bar{4}c2$	(#116)	20.7	22.6	OT4	1.402	1.473	1.670	30.4	1.05	0.50
372.	$HgIn_2Se_4$	mp-20731	$I\bar{4}$	(#82)	20.6	23.0	OT1	1.876	1.876	1.876	-	0.15	1.21
373.	$KSnAs$	mp-3481	$P6_3mc$	(#186)	20.6	22.6	OT3	0.984	1.103	1.103	-	0.15	0.56
374.	$GeTe$	mp-938	$R3m$	(#160)	20.6	21.0	OT3	0.957	1.152	1.152	-	0.32	0.33
375.	$Ca_5Sn_2As_6$	mp-18670	$Pbam$	(#55)	20.6	21.6	OT4	0.893	0.968	1.013	-	0.24	1.34
376.	Ag_3PSe_4	mp-30908	$Pmn2_1$	(#31)	20.6	23.0	OT2	1.448	1.448	1.554	-	0.15	1.22
377.	Ba_2PtH_6	mp-643253	$Cmca$	(#64)	20.4	20.5	OT3	2.087	2.110	2.110	-	0.37	1.27
378.	$BaCu_2S_2$	mp-5970	$Pnma$	(#62)	20.4	22.8	OT1	1.902	1.902	1.902	2.4	0.40	1.26
379.	InI	mp-23202	$Cmcm$	(#63)	20.4	21.7	OT1	2.028	2.028	2.028	-	0.22	0.27
380.	$RbAg_2SbS_4$	mp-17756	$P3_221$	(#154)	20.4	23.0	OT3	1.699	1.809	1.809	-	0.24	0.74
381.	$CdGeP_2$	mp-3668	$I\bar{4}2d$	(#122)	20.4	23.4	OT1	1.793	1.793	1.793	-	0.12	0.36
382.	Rb_2TeI_6	mp-28070	$P4/mnc$	(#128)	20.4	20.5	OT3	2.028	2.138	2.138	-	0.55	0.82
383.	$CuAlTe_2$	mp-8017	$I\bar{4}2d$	(#122)	20.3	22.6	OT1	1.934	1.934	1.934	-	0.15	0.56
384.	SrS_3	mp-1175	$Aea2$	(#41)	20.3	24.3	OT1	1.739	1.739	1.739	-	0.93	0.84
385.	NaK_2TlO_3	mp-560950	$P2_1/c$	(#14)	20.2	21.3	OT1	2.040	2.040	2.040	-	0.42	1.20
386.	$LiCaSb$	mp-16264	$Pnma$	(#62)	20.2	23.4	OT2	1.209	1.209	1.330	-	0.94	0.45
387.	$GaTlSe_2$	mp-17254	$C2/c$	(#15)	20.1	22.6	OT1	1.936	1.936	1.936	-	0.38	0.68
388.	Cu_2P_7	mp-28034	$C2/m$	(#12)	20.1	22.8	OT2	1.424	1.424	1.638	-	1.39	0.77

	Formula	Materials	Space		SLME (%)		Optical	Bandgap (eV)			ΔE_{hull}	m^* (m_0)	
		Project ID	Group		L=500 nm	L=1 μm	Type	E_g	E_g^{d}	E_g^{da}	(meV atom^{-1})	m_e^*	m_h^*
389.	$BaCu_4S_3$	mp-654109	$Pnma$	(#62)	20.1	23.2	OT1	1.787	1.787	1.787	19.3	0.29	1.11
390.	Sr_2GeN_2	mp-29089	$P4_2/mbc$	(#135)	20.1	20.0	OT2	0.684	0.684	0.729	-	1.38	1.43
391.	GaTe	mp-10009	$P6_3/mmc$	(#194)	20.1	24.0	OT3	1.460	1.549	1.549	4.0	0.41	0.78
392.	$Cu_2CdGeSe_4$	mp-10967	$I\bar{4}2m$	(#121)	20.1	21.0	OT2	1.163	1.163	1.436	-	0.12	1.09
393.	InTeI	mp-29234	$P2_1/c$	(#14)	20.0	20.3	OT1	2.108	2.108	2.108	-	0.38	1.42
394.	$RbCu_3S_2$	mp-10985	$C2/m$	(#12)	20.0	23.1	OT3	1.752	1.795	1.795	1.2	0.31	1.44
395.	Ag_3AuSe_2	mp-3172	$I4_132$	(#214)	19.9	21.0	OT2	1.240	1.240	1.523	-	0.20	0.97
396.	Na_5InTe_4	mp-28597	$Pbcn$	(#60)	19.9	22.4	OT1	1.923	1.923	1.923	-	0.29	1.10
397.	$MgGeP_2$	mp-34903	$I\bar{4}2d$	(#122)	19.8	21.2	OT4	1.963	2.000	2.081	13.0	1.15	0.44
398.	$AuTlPSe_3$	mp-569287	$C2/m$	(#12)	19.8	23.3	OT4	1.535	1.570	1.656	2.6	0.68	0.62
399.	$Na_2ZrCu_2S_4$	mp-556536	$C2/m$	(#12)	19.8	24.7	OT4	1.294	1.309	1.367	-	1.05	0.96
400.	In_6Se_7	mp-567596	$P2_1$	(#4)	19.8	22.0	OT2	0.979	0.979	1.104	42.8	0.33	0.35
401.	$Pb_4As_2S_6ClI$	mp-561299	$Pmn2_1$	(#31)	19.8	20.6	OT3	2.059	2.108	2.108	5.4	1.46	0.55
402.	$Ag_2In_2GeSe_6$	mp-505607	Cc	(#9)	19.8	23.1	OT1	1.632	1.632	1.632	17.3	0.22	1.48
403.	$TlPbI_3$	mp-27552	$Cmcm$	(#63)	19.8	20.6	OT1	2.087	2.087	2.087	11.4	0.74	0.92
404.	$NbTe_4I_6$	mp-570873	$P\bar{1}$	(#2)	19.7	23.4	OT4	1.479	1.573	1.604	-	0.69	1.42
405.	$AgGaSe_2$	mp-5518	$I\bar{4}2d$	(#122)	19.7	22.1	OT1	1.815	1.815	1.815	-	0.09	0.60
406.	$CdSiAs_2$	mp-3078	$I\bar{4}2d$	(#122)	19.6	22.8	OT1	1.722	1.722	1.722	-	0.07	0.30
407.	KCu_3S_2	mp-9868	$C2/m$	(#12)	19.6	22.6	OT3	1.733	1.809	1.809	1.5	0.32	1.31
408.	Ag_2S	mp-610517	$P2_1/c$	(#14)	19.6	22.1	OT4	1.858	1.940	1.955	23.6	0.50	1.21
409.	Ba_4P_3	mp-28823	$Pbam$	(#55)	19.5	21.4	OT4	1.176	1.283	1.418	-	0.94	1.04
410.	Sr_2VN_3	mp-17012	$C2/c$	(#15)	19.5	20.0	OT3	2.113	2.123	2.123	-	1.35	1.46
411.	$LaCuS_2$	mp-4841	$P2_1/c$	(#14)	19.2	21.0	OT1	2.038	2.038	2.038	-	0.54	0.35
412.	TcP_3	mp-28029	$Pnma$	(#62)	19.2	19.5	OT3	0.823	0.951	0.951	-	0.86	0.96
413.	Ba_3AlSb_3	mp-18439	$Cmca$	(#64)	19.2	19.7	OT2	0.732	0.732	0.799	-	0.67	1.05
414.	$Pb_5S_2I_6$	mp-23066	$C2/m$	(#12)	19.1	20.7	OT2	2.037	2.037	2.077	25.5	1.46	1.34
415.	$BTlS_2$	mp-8946	$R\bar{3}m$	(#166)	19.1	20.2	OT3	2.004	2.142	2.142	-	1.42	1.42
416.	Hg_3Te_2BrI	mp-571177	$C2$	(#5)	19.1	21.1	OT4	1.852	1.966	2.043	9.5	0.36	1.21
417.	Ca_3AlSb_3	mp-18300	$Pnma$	(#62)	19.1	21.7	OT2	0.988	0.988	1.086	-	1.05	0.78
418.	LiZnAs	mp-9124	$F\bar{4}3m$	(#216)	19.1	21.5	OT1	1.917	1.917	1.917	-	0.11	0.61
419.	$La_9Sb_{16}Br_3$	mp-567777	$P6_3/m$	(#176)	19.0	18.8	OT1	0.626	0.633	0.633	-	0.84	1.44
420.	K_2AgSbS_4	mp-553923	$Pnn2$	(#34)	19.0	21.6	OT1	1.940	1.940	1.940	11.9	0.44	0.69
421.	SiP_2	mp-9996	$Pbam$	(#55)	19.0	22.3	OT1	1.902	1.902	1.902	-	1.37	0.75
422.	LaTeCl	mp-1018752	$P4/nmm$	(#129)	18.9	22.9	OT2	1.427	1.427	1.535	-	0.57	1.47
423.	$BaSnS_2$	mp-12181	$P2_1/c$	(#14)	18.9	19.7	OT4	2.065	2.130	2.161	-	0.96	0.90
424.	BiSCl	mp-23318	$Pnma$	(#62)	18.9	20.3	OT4	2.008	2.090	2.125	-	0.99	1.35
425.	$GeAs_2Te_4$	mp-14790	$R\bar{3}m$	(#166)	18.9	18.7	OT3	0.827	0.968	0.968	8.4	0.27	0.29
426.	$MgSiAs_2$	mp-1016197	$I\bar{4}2d$	(#122)	18.8	21.1	OT2	1.926	1.926	2.037	0.1	0.40	0.40
427.	$Na_2Ge_2Se_5$	mp-18619	$Cmcm$	(#63)	18.8	19.8	OT3	2.095	2.126	2.126	6.8	0.35	1.23
428.	$CaIr_2P_2$	mp-11168	$P3_221$	(#154)	18.8	18.7	OT3	0.630	0.640	0.640	-	0.78	0.97
429.	InSe	mp-20485	$P6_3/mmc$	(#194)	18.8	22.3	OT1	1.779	1.779	1.779	1.4	0.13	1.43
430.	$CaO_7I_{10}H_{14}$	mp-721650	$P\bar{1}$	(#2)	18.7	20.3	OT2	2.000	2.001	2.110	11.7	0.14	1.37
431.	Rb_2AgSbS_4	mp-557540	$P2_1/c$	(#14)	18.7	20.1	OT2	2.015	2.015	2.118	-	0.47	1.45
432.	Ba_2GeP_2	mp-8194	$P2_1/c$	(#14)	18.7	19.5	OT3	0.961	1.172	1.172	-	0.83	0.57
433.	$Hg_3TlSb_2Br_3$	mp-571582	$Pbcm$	(#57)	18.7	21.4	OT3	1.776	1.895	1.895	-	0.25	0.62
434.	$Ta_2Ni_3Se_8$	mp-541509	$Pbam$	(#55)	18.6	18.7	OT4	0.788	0.854	0.911	-	0.40	0.98
435.	$Sr_3Al_2P_4$	mp-9843	$C2/c$	(#15)	18.6	21.3	OT2	1.889	1.889	1.998	-	1.02	1.06
436.	$CsLu_2Cu_3Se_5$	mp-581696	$Cmcm$	(#63)	18.6	20.1	OT1	2.078	2.078	2.078	-	0.98	1.17
437.	$GaIn_2BiS_6$	mp-556231	$P2_1/m$	(#11)	18.5	19.4	OT3	2.114	2.159	2.159	2.7	0.97	0.89
438.	Sb_2OS_2	mp-28711	$P\bar{1}$	(#2)	18.5	20.8	OT1	2.007	2.016	2.016	1.5	0.24	0.70
439.	Sc_2PbS_4	mp-22630	$Pnma$	(#62)	18.5	19.9	OT4	1.920	2.017	2.164	7.6	0.87	0.82
440.	$NaTe_3$	mp-28478	$P\bar{3}c1$	(#165)	18.5	18.5	OT3	0.705	0.783	0.783	-	0.35	0.82
441.	$ZrTe_5$	mp-605	$Cmcm$	(#63)	18.5	18.3	OT3	0.685	0.761	0.761	-	0.25	0.05

	Formula	Materials	Space		SLME (%)		Optical	Bandgap (eV)			ΔE_{hull}	m^* (m_0)	
		Project ID	Group		L=500 nm	L=1 μm	Type	E_g	E_g^{d}	E_g^{da}	(meV atom^{-1})	m_e^*	m_h^*
442.	$\mathrm{InBi_2S_4Cl}$	mp-559521	$C2/m$	(#12)	18.4	19.8	OT3	2.030	2.150	2.150	0.8	0.34	0.68
443.	$\mathrm{In_2Se_3}$	mp-612740	$P6_1$	(#169)	18.3	20.7	OT1	1.985	1.985	1.985	-	0.18	1.44
444.	LaCuOTe	mp-546790	$P4/nmm$	(#129)	18.3	20.5	OT2	2.001	2.001	2.052	6.9	1.07	1.24
445.	$\mathrm{HgGa_2Se_4}$	mp-4730	$I\bar{4}$	(#82)	18.1	20.1	OT1	2.049	2.049	2.049	-	0.17	1.09
446.	$\mathrm{CaZn_2As_2}$	mp-9571	$P\bar{3}m1$	(#164)	18.1	21.8	OT2	1.572	1.572	1.644	-	0.75	0.46
447.	$\mathrm{KInSnSe_4}$	mp-568379	$P2_1/c$	(#14)	18.1	19.5	OT1	2.117	2.117	2.117	-	0.28	0.73
448.	$\mathrm{La_3CI_5}$	mp-568591	$P\bar{1}$	(#2)	18.1	18.5	OT3	0.699	0.773	0.773	-	0.94	1.00
449.	$\mathrm{Ca_3Si_2As_4}$	mp-540696	$P2_1/c$	(#14)	18.0	20.6	OT2	1.377	1.377	1.667	-	0.74	0.59
450.	LiZnSb	mp-9919	$P6_3mc$	(#186)	18.0	19.7	OT2	1.148	1.148	1.415	-	0.44	0.36
451.	$\mathrm{Ag_3AuS_2}$	mp-27554	$P4_132$	(#213)	18.0	19.9	OT2	1.436	1.436	1.707	22.5	0.25	0.68
452.	$\mathrm{TlGeI_3}$	mp-29288	$Pnma$	(#62)	18.0	18.7	OT3	2.147	2.204	2.204	14.2	0.61	0.69
453.	$\mathrm{BTl_3O_3}$	mp-4584	$P6_3/m$	(#176)	18.0	20.2	OT4	1.937	1.976	2.090	-	0.45	1.44
454.	$\mathrm{Pb_3O_4}$	mp-21452	$Pbam$	(#55)	18.0	20.0	OT3	2.049	2.087	2.087	0.4	0.47	1.39
455.	$\mathrm{Tl_4SnS_3}$	mp-9622	$P4/ncc$	(#130)	17.9	20.0	OT4	1.289	1.317	1.580	34.1	0.37	0.85
456.	$\mathrm{K_2TeI_6}$	mp-27688	$P2_1/c$	(#14)	17.9	18.0	OT3	2.150	2.273	2.273	-	0.84	0.91
457.	$\mathrm{AgInS_2}$	mp-19833	$I\bar{4}2d$	(#122)	17.9	20.3	OT1	1.932	1.932	1.932	-	0.15	0.80
458.	$\mathrm{K_3GeSe_3}$	mp-14435	$C2/m$	(#12)	17.9	18.1	OT3	2.191	2.223	2.223	-	0.88	0.52
459.	$\mathrm{Ag_4CdGe_2S_7}$	mp-542200	Cc	(#9)	17.9	20.1	OT3	1.939	2.002	2.002	1.5	1.37	1.20
460.	SiAs	mp-1863	$C2/m$	(#12)	17.9	20.4	OT3	1.918	2.071	2.071	-	0.77	0.41
461.	$\mathrm{Sr_5As_3H}$	mp-24338	$P6_3/mcm$	(#193)	17.8	20.9	OT2	1.425	1.425	1.644	-	1.34	0.32
462.	$\mathrm{CuInSe_2}$	mp-22811	$I\bar{4}2d$	(#122)	17.8	19.0	OT2	1.285	1.285	1.627	-	0.12	0.98
463.	OsSi	mp-2488	$P2_13$	(#198)	17.7	17.7	OT3	0.654	0.707	0.707	11.9	1.05	0.77
464.	RbTe	mp-8360	$Pbam$	(#55)	17.7	19.3	OT4	1.175	1.278	1.475	25.6	0.55	1.03
465.	NaCdAs	mp-7378	$Pnma$	(#62)	17.7	19.2	OT2	1.270	1.272	1.579	-	0.14	1.32
466.	$\mathrm{CdSnAs_2}$	mp-3829	$I\bar{4}2d$	(#122)	17.6	18.7	OT4	1.199	1.246	1.522	-	0.13	0.25
467.	$\mathrm{As_5Te_7I}$	mp-541032	Cm	(#8)	17.6	17.9	OT3	0.889	1.098	1.098	28.3	0.22	0.64
468.	SbSBr	mp-22971	$Pna2_1$	(#33)	17.5	18.3	OT3	2.185	2.213	2.213	-	1.08	0.94
469.	$\mathrm{SrIr_2P_2}$	mp-15074	$P3_221$	(#154)	17.5	17.4	OT1	0.590	0.594	0.594	-	0.76	0.96
470.	$\mathrm{Ge_5As_2Te_8}$	mp-28487	$P\bar{3}m1$	(#164)	17.5	17.4	OT3	0.762	0.896	0.896	16.8	0.53	0.34
471.	$\mathrm{Ag_2In_2SiSe_6}$	mp-640614	Cc	(#9)	17.4	20.5	OT1	1.784	1.784	1.784	9.2	0.20	1.49
472.	$\mathrm{Na_3SbSe_4}$	mp-8703	$I\bar{4}3m$	(#217)	17.4	20.2	OT2	1.520	1.520	1.813	-	0.59	1.20
473.	AlAs	mp-8881	$P6_3mc$	(#186)	17.3	19.3	OT2	2.056	2.056	2.146	6.3	0.41	0.95
474.	$\mathrm{Ca_3Ge_2P_4}$	mp-17817	$P2_1/c$	(#14)	17.3	19.8	OT4	1.340	1.391	1.642	-	1.07	0.61
475.	$\mathrm{LiNa_2AlP_2}$	mp-9719	$Cmca$	(#64)	17.2	18.2	OT3	2.190	2.212	2.212	-	0.86	1.44
476.	$\mathrm{Ag_8GeS_6}$	mp-9770	$Pna2_1$	(#33)	17.2	19.6	OT1	2.013	2.013	2.013	-	0.22	1.38
477.	$\mathrm{MnP_4}$	mp-487	$P\bar{1}$	(#2)	17.1	18.2	OT4	0.963	1.075	1.190	0.3	0.73	1.38
478.	$\mathrm{CsLa_2CuSe_4}$	mp-505815	$Cmcm$	(#63)	17.1	21.6	OT4	1.726	1.769	1.805	-	1.16	1.37
479.	$\mathrm{Tl_6SeI_4}$	mp-28517	$P4/mnc$	(#128)	16.9	18.5	OT1	2.169	2.169	2.169	-	0.47	0.76
480.	$\mathrm{TlPS_3}$	mp-8249	$Immm$	(#71)	16.9	18.5	OT2	2.146	2.146	2.167	-	0.85	1.26
481.	$\mathrm{CdSb_6S_8I_4}$	mp-560411	$P\bar{1}$	(#2)	16.9	18.1	OT3	2.159	2.234	2.234	2.7	0.51	0.56
482.	$\mathrm{Tl_5Se_2Br}$	mp-28921	$I4/mcm$	(#140)	16.9	19.1	OT2	1.160	1.160	1.400	-	0.28	0.39
483.	$\mathrm{In_3SnI_5}$	mp-568493	$P2_1/c$	(#14)	16.8	16.9	OT1	2.268	2.276	2.276	0.3	0.60	1.04
484.	$\mathrm{Hg_3TlAs_2Cl_3}$	mp-628647	$Pbcm$	(#57)	16.8	19.3	OT3	1.951	2.070	2.070	-	0.34	0.70
485.	CoGeTe	mp-3715	$Pbca$	(#61)	16.8	17.4	OT4	0.708	0.781	0.820	-	1.25	0.56
486.	$\mathrm{Ga_2Pb_2S_5}$	mp-557672	$Pbca$	(#61)	16.8	17.5	OT4	2.132	2.230	2.318	-	0.68	0.58
487.	$\mathrm{MgP_4}$	mp-384	$P2_1/c$	(#14)	16.7	20.3	OT4	1.345	1.494	1.552	-	1.32	0.39
488.	TlI	mp-22858	$Cmcm$	(#63)	16.7	17.2	OT3	2.240	2.263	2.263	23.3	0.32	0.46
489.	$\mathrm{BaHgS_2}$	mp-28007	$Pmc2_1$	(#26)	16.6	17.6	OT3	2.198	2.239	2.239	-	0.54	1.32
490.	$\mathrm{Rb_4Pb_9}$	mp-680463	$P2_1/m$	(#11)	16.6	16.5	OT1	0.547	0.547	0.547	-	0.72	0.34
491.	$\mathrm{In_3SnI_5}$	mp-568522	$P2_1/c$	(#14)	16.5	16.6	OT3	2.282	2.292	2.292	-	0.86	1.19
492.	KSnSb	mp-3486	$P6_3mc$	(#186)	16.5	17.6	OT3	0.795	0.932	0.932	-	0.14	0.43
493.	$\mathrm{ZnSnAs_2}$	mp-5190	$I\bar{4}2d$	(#122)	16.5	18.4	OT2	1.313	1.313	1.581	-	0.06	0.76
494.	$\mathrm{In_4GeS_4}$	mp-556528	$Pa\bar{3}$	(#205)	16.4	17.9	OT1	2.184	2.184	2.184	-	0.18	1.25

	Formula	Materials Project ID	Space Group		SLME (%)		Optical Type	Bandgap (eV)			ΔE_{hull}	m^* (m_0)	
					L=500 nm	L=1 μm		E_g	E_g^{d}	E_g^{da}	(meV atom^{-1})	m_e^*	m_h^*
495.	$Ge_4As_2Te_7$	mp-568730	$R\bar{3}m$	(#166)	16.4	16.3	OT3	0.749	0.894	0.894	7.0	0.62	0.46
496.	$TaTlSe_3$	mp-12027	$Pnma$	(#62)	16.4	16.4	OT3	0.717	0.837	0.840	21.0	1.32	0.67
497.	$BaSc_2Te_4$	mp-17501	$Pnma$	(#62)	16.3	18.0	OT2	0.988	0.988	1.199	2.0	0.83	1.03
498.	Na_4SnSe_4	mp-28768	$P\bar{4}2_1c$	(#114)	16.3	18.3	OT1	2.145	2.145	2.145	-	0.30	1.34
499.	BaY_2Te_4	mp-17872	$Pnma$	(#62)	16.1	19.3	OT2	1.373	1.373	1.647	-	0.68	0.92
500.	$CsLuCdTe_3$	mp-12492	$Cmcm$	(#63)	16.0	18.0	OT1	2.170	2.170	2.170	-	1.45	1.42
501.	$CdIn_2Se_4$	mp-22304	$I\bar{4}$	(#82)	16.0	17.7	OT1	2.174	2.174	2.174	-	0.17	1.40
502.	Y_2HfS_5	mp-16919	$Pnma$	(#62)	16.0	19.5	OT1	1.980	1.980	1.980	12.3	0.77	0.64
503.	$Na_7In_3Se_8$	mp-541689	$P\bar{1}$	(#2)	15.9	18.1	OT1	2.124	2.124	2.124	-	0.22	1.04
504.	LiCaBi	mp-569501	$Pnma$	(#62)	15.9	16.7	OT2	0.765	0.765	0.902	-	0.82	0.45
505.	$CuAg_3S_2$	mp-5725	$I4_1/amd$	(#141)	15.9	19.1	OT2	1.617	1.617	1.735	43.4	0.47	1.22
506.	$Sr_3Tl_2O_6$	mp-31355	$Pbam$	(#55)	15.8	18.6	OT1	1.936	1.940	1.940	-	0.37	1.11
507.	$AgAlTe_2$	mp-14092	$I\bar{4}2d$	(#122)	15.8	18.0	OT1	2.137	2.137	2.137	-	0.15	0.51
508.	$SrZrSe_3$	mp-541570	$Pnma$	(#62)	15.8	18.7	OT2	1.121	1.121	1.311	27.5	0.93	0.60
509.	$HgTl_4I_6$	mp-27375	$P4/mnc$	(#128)	15.6	18.3	OT2	1.869	1.869	2.089	23.1	0.71	0.57
510.	$Li_2B_2Se_5$	mp-30100	$C2/c$	(#15)	15.5	16.4	OT4	2.187	2.337	2.362	-	1.19	1.07
511.	Ca_4TiN_4	mp-568469	$P\bar{1}$	(#2)	15.5	17.9	OT3	2.063	2.183	2.183	-	0.54	1.24
512.	Ag_8SiS_6	mp-7614	$Pna2_1$	(#33)	15.5	17.7	OT1	2.125	2.125	2.125	-	0.26	1.36
513.	$CuGaS_2$	mp-5238	$I\bar{4}2d$	(#122)	15.4	17.8	OT1	2.108	2.108	2.108	1.1	0.18	0.73
514.	Sr_2Sn	mp-978	$Pnma$	(#62)	15.4	15.7	OT2	0.634	0.634	0.714	-	0.45	1.32
515.	$BaLaCuTe_3$	mp-17063	$Pnma$	(#62)	15.4	18.2	OT2	1.473	1.473	1.797	-	0.74	0.98
516.	$BaGa_2Sb_2$	mp-29938	$Pnma$	(#62)	15.4	15.3	OT3	0.637	0.759	0.759	-	0.91	0.21
517.	$Na_2Ga_3Sb_3$	mp-28413	$Pnma$	(#62)	15.4	16.0	OT4	0.868	0.988	1.093	-	0.19	0.40
518.	$NaLaGa_4Se_8$	mp-569491	$Fddd$	(#70)	15.3	17.1	OT2	2.096	2.096	2.306	-	1.04	1.23
519.	InTeBr	mp-29236	$P2_1/c$	(#14)	15.2	15.9	OT1	2.311	2.311	2.311	-	0.28	1.40
520.	Ba_3P_4	mp-14289	$Fdd2$	(#43)	15.2	16.0	OT2	0.909	0.909	1.157	-	0.85	0.97
521.	TlBr	mp-22875	$Pm\bar{3}m$	(#221)	15.1	15.8	OT1	2.318	2.318	2.318	45.2	0.25	0.48
522.	InI_2	mp-29312	$Pnna$	(#52)	15.0	16.7	OT4	2.187	2.245	2.284	-	0.59	1.33
523.	$K_2Pb_2O_3$	mp-20694	$I2_13$	(#199)	15.0	16.1	OT3	2.219	2.356	2.356	-	1.35	0.40
524.	$BaAl_2Te_4$	mp-28505	$P4/nbm$	(#125)	14.9	18.4	OT1	2.056	2.056	2.056	-	0.33	0.95
525.	$CdAl_2Te_4$	mp-7909	$I\bar{4}$	(#82)	14.8	15.8	OT1	2.311	2.311	2.311	-	0.23	1.36
526.	$Ba_2LaAg_5S_6$	mp-553874	$C2/m$	(#12)	14.8	16.5	OT1	2.244	2.244	2.244	-	0.70	1.09
527.	Sr_3GaSb_3	mp-542625	$P2_1/c$	(#14)	14.8	15.5	OT4	0.774	0.862	0.942	-	0.42	0.39
528.	TlI	mp-571102	$Fm\bar{3}m$	(#225)	14.8	15.4	OT1	2.337	2.337	2.337	-	0.34	0.49
529.	$AgInP_2Se_6$	mp-20902	$P\bar{3}1c$	(#163)	14.7	17.7	OT4	1.483	1.622	1.738	-	0.30	0.87
530.	$ScYS_3$	mp-7792	$Pnma$	(#62)	14.7	15.6	OT3	2.277	2.382	2.382	7.6	1.48	1.12
531.	$Rb_2Sn_2O_3$	mp-7863	$R\bar{3}m$	(#166)	14.6	15.9	OT1	2.291	2.291	2.291	-	0.50	0.32
532.	CdTe	mp-406	$F\bar{4}3m$	(#216)	14.6	16.6	OT1	2.186	2.186	2.186	-	0.12	0.83
533.	$CaZn_2P_2$	mp-9569	$P\bar{3}m1$	(#164)	14.6	18.3	OT4	1.804	1.904	1.969	-	0.84	0.56
534.	$BaAg_2S_2$	mp-8579	$P\bar{3}m1$	(#164)	14.6	16.5	OT1	2.220	2.220	2.220	-	0.22	0.96
535.	Sc_2CdS_4	mp-10953	$Fd\bar{3}m$	(#227)	14.5	18.4	OT1	2.052	2.052	2.052	-	0.32	1.04
536.	RbAuTe	mp-9008	$Pmma$	(#51)	14.5	17.0	OT2	1.817	1.817	2.183	-	0.83	0.82
537.	$RbInSe_2$	mp-31309	$C2/c$	(#15)	14.5	16.1	OT2	2.252	2.252	2.293	-	0.22	1.15
538.	Tl_6SI_4	mp-27938	$P4/mnc$	(#128)	14.5	16.3	OT1	2.264	2.264	2.264	-	0.49	0.66
539.	KPS_3	mp-8267	$Immm$	(#71)	14.4	16.6	OT2	2.194	2.198	2.222	-	0.75	1.13
540.	$LiAg_3O_2$	mp-27227	$Ibam$	(#72)	14.4	17.6	OT2	1.752	1.752	1.959	-	1.16	1.41
541.	$InTlSe_2$	mp-22232	$I4/mcm$	(#140)	14.3	17.9	OT2	1.555	1.555	1.815	-	0.45	1.11
542.	K_3AuSn_4	mp-18500	$Pmmn$	(#59)	14.3	14.1	OT3	0.597	0.669	0.669	-	0.68	0.65
543.	$Hg_3Se_2I_2$	mp-571404	$C2/m$	(#12)	14.1	16.3	OT4	2.099	2.118	2.273	4.5	0.24	1.24
544.	Ge_3As_4	mp-569600	$P\bar{4}3m$	(#215)	14.1	14.8	OT4	0.812	0.934	1.027	49.8	0.31	1.27
545.	$SrZrS_3$	mp-558760	$Pnma$	(#62)	14.0	17.8	OT2	1.538	1.538	1.724	-	0.86	0.81
546.	Ca_3AsBr_3	mp-27294	$Pm\bar{3}m$	(#221)	14.0	14.5	OT1	2.387	2.387	2.387	-	0.64	0.53
547.	GaP	mp-8882	$P6_3mc$	(#186)	14.0	16.9	OT2	1.893	1.893	2.203	9.9	0.49	0.74

	Formula	Materials	Space		SLME (%)		Optical	Bandgap (eV)			ΔE_{hull}	m^* (m_0)	
		Project ID	Group		L=500 nm	L=1 μm	Type	E_g	E_g^{d}	E_g^{da}	(meV atom^{-1})	m_e^*	m_h^*
548.	$AgTlI_2$	mp-27801	$I4/mcm$	(#140)	14.0	16.7	OT4	2.088	2.156	2.226	31.9	0.50	1.40
549.	Tl_2SnTe_3	mp-28662	$Pnma$	(#62)	13.9	14.1	OT4	0.824	0.980	1.060	-	0.53	0.43
550.	$K_2Sn_2O_3$	mp-7502	$R\bar{3}m$	(#166)	13.7	14.9	OT1	2.342	2.342	2.342	8.2	0.51	0.32
551.	$CsIn_5S_8$	mp-22007	$C2/m$	(#12)	13.7	16.2	OT4	2.084	2.203	2.248	1.2	0.21	1.45
552.	Al_3Te_3I	mp-28693	$Pnma$	(#62)	13.7	14.7	OT3	2.357	2.394	2.394	-	1.43	1.30
553.	$SrSc_2Te_4$	mp-18660	$Pnma$	(#62)	13.7	15.0	OT2	1.080	1.080	1.422	18.6	0.97	0.72
554.	$InTlS_2$	mp-865274	$C2/c$	(#15)	13.6	16.1	OT1	2.230	2.230	2.230	-	0.30	0.67
555.	CaSrPb	mp-21166	$Pnma$	(#62)	13.6	13.4	OT1	0.480	0.481	0.481	-	0.79	1.31
556.	$CdIn_4I_6$	mp-616218	$P4/mnc$	(#128)	13.5	15.3	OT2	2.259	2.259	2.353	7.7	0.38	0.97
557.	$RbPS_3$	mp-556953	$Immm$	(#71)	13.5	15.3	OT2	2.264	2.270	2.306	-	0.96	1.31
558.	$VBiO_4$	mp-504878	$C2/c$	(#15)	13.5	13.5	OT3	2.429	2.473	2.473	16.4	0.96	0.52
559.	$AlTlSe_2$	mp-867359	$C2/c$	(#15)	13.4	15.6	OT4	2.153	2.254	2.357	-	0.49	0.72
560.	$Hg_7O_3Cl_2$	mp-541193	$Pbcm$	(#57)	13.3	15.7	OT2	2.155	2.155	2.261	-	0.58	1.44
561.	Cd_4GeSe_6	mp-18163	Cc	(#9)	13.2	15.6	OT1	2.181	2.181	2.181	22.6	0.19	1.02
562.	$MgSc_2S_4$	mp-14307	$Fd\bar{3}m$	(#227)	13.2	15.5	OT2	2.172	2.172	2.344	-	0.62	1.09
563.	Cu_6PS_5Br	mp-554627	Cc	(#9)	13.2	16.5	OT1	2.053	2.053	2.053	1.1	0.58	1.09
564.	Cu_2PbO_2	mp-29396	$C2/c$	(#15)	12.9	16.2	OT4	1.672	1.816	1.925	-	0.41	1.46
565.	SbI_3	mp-569224	$P2_1/c$	(#14)	12.9	12.9	OT4	2.455	2.503	2.517	47.3	1.04	1.30
566.	CdTe	mp-12779	$P6_3mc$	(#186)	12.9	14.9	OT1	2.258	2.258	2.258	4.0	0.12	1.07
567.	$RuSi_2$	mp-569815	$Cmca$	(#64)	12.8	14.7	OT4	1.321	1.465	1.768	-	0.53	0.23
568.	$Ba_3Bi_2O_9Te$	mp-556407	$P\bar{3}c1$	(#165)	12.7	13.1	OT4	2.395	2.448	2.570	-	0.58	0.94
569.	$La_{17}Al_4Si_9N_{33}$	mp-866690	$F\bar{4}3m$	(#216)	12.6	14.0	OT2	2.334	2.334	2.453	-	1.38	0.99
570.	$In_2P_3S_9$	mp-27753	$P2_1/c$	(#14)	12.6	15.7	OT4	2.119	2.136	2.177	-	0.37	0.87
571.	Nb_3I_8	mp-27772	$R\bar{3}m$	(#166)	12.4	12.1	OT3	0.491	0.523	0.523	-	0.90	1.47
572.	$LiInSe_2$	mp-20187	$I\bar{4}2d$	(#122)	12.4	13.3	OT1	2.437	2.437	2.437	-	0.27	0.87
573.	$HgPS_3$	mp-27178	$P\bar{1}$	(#2)	12.4	13.5	OT4	2.352	2.496	2.516	-	0.69	1.45
574.	MgSrSi	mp-15642	$Pnma$	(#62)	12.4	12.0	OT3	0.462	0.495	0.495	-	0.40	0.45
575.	$CdSnSb_2$	mp-10063	$I\bar{4}2d$	(#122)	12.3	12.6	OT4	0.906	0.917	1.256	-	0.08	0.24
576.	$CdSiP_2$	mp-4666	$I\bar{4}2d$	(#122)	12.3	14.2	OT2	2.166	2.166	2.517	-	0.46	0.40
577.	$BaLaCuSe_3$	mp-541430	$Pnma$	(#62)	12.3	14.9	OT2	1.970	1.970	2.313	-	0.79	1.35
578.	$KInP_2S_7$	mp-22583	$C2$	(#5)	12.2	13.2	OT1	2.445	2.445	2.445	-	1.35	1.46
579.	Tl_2GeTe_3	mp-29034	$Pnma$	(#62)	12.2	12.1	OT4	0.751	0.836	0.978	-	0.50	0.40
580.	$MgPSe_3$	mp-30943	$R\bar{3}$	(#148)	12.1	13.0	OT2	2.433	2.434	2.503	-	0.50	0.65
581.	$RbIn_5S_8$	mp-20938	$C2/m$	(#12)	12.0	14.6	OT3	2.175	2.321	2.321	0.6	0.20	1.49
582.	$CsPbBr_3$	mp-567629	$Pnma$	(#62)	12.0	12.9	OT1	2.460	2.460	2.460	-	0.96	0.30
583.	$BaGe_2P_2$	mp-27809	$P4_2mc$	(#105)	12.0	13.5	OT4	1.229	1.332	1.687	-	0.48	0.37
584.	$NaInTe_2$	mp-22483	$I4/mcm$	(#140)	11.9	14.1	OT4	1.281	1.429	1.710	-	0.26	0.78
585.	Tl_2SiS_3	mp-8190	$P\bar{1}$	(#2)	11.9	12.4	OT3	2.451	2.564	2.564	-	1.45	0.89
586.	NaSb	mp-7944	$P2_1/c$	(#14)	11.9	11.8	OT3	0.742	0.968	0.968	-	0.79	0.49
587.	MgY_2Se_4	mp-15803	$Fd\bar{3}m$	(#227)	11.9	15.8	OT1	2.091	2.091	2.091	-	0.39	1.01
588.	$ZnCdTe_2$	mp-971837	$I\bar{4}2d$	(#122)	11.8	13.8	OT1	2.324	2.324	2.324	4.7	0.12	0.85
589.	$GaTlS_2$	mp-4016	$C2/c$	(#15)	11.8	13.8	OT4	2.294	2.397	2.453	-	0.55	0.79
590.	$Rb_2Hg_3Sn_2S_8$	mp-561434	$P2_1/c$	(#14)	11.7	12.6	OT3	2.452	2.506	2.506	-	0.42	1.41
591.	CsAuTe	mp-573755	$Pmma$	(#51)	11.6	14.8	OT2	2.057	2.057	2.252	-	0.64	0.88
592.	La_3NS_3	mp-555129	$Pnma$	(#62)	11.6	14.5	OT4	1.966	2.014	2.293	-	0.65	0.86
593.	Tl_6SBr_4	mp-28518	$P4/mnc$	(#128)	11.6	12.9	OT2	2.426	2.426	2.495	0.9	0.48	0.80
594.	$MoBi_2O_6$	mp-567326	$Cmca$	(#64)	11.5	13.9	OT4	1.983	2.071	2.259	45.5	1.42	0.76
595.	CaTe	mp-569170	$Pnma$	(#62)	11.5	13.8	OT2	2.168	2.168	2.471	34.3	0.74	0.63
596.	$K_{12}In_2Se_9$	mp-570411	$P2_1/c$	(#14)	11.5	12.9	OT1	2.439	2.439	2.439	-	0.32	1.47
597.	KIn_5S_8	mp-22199	$C2/m$	(#12)	11.5	14.0	OT3	2.215	2.335	2.335	2.6	0.20	1.44
598.	$KAlTe_2$	mp-18347	$C2/c$	(#15)	11.4	13.1	OT2	2.343	2.343	2.537	-	0.31	0.81
599.	CaSrSn	mp-20726	$Pnma$	(#62)	11.4	11.5	OT2	0.697	0.700	0.904	-	0.52	1.26
600.	La_3GaOS_5	mp-561076	$Pnma$	(#62)	11.4	14.6	OT2	2.075	2.075	2.232	-	0.73	1.14

	Formula	Materials	Space		SLME (%)		Optical	Bandgap (eV)			ΔE_{hull}	m^* (m_0)	
		Project ID	Group		L=500 nm	L=1 μm	Type	E_g	E_g^{d}	E_g^{da}	(meV atom^{-1})	m_e^*	m_h^*
601.	$CdGa_2Se_4$	mp-3772	$I\bar{4}$	(#82)	11.3	12.5	OT1	2.465	2.465	2.465	-	0.18	1.32
602.	ZnTe	mp-2176	$F\bar{4}3m$	(#216)	11.2	12.9	OT1	2.418	2.418	2.418	-	0.13	0.76
603.	Na_3SbS_4	mp-10167	$I\bar{4}3m$	(#217)	11.2	12.6	OT4	2.340	2.361	2.616	-	0.46	1.45
604.	La_2S_3	mp-7475	$Pnma$	(#62)	11.2	14.2	OT2	1.787	1.787	2.192	-	0.52	0.84
605.	Tl_6SCl_4	mp-28242	$P4/mnc$	(#128)	11.2	12.4	OT2	2.427	2.427	2.553	11.2	0.47	0.93
606.	$BaSe_2$	mp-7547	$C2/c$	(#15)	11.1	11.5	OT4	0.795	0.897	1.061	-	0.19	1.34
607.	Ta_4SiTe_4	mp-28509	$Pbam$	(#55)	11.1	10.9	OT4	0.556	0.599	0.676	-	0.14	0.19
608.	$CuAlSe_2$	mp-8016	$I\bar{4}2d$	(#122)	11.1	13.2	OT1	2.332	2.332	2.332	-	0.16	0.75
609.	$CdTl_4I_6$	mp-570339	$P4/mnc$	(#128)	11.0	12.0	OT2	2.412	2.412	2.674	14.3	0.81	0.66
610.	$NaSr_2AlP_3$	mp-620652	$C2/m$	(#12)	10.9	14.3	OT2	1.284	1.284	1.562	-	1.10	1.46
611.	LaAgOS	mp-6625	$P4/nmm$	(#129)	10.9	12.4	OT1	2.452	2.452	2.452	1.3	0.39	1.12
612.	Ca_3AsCl_3	mp-28069	$Pm\bar{3}m$	(#221)	10.9	11.3	OT1	2.561	2.561	2.561	-	0.70	0.56
613.	ZnTe	mp-8884	$P6_3mc$	(#186)	10.7	12.6	OT1	2.419	2.419	2.419	6.3	0.14	0.91
614.	CdSe	mp-2691	$F\bar{4}3m$	(#216)	10.6	12.3	OT1	2.415	2.415	2.415	-	0.12	1.01
615.	$CdTl_2GeTe_4$	mp-568890	$I\bar{4}2m$	(#121)	10.6	11.1	OT4	0.886	0.961	1.224	5.5	0.14	1.27
616.	YZnPO	mp-12509	$R\bar{3}m$	(#166)	10.6	13.5	OT4	2.243	2.311	2.358	-	0.70	1.22
617.	ZrNI	mp-23052	$Pmmn$	(#59)	10.6	12.8	OT1	2.389	2.389	2.389	-	0.45	1.09
618.	Ca_3PCl_3	mp-29342	$Pm\bar{3}m$	(#221)	10.5	10.9	OT1	2.579	2.579	2.579	-	0.69	0.60
619.	$CuBSe_2$	mp-983565	$I\bar{4}2d$	(#122)	10.5	12.3	OT2	2.343	2.343	2.591	-	0.53	0.48
620.	LaP_5	mp-645421	$P2_1/m$	(#11)	10.4	10.5	OT2	0.699	0.699	0.946	-	0.38	0.50
621.	Ba_2TiS_4	mp-17908	$Pnma$	(#62)	10.4	10.9	OT2	2.525	2.525	2.701	-	1.25	1.48
622.	$AgGaS_2$	mp-5342	$I\bar{4}2d$	(#122)	10.3	12.3	OT1	2.396	2.396	2.396	-	0.18	0.93
623.	LaSeF	mp-7738	$P6_3/mmc$	(#194)	10.1	11.2	OT1	2.546	2.546	2.546	-	0.53	0.95
624.	C	mp-569416	$R\bar{3}m$	(#166)	10.0	10.3	OT1	2.613	2.613	2.613	27.5	0.08	0.09
625.	Ca_2Si	mp-2517	$Pnma$	(#62)	9.8	10.1	OT2	0.800	0.800	1.104	-	0.50	1.37
626.	TlBr	mp-568949	$Cmcm$	(#63)	9.7	10.4	OT1	2.596	2.596	2.596	22.6	0.28	0.41
627.	$AgGaS_2$	mp-556916	Cc	(#9)	9.7	11.6	OT1	2.441	2.441	2.441	2.6	0.19	1.19
628.	Ca_2Pb	mp-30478	$Pnma$	(#62)	9.6	9.1	OT3	0.383	0.398	0.398	-	0.36	0.60
629.	$LiBiO_2$	mp-28253	$Ibam$	(#72)	9.6	9.8	OT1	2.633	2.635	2.635	-	0.22	0.55
630.	Zn_3P_2	mp-2071	$P4_2/nmc$	(#137)	9.6	12.0	OT2	1.557	1.557	1.987	-	0.23	0.88
631.	Y_2CdS_4	mp-35785	$Fd\bar{3}m$	(#227)	9.5	12.6	OT1	2.346	2.346	2.346	-	0.27	1.22
632.	$NaAlTe_2$	mp-10163	$I4/mcm$	(#140)	9.4	12.0	OT2	1.998	1.998	2.536	-	0.32	1.29
633.	Tl_2O_3Te	mp-543028	$Pban$	(#50)	9.4	10.9	OT1	2.545	2.545	2.545	-	0.76	1.49
634.	Cu_3N^*	mp-1933	$Pm\bar{3}m$	(#221)	9.4	10.6	OT4	1.492	2.032	2.110	189.8	0.93	0.90
635.	TlBr	mp-568560	$Fm\bar{3}m$	(#225)	9.3	9.8	OT1	2.635	2.635	2.635	-	0.36	0.49
636.	Cd_4SiSe_6	mp-17791	Cc	(#9)	9.3	11.3	OT1	2.407	2.407	2.407	13.5	0.18	1.05
637.	$MgSiP_2$	mp-2961	$I\bar{4}2d$	(#122)	9.2	11.9	OT2	2.122	2.122	2.565	-	0.39	0.45
638.	$Ag_{15}P_4S_{16}Cl_3$	mp-560328	$I\bar{4}3d$	(#220)	9.2	11.3	OT4	2.339	2.418	2.542	-	0.25	1.20
639.	PbFI	mp-22969	$P4/nmm$	(#129)	9.2	11.3	OT2	2.395	2.395	2.638	21.0	0.61	1.32
640.	Ca_2As_3	mp-31010	$P2/c$	(#13)	9.1	9.0	OT4	0.743	0.966	1.041	-	1.18	1.32
641.	AgHgSBr	mp-560067	$Pmma$	(#51)	9.0	10.6	OT4	2.479	2.576	2.598	-	0.36	1.27
642.	Zr_3N_4	mp-11661	$I\bar{4}3d$	(#220)	9.0	11.5	OT2	1.719	1.719	2.281	45.1	0.42	1.07
643.	$NaBiO_2$	mp-22984	$C2/c$	(#15)	9.0	11.8	OT1	2.324	2.327	2.327	-	0.40	1.43
644.	Na_5TlSn_3	mp-31483	$P2_1/c$	(#14)	8.9	8.4	OT3	0.450	0.551	0.551	-	0.25	0.91
645.	K_5SnBi_3	mp-29387	$P2_1/c$	(#14)	8.9	8.2	OT3	0.376	0.413	0.413	1.4	0.18	1.15
646.	$HgGa_2S_4$	mp-4809	$I\bar{4}$	(#82)	8.7	9.5	OT1	2.636	2.636	2.636	-	0.23	1.39
647.	ZrOS	mp-8231	$P4/nmm$	(#129)	8.7	11.8	OT2	2.184	2.184	2.276	25.5	0.53	0.86
648.	TlCl	mp-23167	$Pm\bar{3}m$	(#221)	8.5	9.0	OT1	2.682	2.682	2.682	47.0	0.29	0.56
649.	La_3RuI_3	mp-29824	$P2_1/m$	(#11)	8.5	7.9	OT3	0.415	0.458	0.458	-	0.24	0.17
650.	Ca_2Ge	mp-304	$Pnma$	(#62)	8.4	8.6	OT2	0.806	0.806	1.147	-	0.52	1.33
651.	CdSe	mp-1070	$P6_3mc$	(#186)	8.4	9.9	OT1	2.529	2.529	2.529	1.1	0.12	1.33
652.	Tl_4SnTe_3	mp-3019	$I4/mcm$	(#140)	8.4	8.6	OT2	0.756	0.756	1.105	5.3	0.21	0.28
653.	$K_2Au_4CdS_4$	mp-557832	$Ibam$	(#72)	8.3	9.7	OT4	2.557	2.650	2.733	-	0.70	1.18

	Formula	Materials	Space	SLME (%)		Optical	Bandgap (eV)			ΔE_{hull}	m^* (m_0)	
		Project ID	Group	L=500 nm	L=1 μm	Type	E_g	E_g^{d}	E_g^{da}	(meV atom^{-1})	m_e^*	m_h^*
654.	PtP_2O_7	mp-29282	$P2_1/c$ (#14)	8.1	9.5	OT2	2.506	2.506	2.744	-	0.59	1.46
655.	Cd_2AsCl_2	mp-27776	$P2_1/c$ (#14)	8.0	10.0	OT4	2.381	2.569	2.621	1.5	0.39	0.34
656.	$MoHg_2O_4$	mp-505677	$P2_1/c$ (#14)	8.0	8.4	OT3	2.692	2.781	2.781	-	1.11	1.31
657.	Ca_2NI	mp-28553	$P6_3/mmc$ (#194)	8.0	8.2	OT3	2.719	2.786	2.786	-	0.94	1.35
658.	Ag_3PS_4	mp-12459	$Pmn2_1$ (#31)	7.9	10.2	OT2	2.264	2.264	2.546	-	0.25	1.18
659.	$MgSr_3GeN_4$	mp-567398	$Pnna$ (#52)	7.7	9.9	OT1	2.470	2.470	2.470	-	0.29	1.22
660.	$AgPb_4O_4Cl$	mp-560923	$P4/n$ (#85)	7.6	8.0	OT3	2.729	2.776	2.776	12.0	0.67	1.44
661.	$LiAlTe_2$	mp-4586	$I\bar{4}2d$ (#122)	7.4	7.6	OT1	2.764	2.764	2.764	-	0.53	0.56
662.	$KYGeS_4$	mp-867334	$P2_1$ (#4)	7.4	7.9	OT1	2.736	2.739	2.739	-	0.83	0.86
663.	C	mp-606949	$P6_3mc$ (#186)	7.4	7.5	OT1	2.771	2.771	2.771	2.3	0.10	0.11
664.	$Sr_3Ga_3N_5$	mp-570971	$P\bar{1}$ (#2)	7.3	8.7	OT1	2.642	2.642	2.642	-	0.23	1.28
665.	$AgAlSe_2$	mp-14091	$I\bar{4}2d$ (#122)	7.3	8.9	OT1	2.589	2.589	2.589	-	0.17	0.90
666.	$Ba_2Bi_2O_5$	mp-28670	$P2_1/c$ (#14)	7.2	8.4	OT3	2.677	2.709	2.709	-	0.70	1.17
667.	$HgTl_4Br_6$	mp-27293	$P4/mnc$ (#128)	7.2	9.1	OT2	2.526	2.526	2.703	9.7	1.35	0.74
668.	$BaLa_2ZnS_5$	mp-16452	$I4/mcm$ (#140)	7.2	9.6	OT2	2.332	2.332	2.687	-	0.63	0.77
669.	CuI	mp-22895	$R3m$ (#160)	7.2	8.5	OT1	2.655	2.655	2.655	6.0	0.20	1.06
670.	$Cd_2Tl_3I_7$	mp-28432	$Pbam$ (#55)	7.1	9.2	OT3	2.537	2.651	2.651	-	0.37	1.44
671.	In_7Cl_9	mp-28730	$Pa\bar{3}$ (#205)	7.1	7.8	OT2	2.679	2.679	2.933	-	1.31	1.41
672.	TlF	mp-2175	$Fm\bar{3}m$ (#225)	7.1	7.3	OT1	2.786	2.786	2.786	34.7	0.44	1.05
673.	$SrGa_2Te_4$	mp-6987	$Cccm$ (#66)	6.9	8.6	OT4	1.330	1.447	1.926	-	0.26	0.85
674.	$LiGaSe_2$	mp-11582	$Pna2_1$ (#33)	6.9	7.4	OT1	2.771	2.771	2.771	-	0.31	1.47
675.	$Hg_5O_4Cl_2$	mp-23358	$Ibam$ (#72)	6.8	9.0	OT4	1.909	1.987	2.229	-	0.25	1.43
676.	Ag_6SiO_8S	mp-555015	$I4_1/amd$ (#141)	6.8	8.9	OT2	1.470	1.471	2.161	-	0.46	0.35
677.	$Ta_9Fe_2S_6$	mp-3652	$P\bar{6}2m$ (#189)	6.7	6.1	OT3	0.411	0.507	0.507	-	0.66	1.23
678.	$LiZnN$	mp-7575	$F\bar{4}3m$ (#216)	6.7	7.8	OT1	2.691	2.691	2.691	-	0.15	1.24
679.	$ZnSiP_2$	mp-4763	$I\bar{4}2d$ (#122)	6.7	8.5	OT2	2.138	2.138	2.977	-	0.68	0.40
680.	AgI	mp-22925	$F\bar{4}3m$ (#216)	6.7	7.6	OT1	2.741	2.741	2.741	-	0.22	1.05
681.	$Sr_3Ga_2N_4$	mp-16945	$Pnna$ (#52)	6.7	7.9	OT1	2.691	2.691	2.691	-	0.27	1.28
682.	$MgLu_2Se_4$	mp-10191	$Fd\bar{3}m$ (#227)	6.5	9.2	OT1	2.490	2.490	2.490	-	0.38	1.00
683.	Na_2CdSnS_4	mp-561075	$C2$ (#5)	6.4	7.0	OT1	2.789	2.789	2.789	-	0.35	0.99
684.	AgI	mp-567809	$P4/nmm$ (#129)	6.4	7.4	OT1	2.741	2.741	2.741	25.2	0.29	1.33
685.	$AgHg_2AsO_4$	mp-558188	$Pbam$ (#55)	6.4	8.7	OT1	2.454	2.454	2.454	-	0.32	1.24
686.	Ba_3GaSb_3	mp-28296	$Pnma$ (#62)	6.3	5.9	OT2	0.542	0.542	0.736	-	1.02	1.29
687.	CuI	mp-569346	$P6_3mc$ (#186)	6.2	7.4	OT1	2.716	2.716	2.716	8.8	0.20	1.21
688.	$LuNiBi$	mp-30457	$F\bar{4}3m$ (#216)	6.1	6.0	OT3	1.005	1.811	1.811	-	0.11	0.39
689.	C	mp-569304	$R\bar{3}m$ (#166)	6.0	6.1	OT1	2.865	2.865	2.865	28.7	0.08	0.08
690.	Ba_2Pb	mp-21246	$Pnma$ (#62)	6.0	5.5	OT1	0.309	0.309	0.309	-	1.03	1.19
691.	$RbTaN_2$	mp-568557	$Pbca$ (#61)	6.0	6.0	OT2	2.859	2.859	2.920	-	0.91	1.34
692.	$InPS_4$	mp-20790	$I\bar{4}$ (#82)	6.0	6.3	OT3	2.830	2.934	2.934	-	0.46	1.12
693.	Cu_2O^*	mp-361	$Pn\bar{3}m$ (#224)	5.8	7.3	OT2	1.745	1.745	2.527	-	0.95	1.71
694.	$Sr_{14}Al_8Ge_3$	mp-571416	$R\bar{3}$ (#148)	5.7	5.0	OT3	0.344	0.403	0.403	-	1.01	0.98
695.	$AgZnPS_4$	mp-558807	$Pna2_1$ (#33)	5.7	6.4	OT2	2.782	2.782	2.959	-	0.37	1.29
696.	$CaTl_2O_4$	mp-5402	$Cmcm$ (#63)	5.6	6.9	OT4	1.789	1.924	2.425	9.4	0.20	1.42
697.	$Ba_3Si_4P_6$	mp-27887	$P2_1/m$ (#11)	5.6	6.7	OT2	1.181	1.181	1.786	-	1.01	0.54
698.	PbF_3	mp-20652	$P4_2/mcm$ (#132)	5.6	6.4	OT2	2.754	2.754	2.997	-	0.78	1.05
699.	$Hg_3S_2Br_2$	mp-29096	$C2/m$ (#12)	5.4	6.9	OT4	2.666	2.699	2.866	-	0.30	1.28
700.	AgI	mp-22894	$P6_3mc$ (#186)	5.4	6.2	OT1	2.825	2.825	2.825	1.0	0.22	1.25
701.	$CuAlS_2$	mp-4979	$I\bar{4}2d$ (#122)	5.3	6.4	OT1	2.792	2.792	2.792	-	0.24	1.09
702.	$LaZnPO$	mp-7060	$P4/nmm$ (#129)	5.3	8.0	OT2	2.055	2.055	2.441	-	0.54	1.35
703.	$CuBS_2$	mp-12954	$I\bar{4}2d$ (#122)	5.3	6.8	OT2	2.676	2.676	2.937	-	0.53	0.75
704.	$CaPdAs$	mp-28763	$Pnma$ (#62)	5.3	4.8	OT4	0.512	0.641	0.699	-	0.93	0.58
705.	Li_3AuS_2	mp-15999	$Ibam$ (#72)	5.2	6.3	OT1	2.816	2.822	2.822	-	0.40	1.26
706.	Sr_2Pb	mp-30828	$Pnma$ (#62)	5.1	4.6	OT3	0.437	0.619	0.619	-	0.22	0.55

	Formula	Materials	Space	SLME (%)		Optical	Bandgap (eV)			ΔE_{hull}	m^* (m_0)	
		Project ID	Group	L=500 nm	L=1 μm	Type	E_g	E_g^{d}	E_g^{da}	(meV atom^{-1})	m_e^*	m_h^*
707.	$PbBiO_2Cl$	mp-23084	$Cmcm$ (#63)	5.1	6.2	OT3	2.809	2.837	2.837	-	0.43	1.01
708.	$Li_2Ga_2GeS_6$	mp-554782	$Fdd2$ (#43)	5.1	5.3	OT1	2.932	2.932	2.932	36.1	0.36	1.43
709.	CaO_8Te_3	mp-15511	$C2/c$ (#15)	4.8	5.4	OT4	2.883	2.994	3.027	-	0.66	0.70
710.	$RbGeBr_3$	mp-28558	$Pna2_1$ (#33)	4.8	5.2	OT1	2.934	2.934	2.934	-	1.39	0.42
711.	CdS	mp-2469	$F\bar{4}3m$ (#216)	4.8	5.5	OT1	2.873	2.873	2.873	1.2	0.17	1.12
712.	Pb_5O_8S	mp-505603	$P2_1/c$ (#14)	4.6	5.0	OT3	2.948	2.960	2.960	-	0.83	1.14
713.	$LiBaBS_3$	mp-554076	$P2_1/c$ (#14)	4.5	5.9	OT2	2.770	2.770	2.849	-	0.75	1.06
714.	K_2Ga_3	mp-568052	$I4/mmm$ (#139)	4.3	3.8	OT2	0.522	0.523	0.739	-	0.66	1.15
715.	Lu_2CdS_4	mp-8269	$Fd\bar{3}m$ (#227)	4.2	5.7	OT1	2.791	2.791	2.791	-	0.27	1.23
716.	$Ba_3P_2S_8$	mp-561443	$C2/m$ (#12)	4.2	5.6	OT2	2.679	2.686	3.111	10.7	0.49	0.63
717.	RuSi	mp-189	$P2_13$ (#198)	4.0	3.8	OT3	0.415	0.522	0.522	0.1	0.45	0.75
718.	$Rb_2In_4O_7$	mp-27563	$P\bar{3}1m$ (#162)	3.9	4.7	OT4	2.878	2.914	3.054	-	0.25	0.79
719.	$LiCaGaN_2$	mp-570948	$P2_1/c$ (#14)	3.8	4.2	OT1	3.024	3.024	3.024	-	0.30	0.85
720.	CdS	mp-672	$P6_3mc$ (#186)	3.8	4.5	OT1	2.966	2.966	2.966	-	0.17	1.46
721.	$Ca_3Ga_2N_4$	mp-571162	$C2/c$ (#15)	3.5	4.1	OT1	3.010	3.010	3.010	-	0.29	1.49
722.	$CsCu_2I_3$	mp-23431	$Cmcm$ (#63)	3.5	4.3	OT1	2.957	2.957	2.957	4.3	0.30	1.47
723.	$NaGaTe_2$	mp-10164	$I4/mcm$ (#140)	3.4	4.1	OT4	1.152	1.282	1.842	6.1	0.24	0.84
724.	$AgHg_2PO_4$	mp-556798	$Pbam$ (#55)	3.4	4.9	OT2	2.712	2.712	2.819	-	0.42	0.77
725.	$NaAlSe_2$	mp-17060	$C2/c$ (#15)	3.3	4.1	OT2	2.968	2.968	3.117	-	0.23	1.16
726.	ZnSe	mp-1190	$F\bar{4}3m$ (#216)	3.3	3.9	OT1	3.010	3.010	3.010	-	0.14	0.95
727.	Cd_4SiS_6	mp-18179	Cc (#9)	3.2	4.0	OT1	2.977	2.977	2.977	6.6	0.24	1.43
728.	$CsPbCl_3$	mp-23037	$Pm\bar{3}m$ (#221)	3.2	3.5	OT1	3.080	3.080	3.080	5.5	0.72	0.28
729.	$CaLu_2S_4$	mp-505362	$Pnma$ (#62)	3.1	4.5	OT2	2.778	2.778	2.989	-	0.65	1.24
730.	Be_3P_2	mp-567841	$Ia\bar{3}$ (#206)	3.1	4.2	OT2	1.739	1.739	2.785	-	0.42	0.58
731.	Cd_3AsCl_3	mp-27899	$Pnma$ (#62)	3.0	3.7	OT4	3.003	3.083	3.119	-	0.24	1.38
732.	KGa_3	mp-181	$I\bar{4}m2$ (#119)	2.9	2.5	OT3	0.380	0.488	0.488	-	0.23	0.11
733.	LaZnAsO	mp-549589	$P4/nmm$ (#129)	2.9	4.0	OT2	1.849	1.849	2.900	-	0.55	1.41
734.	$CdCN_2$	mp-10969	$R\bar{3}m$ (#166)	2.8	3.9	OT4	2.918	2.974	3.082	-	0.75	0.59
735.	ZnSe	mp-380	$P6_3mc$ (#186)	2.8	3.4	OT1	3.057	3.057	3.057	4.8	0.14	1.14
736.	$K_2Zn_3O_4$	mp-28371	$C2/c$ (#15)	2.7	3.0	OT1	3.137	3.137	3.137	-	1.47	1.15
737.	$MgLu_2S_4$	mp-14304	$Fd\bar{3}m$ (#227)	2.7	3.8	OT1	2.960	2.960	2.960	-	0.46	1.26
738.	Sb_2O_3	mp-2136	$Pccn$ (#56)	2.6	3.2	OT2	3.047	3.047	3.269	-	0.59	1.31
739.	$BaHg_2O_2Cl_2$	mp-555736	$P4/mbm$ (#127)	2.4	3.4	OT4	2.851	2.924	3.177	-	0.41	1.48
740.	Lu_2ZnS_4	mp-18332	$Pnma$ (#62)	2.4	2.8	OT1	3.168	3.168	3.168	1.1	1.14	0.85
741.	$ZnCdS_2$	mp-971712	$P\bar{4}m2$ (#115)	2.3	2.7	OT1	3.167	3.167	3.167	17.6	0.18	1.14
742.	$Rb_2Zn_3O_4$	mp-29606	$C2/c$ (#15)	2.3	2.6	OT1	3.203	3.203	3.203	-	0.29	1.50
743.	$ZnGa_2S_4$	mp-5350	$I\bar{4}$ (#82)	2.3	2.4	OT1	3.260	3.260	3.260	-	0.26	1.43
744.	$O_8TeBr_6H_{18}$	mp-740696	$P2_1/c$ (#14)	2.2	2.2	OT3	3.295	3.306	3.306	-	0.44	0.44
745.	$ZnSnSb_2$	mp-4756	$I\bar{4}2d$ (#122)	2.0	2.0	OT4	0.929	1.580	2.019	-	0.07	0.58
746.	$RbGaS_2$	mp-561407	$C2/c$ (#15)	1.9	2.3	OT2	3.246	3.246	3.383	-	0.29	1.19
747.	SrN_2H_4	mp-643905	$P2_1/c$ (#14)	1.9	2.4	OT3	3.139	3.279	3.279	-	0.47	0.94
748.	Na_3PS_4	mp-28782	$P\bar{4}2_1c$ (#114)	1.9	2.8	OT2	2.963	2.963	3.489	-	0.67	1.25
749.	Ba_2AgSi_3	mp-9867	$Fddd$ (#70)	1.8	1.4	OT3	0.268	0.346	0.349	-	0.88	0.44
750.	ZnO^*	mp-2133	$P6_3mc$ (#186)	1.8	2.1	OT1	3.268	3.268	3.268	-	0.19	2.13
751.	LiB_6C	mp-569450	$Amm2$ (#38)	1.7	2.5	OT2	2.924	2.924	3.396	-	0.41	0.61
752.	Hg_2PO_3F	mp-561472	$Ibam$ (#72)	1.5	2.2	OT1	3.123	3.123	3.123	-	0.36	0.53
753.	MgO_5Te_2	mp-5746	$Pbcn$ (#60)	1.4	1.7	OT2	3.367	3.367	3.424	7.1	1.40	1.14
754.	Zn_3CdS_4	mp-981379	$P\bar{4}3m$ (#215)	1.2	1.5	OT1	3.425	3.425	3.425	15.9	0.19	1.21
755.	GaN	mp-830	$F\bar{4}3m$ (#216)	1.1	1.3	OT1	3.454	3.454	3.454	5.2	0.18	1.40
756.	BaZnOS	mp-548469	$Cmcm$ (#63)	1.1	1.4	OT1	3.405	3.405	3.405	-	0.30	1.36
757.	Na_3AlH_6	mp-568950	$Pbcm$ (#57)	0.9	1.5	OT2	3.174	3.174	3.501	13.2	0.44	1.21
758.	NaK_2AlH_6	mp-24412	$P4/mnc$ (#128)	0.9	1.5	OT2	3.032	3.037	3.591	-	0.41	1.16
759.	Ga_2O_6Te	mp-28931	$P4_2/mnm$ (#136)	0.7	1.2	OT2	2.913	2.913	3.305	-	0.24	1.49

	Formula	Materials	Space		SLME (%)		Optical	Bandgap (eV)			ΔE_{hull}	m^* (m_0)	
		Project ID	Group		L=500 nm	L=1 μm	Type	E_g	E_g^{d}	E_g^{da}	(meV atom^{-1})	m_e^*	m_h^*
760.	ZnS	mp-556775	$P3m1$	(#156)	0.5	0.6	OT1	3.671	3.671	3.671	1.0	0.20	1.46
761.	ZnS	mp-556392	$P3m1$	(#156)	0.4	0.5	OT1	3.698	3.698	3.698	0.8	0.20	1.47
762.	ZnS	mp-555858	$R3m$	(#160)	0.4	0.5	OT1	3.705	3.705	3.705	10.9	0.20	1.37
763.	ZnS	mp-561196	$P6_3mc$	(#186)	0.4	0.5	OT1	3.714	3.714	3.714	0.4	0.20	1.47
764.	ZnS	mp-10695	$F\bar{4}3m$	(#216)	0.4	0.5	OT1	3.708	3.708	3.708	-	0.20	1.06
765.	ZnS	mp-556468	$R3m$	(#160)	0.4	0.5	OT1	3.721	3.721	3.721	11.4	0.21	1.47
766.	ZnS	mp-557151	$R3m$	(#160)	0.4	0.5	OT1	3.721	3.721	3.721	11.3	0.21	1.44
767.	ZnS	mp-555280	$R3m$	(#160)	0.4	0.5	OT1	3.719	3.719	3.719	11.7	0.20	1.39
768.	ZnS	mp-543011	$R3m$	(#160)	0.4	0.5	OT1	3.721	3.721	3.721	12.5	0.21	1.39
769.	ZnS	mp-13456	$R3m$	(#160)	0.4	0.4	OT1	3.723	3.723	3.723	1.6	0.21	1.37
770.	ZnS	mp-557308	$P3m1$	(#156)	0.4	0.5	OT1	3.715	3.715	3.715	0.6	0.21	1.48
771.	ZnS	mp-561118	$P6_3mc$	(#186)	0.4	0.5	OT1	3.710	3.710	3.710	0.7	0.20	1.44
772.	ZnS	mp-561258	$P6_3mc$	(#186)	0.4	0.5	OT1	3.714	3.714	3.714	0.5	0.20	1.47
773.	ZnS	mp-9946	$P6_3mc$	(#186)	0.3	0.4	OT1	3.719	3.719	3.719	0.9	0.20	1.38
774.	ZnS	mp-10281	$P6_3mc$	(#186)	0.3	0.4	OT1	3.721	3.721	3.721	1.4	0.21	1.35
775.	ZnS	mp-555410	$R3m$	(#160)	0.3	0.4	OT1	3.733	3.733	3.733	2.1	0.21	1.31
776.	ZnS	mp-555763	$R3m$	(#160)	0.3	0.4	OT1	3.731	3.731	3.731	2.5	0.21	1.34
777.	$LiBa_2Ge_3$	mp-17491	$Fddd$	(#70)	0.3	0.2	OT3	0.212	0.291	0.291	-	0.85	0.87
778.	ZnS	mp-554405	$R3m$	(#160)	0.3	0.4	OT1	3.738	3.738	3.738	2.8	0.21	1.32
779.	ZnS	mp-560588	$P6_3mc$	(#186)	0.3	0.4	OT1	3.731	3.731	3.731	3.0	0.21	1.29
780.	ZnS	mp-556005	$P3m1$	(#156)	0.3	0.4	OT1	3.730	3.730	3.730	1.4	0.21	1.38
781.	B_6O	mp-1346	$R\bar{3}m$	(#166)	0.1	0.2	OT2	3.672	3.672	4.246	-	0.36	0.59
782.	KTl	mp-863730	$Cmca$	(#64)	0.1	0.0	OT3	0.215	0.346	0.346	-	0.21	0.42
783.	GeO_2	mp-470	$P4_2/mnm$	(#136)	0.0	0.0	OT2	3.790	3.790	4.015	3.7	0.24	1.41
784.	Si*	mp-149	$Fd\bar{3}m$	(#227)	0.0	0.0	OT4	1.147	3.091	3.091	-	1.00	0.59
785.	Tl_4PbTe_3	mp-20740	$I4/mcm$	(#140)	0.0	0.0	OT2	0.810	0.810	1.524	-	0.20	0.29
786.	YH_3	mp-23706	$P\bar{3}c1$	(#165)	0.0	0.0	OT4	1.180	1.202	2.701	-	0.17	0.18
787.	Na_3InBi_2	mp-580161	$P2_1/c$	(#14)	0.0	0.0	OT4	0.168	0.213	0.295	-	0.25	0.69
788.	Ca_2Sn	mp-22735	$Pnma$	(#62)	0.0	0.0	OT2	0.535	0.535	1.088	-	0.63	1.18

Phases for which calculations did not successfully finish

Ab initio calculations of absorption spectra, transition dipole matrices, and/or Δ-sol bandgap corrections were not successfully completed for $\approx$30 ($\approx$3.5 %) of the $\approx$800 phases which pass the intermediate screens. For completeness, we list these phases below. On inspection, many are unlikely to be practical photovoltaics (e.g. air-sensitive Zintl phases, phases containing toxic or scarce metals like $RhSb_2$, or extremely narrow-gap semiconductors like Bi_2Te_3).

	Formula	Materials Project ID	Space Group
1.	$HfTe_5$	mp-1168	$Cmcm$ (#63)
2.	$NaAu_3Ge$	mp-13674	$Pa\bar{3}$ (#205)
3.	SnTe	mp-1883	$Fm\bar{3}m$ (#225)
4.	$BaLa_2In_2O_7$	mp-21699	$P4_2/mnm$ (#136)
5.	$Hg_6Sb_5Br_7$	mp-23453	$Pa\bar{3}$ (#205)
6.	GeTe	mp-2612	$Fm\bar{3}m$ (#225)
7.	$RhSb_2$	mp-2682	$P2_1/c$ (#14)
8.	$Cs_3Sb_2Cl_9$	mp-27629	$P\bar{3}m1$ (#164)
9.	Bi_2Te_3	mp-34202	$R\bar{3}m$ (#166)
10.	ZnS	mp-554889	$P3m1$ (#156)
11.	ZnS	mp-555214	$P3m1$ (#156)
12.	ZnS	mp-556161	$P3m1$ (#156)
13.	ZnS	mp-556950	$P3m1$ (#156)
14.	CuO_3Te	mp-558696	$P2_1/c$ (#14)
15.	ZnS	mp-560725	$P6_3mc$ (#186)
16.	$Ca_{14}GaAs_{11}$	mp-568790	$I4_1/acd$ (#142)
17.	$GaBi_4Cl_4$	mp-569237	$P6_3$ (#173)
18.	$CsGeBr_3$	mp-570223	$Pm\bar{3}m$ (#221)
19.	$RbGeI_3$	mp-571458	$Pm\bar{3}m$ (#221)
20.	Na_2SnAs_2	mp-574684	$I4_1/acd$ (#142)
21.	$Tl_8Pb_4As_{19}Sb_{21}S_{68}$	mp-581586	$P1$ (#1)
22.	$CsSnI_3$	mp-614013	$Pm\bar{3}m$ (#221)
23.	Ba_3InAs_3	mp-620346	$Pnma$ (#62)
24.	Cs_3PdH_5	mp-643006	$P4/mbm$ (#127)
25.	$K_{11}In_6Bi_9$	mp-680539	$P\bar{1}$ (#2)
26.	$AuBi_9Br_9$	mp-684015	$P2_1/c$ (#14)
27.	SnSe	mp-8936	$P4/nmm$ (#129)
28.	$CsSe_3Te$	mp-9462	$P2_1/c$ (#14)
29.	KAg_3Se_2	mp-9782	$C2/m$ (#12)

References

(1) Chan, M. K. Y.; Ceder, G. Efficient Band Gap Prediction for Solids. *Phys. Rev. Lett.* **2010**, *105*, 196403.

(2) Yu, L.; Zunger, A. Identification of Potential Photovoltaic Absorbers Based on First-Principles Spectroscopic Screening of Materials. *Phys. Rev. Lett.* **2012**, *108*, 068701.

(3) Shockley, W.; Queisser, H. J. Detailed Balance Limit of Efficiency of p–n Junction Solar Cells. *J. Appl. Phys.* **1961**, *32*, 510–519.

(4) Jain, A.; Ong, S. P.; Hautier, G.; Chen, W.; Richards, W. D.; Dacek, S.; Cholia, S.; Gunter, D.; Skinner, D.; Ceder, G.; Persson, K. A. Commentary: The Materials Project: A Materials Genome Approach to Accelerating Materials innovation. *APL Mater.* **2013**, *1*, 011002.

(5) Setyawan, W.; Gaume, R. M.; Lam, S.; Feigelson, R. S.; Curtarolo, S. High-Throughput Combinatorial Database of Electronic Band Structures for Inorganic Scintillator Materials. *ACS Comb. Sci.* **2011**, *13*, 382–390.

(6) Ricci, F.; Chen, W.; Aydemir, U.; Snyder, G. J.; Rignanese, G.-M.; Jain, A.; Hautier, G. An Ab Initio Electronic Transport Database for Inorganic Materials. *Sci. Data* **2017**, *4*, 170085.

(7) Huck, P.; Jain, A.; Gunter, D.; Winston, D.; Persson, K. A Community Contribution Framework for Sharing Materials Data with Materials Project. 2015 IEEE 11th International Conference on e-Science. 2015.

(8) Huck, P.; Gunter, D.; Cholia, S.; Winston, D.; N'Diaye, A. T.; Persson, K. User Applications Driven by the Community Contribution Framework MPContribs in the Materials Project. *Concurr. Comp.-Pract. E.* **2015**, *28*, 1982–1993.